Crystallisation and Structure Solution of the *c*-Ring of F_oF_1 ATP Synthase from Spinach Chloroplasts

Inaugural-Dissertation

zur

Erlangung des Doktorgrades

der Mathematisch-Naturwissenschaftlichen Fakultät

der Heinrich-Heine-Universität Düsseldorf

vorgelegt von

Melanie Vollmar

aus Kapsweyer

Juli 2009

Aus dem Institut für biochemische Pflanzenphysiologie
der Heinrich-Heine-Universität Düsseldorf

Gedruckt mit der Genehmigung
der Mathematisch-Naturwissenschaftlichen Fakultät
der Heinrich-Heine-Universität Düsseldorf

Referent: Prof. Dr. G. Groth
Koreferent: Prof. Dr. L. Schmitt

Tag der mündlichen Prüfung: 17.09.2009

Meiner Mutter

Summary

ATP synthase from spinach belongs to a group of essential enzymes which produce most of the cell's ATP supply. The energy stored in light is used in photosynthetic active complexes to produce an outward pointing electron/proton gradient across the thylakoid membrane of chloroplasts. This energisation of the membrane is a prerequisite for active F_oF_1 ATP synthase. ATP synthase pumps protons back across the thylakoid membrane into the chloroplast. During this translocation process, the electrical energy of the gradient is transformed into the mechanical energy of a rotation. This rotation takes place in the membrane part F_o and is translated via a stalk into a membrane associated part F_1 which carries the catalytic active sites. Conformational changes in these binding sites result in formation of an anhydride bond between the substrates, ADP and inorganic phosphate, and produces ATP. For F_1 a detailed structure is available and also the reaction mechanism in the binding sites is known on the atomic level. In contrast, for F_o a little information is available, and mechanisms as well as structural details are still at the levels of proposals and hypotheses. In this work X-ray crystallography was used to solve the structure for the main part of F_o, namely the proton translocating rotor, to a resolution of 3.8 Å. This is the first structure of the *c*-ring of a proton pumping ATP synthase and can therefore be used to explain several findings of binding behaviour as well as proposed structural details and mechanism. Crystals produced with new crystallisation conditions had no effect on the resolution. Instead, some of the changes improved the spot quality in diffraction experiments and decreased the mosaicity. Co-crystallisation of the *c*-ring with the inhibitors DCCD (N,N'-dicyclohexylcarbodiimide), phloretin, and phloridzin was also attempted. For DCCD detailed biochemical information about inhibitory effects is already known. However, a structure of the *c*-ring of a proton translocating ATP synthase with covalently bound DCCD has not yet been solved. Phloridzin is a sugar derivative of phloretin. For both substances inhibitory effects have been reported but only a little biochemical information is available and no binding site is identified. Data set analysis of a protein-inhibitor crystal with phloridzin showed extra electron density near one proton binding site, but couldn't be identified for definite because of low resolution of 4.25 Å.

Zusammenfassung

Die ATP Synthase aus Spinat gehört zu einer Gruppe von essentiellen Proteinen, die den größten Teil an ATP in einer Zelle produzieren. Die in Licht gespeicherte Energie wird von den photosynthetisch aktiven Komplexen genutzt, um einen nach außen gerichteten Elektronen-/Protonengradienten über die Thylakoidmembran der Chloroplasten aufzubauen. Diese Energetisierung der Membran ist die Voraussetzung für eine aktive F_oF_1 ATP Synthase. Diese pumpt im Gegenzug die Protonen in den Chloroplasten. Während dieses Transportprozesses, wird die elektrische Energie des Gradienten in die mechanische Energie einer Rotation übersetzt. Diese Rotation findet im Membranteil F_o statt, und wird über einen Stab in den membranassozierten Teil F_1 weiter gegeben, der die katalytisch aktiven Bindungstaschen trägt. Konformationsänderungen in diesen Bindungstaschen resultiert in der Ausbildung einer Anhydridbindung zwischen den Substraten ADP und anorganischem Phosphat, um ATP zu produzieren. Für F_1 ist bereits eine detaillierte Struktur bekannt, und sowohl Reaktionsmechanismus als auch der Aufbau der Bindungstaschen sind auf atomarer Ebene gelöst. Die Methode der Röntgenkristallanalyse wurde in dieser Arbeit genutzt, um die Struktur des Hauptbestandteils von F_o, den protonentransportierenden Rotor aus Untereinheit *c*, aufzuklären. Dies gelang mit einer Auflösung von 3.8 Å. In dieser Arbeit wird die erste detaillierte Struktur des rotierenden Rings einer protonentranslozierenden ATP Synthase vorgestellt. Diese Struktur kann genutzt werden, um Ergebnisse zu Bindungsverhalten sowie vorgeschlagene Strukturdetails und Mechanismen zu erklären. Mit Änderungen in den Kristallisationsbedingungen, an die Kristallisation anschließende Manipulationen und allgemeine Verbesserungen in der Reinigung wurde versucht die Auflösung zu verbessern und eine detailliertere Struktur zu erhalten. Kristalle, die unter neuen Bedingungen gewachsen waren zeigten leider keine Verbesserung in der Auflösung, hatten aber hingegen schärfere Reflexprofile in Beugungsexperimenten und eine niedrigere Mosaizität. In einem weiteren Projekt, sollte der Membranteil zusammen mit den Inhibitoren DCCD (N,N'-Dicyclohexylcarbodiimid), Phloretin und Phloridzin kristallisiert werden. Für DCCD gibt es bereits detaillierte biochemische Informationen, aber noch keine Struktur in kovalent gebundener Form am *c*-Ring einer Protonen ATP Synthase. Phloridzin ist ein Zuckerderivat von Phloretin. Für beide Substanzen werden inhibitorische Effekte berichtet. Es sind aber nur wenige biochemische Informationen vorhanden und eine Bindungstasche ist nicht bekannt. In einem Datensatz mit einem Co-Kristall aus Phloridzin und dem *c*-Ring konnte zusätzlich positive Elektronendichte an einer Protonenbindungstasche identifiziert werden. Eine Zuordnung zu Phloridzin war aber wegen der geringen Auflösung von 4.25 Å nicht möglich.

Content

Abbreviations

Å	Ångström
ADP	Adenosine 5'-diphosphate
AMPPNP	Adenosine 5'-(β,γ-imido)triphosphate
APS	Ammoniumperoxo disulphate
asu	Asymmetric unit
ATP	Adenosine 5'-triphosphate
CMC	Critical micelle concentration
DCCD	N,N'-dicyclohexylcarbodiimide
DDM	Dodecyl-β-D-maltoside
DTT	Dithiothreitol
g	Gram
x g	Multiple of gravity
IC_{50}	Half maximal inhibitory concentration
kDa	Kilo Dalton
kg	Kilogram
l	Litre
M	Molar (mol/l)
mA	Mili Ampere
min	Minute
mV	Milli Volt
µg	Micro gramme
µl	Micro litre
NaPPi	Sodium pyrophosphate
nm	Nanometre
p.a.	Pro analysis
PC	Phosphatidyl choline
PEG	Poly ethylenglycol
pg	Pico gramme
PMSF	Phenylmethanesulfonyl fluoride
SDS-PAGE	SDS-Polyacrylamide gelelectrophoresis
SDS	Sodium dodecyl sulphate
TEMED	N, N, N', N',-Tetramethylethylenediamine
Tris	Tris(hydroxymethyl)-amino methane
V	Volt

1. Introduction

1.1. ATP Synthases

An average human with a standard working behaviour has a turnover of about 200 kg ATP (adenosine 5'-triphosphate) every day (1). ATP is the ultimate energy currency in nature and is mainly produced by the F_oF_1 ATP synthase. This enzyme is a universal protein and can be found in any species: eukaryotes, prokaryotes, and eubacteria. Its location in mitochondria is in the inner membrane and the catalytic active part points into the matrix. The bacterial enzyme can be found in the cytoplasmic membrane with the catalytic part orientated towards the cytoplasm. In chloroplasts the protein is embedded into the thylakoid membrane and the catalytic part points towards the stroma.

Although they differ slightly in their subunit composition, all ATP synthases are constructed after the same scheme and show high functional and structural homologies (2). All F_oF_1 ATP synthases are composed of two portions, the membrane-embedded F_o part and the membrane-associated or soluble F_1 part. Both portions include several subunits with a high variability in the stoichiometry of subunit *c* depending on the species (3, 4, *5*, *6*, *7*, 8). This redundancy supports on one hand the study of structure and function but questions on the other hand why do differences exist and how do they influence the efficiency.

For the chloroplast enzyme it is known that subunits of F_o take part in the proton translocation across the membrane while the synthesis of ATP occurs in F_1. Depending on the actual physiological conditions the ATP synthase can work either as a synthase or as a hydrolase. Both functions cause a rotation of the enzyme. In the synthase situation the enzyme rotates counter-clockwise if seen from the stroma side. A proton gradient across the thylakoid membrane from the lumen to the stroma is established as a result of the rotation. In the hydrolase situation the complex rotates clockwise and protons are translocated from the stroma into the lumen under the expense of ATP. The rotation as well as the synthesis are well-controlled events. A proton gradient and a membrane potential with a threshold of > 40 mV are essential for the rotation (9). A molecular switch in subunit γ can be in an oxidised or reduced form (10). Furthermore, the catalytic part is controlled through the binding or release of inhibitory nucleotides in subunit ε (11, 12, 13, 14). The enzyme does not only show a reaction to general inhibitors which are known for both components, but also responds to plant-specific toxins.

1.2. Structure of ATP Synthase from Spinach Chloroplast

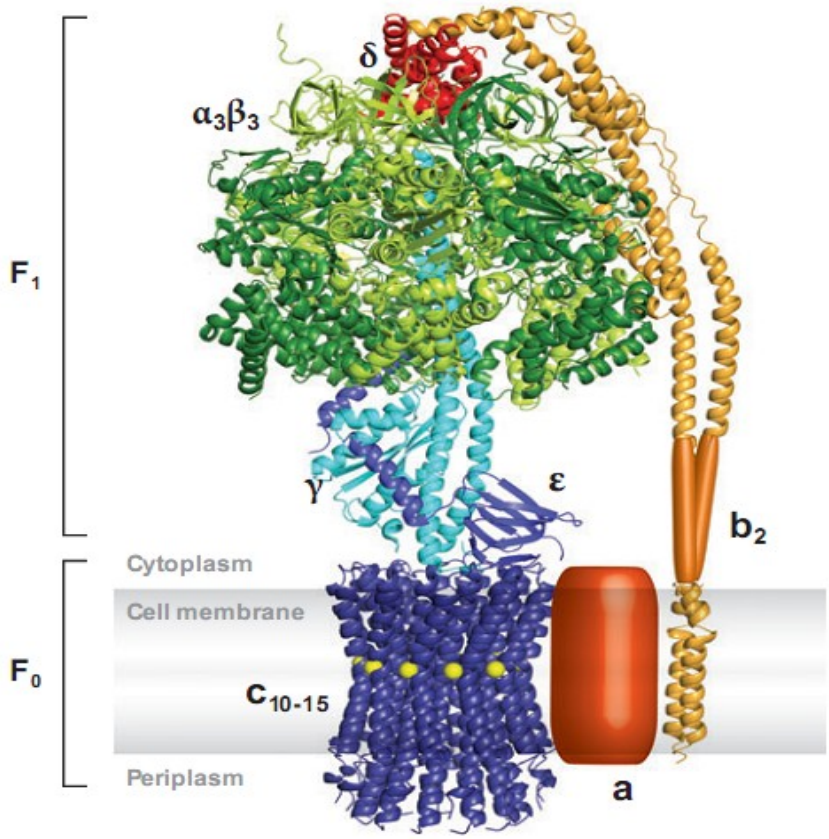

Figure 1.1:
Subunit organisation and secondary structure elements of F_oF_1 synthases. The structures of different subunits are taken from the RCSB Protein Data Bank and combined by hand based on biochemical data. The *c*-ring is taken from *Ilyobacter tartaricus* (1YCE) and F_1 from *Escherichia coli* (1JNV). The outer stalk is combined of *δ* from *E.coli* (2A7U) and the b-dimer from bovine mitochondria (2CLY). No structural information about subunit *a* and the hinge region in *b* is available so their predicted position is symbolised. The binding site in the *c*-ring is indicated by a yellows sphere (taken from von Ballmoos *et al.*, 2008)

The subunit composition of the two portions is given below. For spinach, F_o includes the subunits *IV* (*a*), *I* (*b*), *II* (*b'*), *III* (*c*) in a stoichiometry of 1:1:1:14. In brackets the nomenclature of *Escherichia coli* is given and will be used in this work to facilitate comparisons with structures from other organisms. F_1 contains the subunits *α*, *β*, *γ*, *δ*, *ε* in a stoichiometry of 3:3:1:1:1. For both parts this is a structural assignment for the different subunits. All subunits of F_o are located, completely or partially, in the membrane and those belonging to F_1 point to an aqueous environment

namely cytoplasm, matrix or stroma. An alternative way is to combine the subunits in a functional manner. Subunits α_3, β_3, δ, a, b, b' compose the stator of the enzyme and γ, ε, c form the rotor. Figure 1.1 gives a model of the complete F_oF_1-synthase. The subunits are taken from different organisms.

1.2.1. Structure of CF_1

The first images of chloroplast F_1 were retrieved with electron microscopy which showed a knob-like structure (15, 16, 17). More detailed information was only available after successful structure solution at 3.2 Å (18).

The former knob-like structure was shown to be a hexamer consisting of alternating monomers of α and β subunits arranged like the segments of an orange. Comparison of the structures of α and β subunits with each other, enlightened structural similarities between them. Both, α and β, can be separated into three regions. The N terminus contains six β-sheets. In the central region a mixture of α-helices, β-sheets, and the P-loop with the nucleotide binding site, can be found. Whereas the C terminus consists only of α-helices. The $\alpha\beta$ hexamer has in total six nucleotide binding sites which lie at the interface between subunits α and β. Only those which are mainly built up by residues from the subunit β show catalytic activity. Those having residues predominantly from the subunit α are only regulatory binding sites (19). In the crystal structure at 3.2 Å of Groth and Pohl (18) no nucleotides could be found in any binding site and the catalytic as well as the regulatory sites show a closed conformation. This structure is therefore thought to represent a unique state of the chloroplast ATP synthase namely the latent state of the enzyme.

The structure of Abrahams *et al.* (20) for the mitochondrial F_1 complex at 2.8 Å instead, shows different conformations for each catalytic site. This corresponds to a proposed mechanism for the synthesis of ATP namely the binding-change mechanism (see Figure 1.2). One of the sites was occupied by ADP and showed a closed conformation. The second site contained AMPPNP, a non-hydrolysable nucleotide analogue, and was also in a closed conformation. The last site was empty and open. All regulatory sites were occupied by AMPPNP and showed a closed conformation.

The asymmetric subunit γ works as a shaft and connects the synthesis in the hexamer to the rotation in the membrane ring. The N and C terminus are α-helices and form a coiled-coil structure that protrudes into the central cavity within the $\alpha\beta$ hexamer and almost reaches the top. For the

chloroplast F_1 the density probably representing the γ subunit could not be interpreted (18). However, the situation can clearly be seen in the mitochondrial structure (20, 21). γ as well as ε are in contact with the *c*-ring through the polar loops of the *c*-monomers (22, 23). This couples rotation of the *c*-ring via subunit γ to the conformational change in the catalytic active sites in the $\alpha\beta$ hexamer (24, 25, 26). A specific finding for chloroplast ATP synthase is a molecular switch in subunit γ represented by two cysteine residues. They can form a disulphide bridge and alter the enzyme between a latent and an active ATP synthase (10, 27).

For subunit ε in spinach no structural data is available. Proposals and hypothesis for its appearance are made on the basis of the mitochondrial homologue δ as well as ε from *Escherichia coli*. In mitochondrial δ the N terminus is built of ten β-sheets in a compact sandwich structure and the C terminus consists of two α-helices in a hairpin. Mitochondrial δ has no direct contact to the $\alpha\beta$ hexamer (21). ε from *E. coli* shows the same composition of secondary structure elements as in mitochondria (28, 29), but in contrast to the mitochondrial ε, interaction with subunit γ was identified. The helices of the α-helical hairpin leave their tight packing and wrap around γ (30).

The position of δ in the spinach ATP synthase was determined with cross-linking experiments and FRET measurements (31, 32), but detailed structural information is still not available. It is suggested that subunit δ lies on the outside of the $\alpha\beta$ hexamer. It has its beginning on the top of the hexamer near the N termini of the α and β subunits and reaches down to the level of the nucleotide binding sites. δ is thought to hold the hexamer in a stiff position together with the bb' dimer. A missing δ would allow the hexamer to follow the drag of the rotating ring and the energy stored in the rotation would not result in ATP synthesis (33).

1.2.2. Structure of CF_o

The first images of how the membrane part of spinach chloroplast ATP synthase could look like came from Seelert *et al.* (5). In topology images done with atomic force microscopy, the ring has a doughnut shape in a top view and shows a cylindrical shape from a side view. The authors could identify 14 subunits in the ring. Subunits *a*, *b*, and b' of spinach ATP synthase are not present in these images. With electron microscopy Birkenhäger *et al.* (34) showed for the *E.coli* ATP synthase that the *a* and b_2 subunits of the membrane part are on the outside of the *c*-ring. An alternative model for *E. coli* F_o was suggested by Hatch *et al.* (35) which places subunits *a* and *b* in the centre

of the ring.

The greatest variability between different species is in the number of subunit *c* within the rotating ring. Stoichiometries of 10 in yeast (3), 10 (6) to 12 (4) in *Escherichia coli*, 11 in *Ilyobacter tartaricus* (7), 14 in spinach chloroplasts (5), and 15 in *Spirulina platensis* (8) are known. In addition, the transmembrane *K*-ring of the V-ATPase from *Enterococcus hirae* which arose from gene duplication followed by gene fusion of *c* subunits of F-type ATP synthases, can be compared with the other rings. The *K*-ring has a stoichiometry of 10 subunits (36, 37, 38). As the ATP synthase is a universal enzyme to generate energy stored in an anhydride bond in ATP, one can expect more structures from other organisms with different stoichiometries in future.

In general, a *c*-monomer consists of two anti-parallel α-helices connected by a highly conserved loop. The first structure of the monomer was derived from *E.coli* with NMR (39). Based on this information the orientation of the multimer was proposed with the loop pointing towards the cytoplasm for bacteria or matrix for mitochondria, and with the termini facing the periplasm (40, 39, 3).

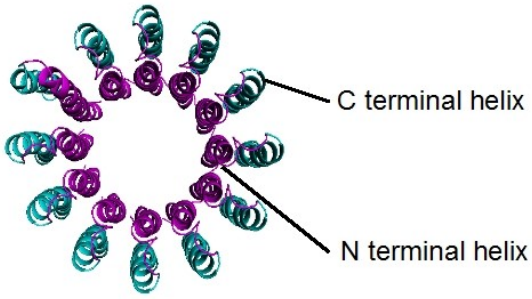

Figure 1.2:
Subunit organisation and secondary structure elements of a *c*-ring model from *Escherichia coli* (adopted from Rastogi and Girvin, 1999). In magenta the inner ring formed by the N terminal helix and in cyan the outer ring build by the C terminal helix viewed from top i.e. the cytoplasmic side in *Escherichia coli* which corresponds to matrix in mitochondria and stroma in chloroplasts

The N-terminal helix of a monomer in the rotor is part of the inner ring whereas the C terminus contributes to the outer ring. In an alternative model probed with trypotophan mutations, the orientation of N and C terminus was reversed (41). In both cases, the loop is suggested to interact with subunits γ and ε to transmit the energy of rotation to the conformational change within subunit β. In addition to the NMR structure of the *c*-monomer (39) at pH 5, a high pH structure for the *E.coli* c-monomer could be solved. It was done at pH 8.0 and showed a dramatic change in the C

terminal helix. The straight C terminal helix of the structure at pH 5.0 shows a pronounced kink at the proton binding site and the whole helix was rotated by about 140° (4; see also Figure 1.5 (A)). Sequence alignments of the *c*-monomer from several species have shown that they all have an essential acidic residue Asp or Glu to bind a proton or sodium ion (7). The hypothesis of an essential acidic residue was already established in the 1950s. Upon addition, DCCD (N,N'-dicyclohexylcarbodiimide) accepts the proton bound at the acidic residue and binds then covalently to this side chain which results in complete inhibition of the enzyme (42, 43).

The ring is thought to disrupt the integrity of the membrane and therefore it is likely that the central pore is sealed to avoid a breakdown of the membrane potential and uncontrolled substrate flow. Oberfeld *et al.* (44) proposed the presence of lipids in the central cavity as a result of photo-cross-linking studies of residues on the inside of the ring with phosphatidylethanolamine. Images taken with atomic force microscopy which show a plug on one side of the ring (45) were the initiation for the experiment of Oberfeld *et al.* (44).

Subunit *a* has not been crystallised for any species, so no structural information is available. Genetic studies done by Hatch *et al.* (35) gave a first impression about a possible orientation of the subunit. It is extremely hydrophobic and Wada *et al.* (46) suggested five transmembrane helices for the *E.coli* enzyme. Most information about position, orientation and function of subunit *a* was retrieved by chemical cross-linking in the Fillingame lab. The loops connecting transmembrane helices one and two as well as three and four on the cytoplasmic side are well pronounced and contain charged residues. The periplasmic loops between helices 2-3 and 4-5 are only small. The N terminus points toward the periplasm and the C terminus can be found in the cytoplasm. It is known that subunit *a* serves as a loading and unloading compound to deliver protons or sodium ions to the *c*-ring. An essential arginine is conserved in all species and points towards the centre of the membrane approximately on the same level as its interaction partner in subunit *c*, i.e. the carboxylate aspartate or glutamate. Mutations in the essential arginine result in loss of function (47). The interface between subunit *a* and the *c*-ring as well as aqueous channels within subunit *a* which allow for access or exit on both sides of the membrane, were mapped by long-range and short-range chemical cross-links (48, 49, 50, 51, 52, 53, 54, 55). Nevertheless there are still controversial debates as to whether two or only one aqueous channel is present.

There is not much detailed information available about subunits *b* and *b′*. They form a functional dimer and extend from the central part of the membrane up to the *αβ* hexamer at the height of the active site. The dimer is located at the periphery of the complex (16) and is in contact with subunit

δ to form the stator. This stator keeps the $\alpha\beta$ hexamer in position, so that it cannot follow the drag of the ring rotation (33). Roughly the first about 30 residues of the N terminus are hydrophobic and inserted in the membrane. The rest of the subunit-dimer is highly hydrophilic (40). It is suggested that the dimer binds to subunit *a* and has a few contacts to the ring. Possibly it stabilises subunit *a* to stay in the proximity of the ring (56). The ability to bind F_1 to depleted F_o within a membrane and to translocate protons could be shown for *E. coli*, upon addition of subunits *b* in stoichiometric amounts (57). Therewith it could be shown that this part of the complex is essential to connect both portions together (58). A structure of peripheral stalk fragments was solved for the mitochondrial enzyme. It shows almost continuous α-helices from the membrane up to the top of F_1, where the C termini of the helices interact with subunit δ (59).

1.3. Functional Mechanisms in F_o and F_1

1.3.1. Catalytic Mechanism within CF_1

The binding-change mechanism to be described here was introduced by Boyer (60, 61). It assumes that during ATP synthesis or hydrolysis the three catalytic binding sites in the β subunits sequentially pass through the same conformations. Cross (62) introduced the nomenclature for the different conformations: O (open), L (loose), and T (tight). They correspond to β_E, β_{TP}, and β_{DP} in the structure of Abrahams *et al.* (20).

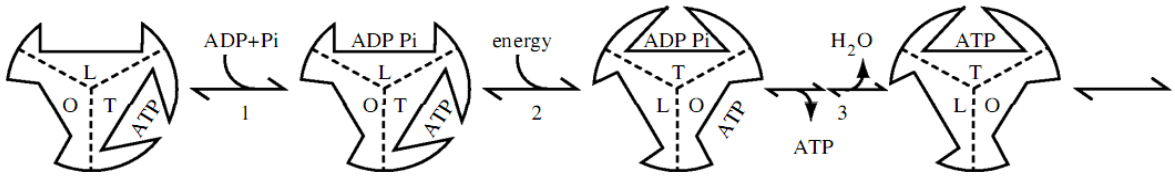

Figure 1.3: Scheme of the binding change mechanism in CF_1. The three states of the catalytic sites are given as O (open), L (loose), and T (tight). Each binding site passes through all three states during a full 360° rotation of CF_1. (after Cross, 1981)

The prerequisite for bond formation or cleavage, is bound substrate in a T-state binding site. In the T conformation Mg^{2+} and ATP or ADP are bound depending on the operation mode of the enzyme, i.e. synthesis or hydrolysis. This initial substrate binding is an intermediate state and does not

correspond to the inhibitory MgADP in the Walker structure (20). In the synthesis mode the bound substrates in a T binding site spontaneously form the product ATP. The next 120° step turns this site into an O conformation with little affinity for ATP. This allows ATP to exit the catalytic site. In the last 120° step the O site becomes an L site which has a high affinity for the substrates ADP and inorganic phosphate. As mentioned before, the $\alpha_3\beta_3$ core complex of F_1 belongs to the stator whereas $\gamma\varepsilon$ are part of the rotor. Changes in the conformation of F_1 are introduced by the rotation of the asymmetric γ in concert with the *c*-ring. This means also that all three catalytic binding sites change their conformations simultaneously with every 120° step. After a full revolution of the *c*-ring, γ has finished a cycle of three 120° steps and all three β subunits have been in each catalytic conformation.

Experiments with attached fluorescent actin filaments to subunit γ and an upside down fixed F_1 showed this 120° rotation in the hydrolysis mode (63, 64, 65). Later this filament was replaced by 40 nm gold particles to reduce the drag due to the filament length. A smaller probe allowed for the determination of substeps in a 120° rotation. In the first step of 90° the ATP becomes bound to a catalytic site in the open state. The second step, after another 30°, releases the hydrolysis products ADP and inorganic phosphate (66).

1.3.2. Energetics and Mechanics of CF_o

In the past, acid-base jump experiments were performed to show the pH dependency of functional ATP synthase (67). Later investigations showed that the buffers used not only formed a concentration gradient across the membrane but also induced a membrane potential (68). Until these findings it was believed that the proton/ion motive force in the form of a transmembrane gradient as well as the membrane potential are thermodynamically and kinetically equivalent. Electrochemical experiments as described above, were the basis for the chemiostatic model introduced by Mitchell (69). The proton/ion motive force Δp is composed of the membrane potential $\Delta\psi + \left(\frac{2.3\,RT}{F}\right)$ and the pH gradient ΔpH .

$$Proton\ motive\ force\,(\Delta p) = \Delta\psi - \left(\frac{2.3\,RT}{F}\right) \times \Delta pH \qquad (1.1)$$

After the finding that the buffers used for the acid-base jump experiments also induced a membrane potential, it became clear, why this potential seems to be independent from the ion gradient in a kinetic manner (68). The membrane potential is proposed to control the idling behaviour of the ring and cannot be replaced even by very high ion/proton concentrations. Without an external power, the rotor is in a stand-by mode. Only a membrane potential has enough kinetic energy, to release the rotor from the stand-by mode and start rotation (70). After reaching a potential threshold of > 40 mV the rotor starts to move and leaves its idling mode. A maximal efficiency in ATP synthesis could be achieved with a membrane potential of > 60 mV for the chloroplast and > 120 mV for the bacterial ATP synthase (9).

As there is a direct coupling between the two portions, F_o and F_1, one would expect that the number of protons needed to produce ATP would have a fixed ratio in relation to the three binding sites in the *β* subunits in every known F_oF_1 ATP synthase. The stoichiometries of different organisms show a mismatch in the number of *β* subunits and *c* subunits in the ring. Such a mismatch must ultimately result in a non-integral value for the H^+/ATP ratio.

Steigmiller *et al.* (71) compared the energetic H^+/ATP ratio in relation to the stoichiometric ratio *c/β* of chloroplasts with those of *E. coli*. In chloroplasts the *c*-ring consists of 14 subunits and in *E. coli* 10 are proposed. Both showed a potential energy of about $\Delta G_p^{0'} \approx 40\, kJ/mol$ which corresponds to a H^+/ATP ratio of four whereas the stoichiometric *c/β* ratio was 4.7 for chloroplasts and 3.3 for *E.coli*. Why this mismatch is present is still under investigation, but in both examples it seems that sufficient energy is produced to synthesize ATP. Structural and functional importance was proposed for the mismatch (38, 3) but an adaptation to physiological conditions is more likely. A greater number of *c* subunits within the ring still allows for the synthesis of ATP even if the proton motive force is small (72).

Another obvious question is how a stepping motor with 3 steps in F_1 can work smoothly with one of 10-15 steps in F_o. The elastic element to couple the two step motors lies in subunit *γ*. The foot of subunit *γ* extends from within the *c* ring up to the entrance area of the *αβ* hexamer and almost reaches the top of F_1. Viewing the system from the point of view of physics and mechanics one can describe the generation of torque as follows:

$$\vec{M} = r' \times \vec{F} \quad (1.2)$$

where r' is the distance between the centre of the ring and the protonated glutamate/aspartate in subunit *c*. $\vec{F}$ is the translational force, which induces an acceleration of the subunits within the ring. As the ring has a fix point in the centre, given as subunit γ, the translational accelerated *c*-monomers of the ring start to move on a circular trajectory and cause a rotation of the ring.

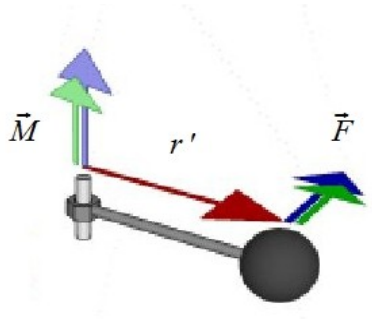

Figure 1.4: Schematic drawing of torque generation

The main components of the elastic buffer are addressed to the globular region of γ, subunit ε, and the loop of subunit *c*. The coiled-coil γ region buried within the $\alpha\beta$ hexamer is necessary for the subunit assembly in F_1 and the change in the catalytic sites, but does not take part in the elastic buffer. This buffer allows for high turn over rates under load (73, 74) and explains, why the enzyme can use the same principles with different F_1F_o compositions (3:10-15) (75). Additionally this may be an explanation for the robustness of chimeric constructs (76) and structural modifications (77, 78, 79).

1.4. Membrane Intrinsic F_o Domain

1.4.1. Subunit *c*

The NMR structures of subunit *c* from *E. coli* at pH 5 (39) and at pH 8 (4) served as the basis for theoretical models. These structures also supported biochemical findings for the binding site.

Matthey *et al.* (80) additionally proposed a structure of subunit *c* for the sodium translocating enzyme from *Propionigenium modestum* derived with NMR. For both NMR structures see Figure 1.5.

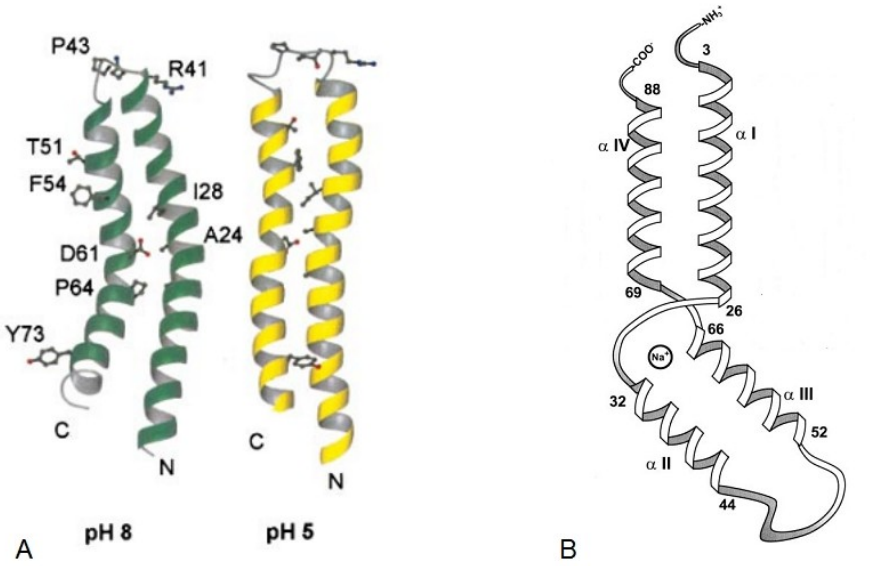

Figure 1.5: (A) NMR structure of subunit *c* from *E. coli* at pH 8 (left) and pH 5 (right) (taken from Rastogi and Girvin (1999) and Girvin *et al.* (1998)); (B) Proposed structure for subunit *c* from *Propionigenium modestum* based on NMR findings from Matthey *et al.* (1999)

As a universal protein, most amino acids of subunit *c* from F_oF_1 ATP synthases are highly conserved. The sequence alignment of subunit *c* from 21 different species (see Appendix 7.3) shows that Asp and Glu are used for proton or sodium ion translocation. The highly conserved acidic residue can generally be found between position 60 and 65 for any known sequence of subunit *c*. Assadi-Porter and Fillingame (81) showed for isolated *c*-rings from *E. coli* that Asp61 in this special position has a remarkably higher pKa value of 7.1, compared to the other two Asp present in the sequence with a pKa of five. They proposed that this pKa difference is based on an unusually high number of hydrophobic residues in the local environment of Asp61. The presence of non polar side chains in the neighbourhood of glutamate or aspartate seems to be necessary for proton binding and could be a common feature for proton translocating enzymes.

Compared to proton translocating F_oF_1 ATP synthases, the binding of ions in the sodium ATP synthases seems to follow a different way. The environment contains more polar side chains which allows stabilisation of the bound ion within a cluster of several residues (82). This implies that not

only one subunit is involved. As shown for *Ilyobacter tartaricus* or the V-ATPase of *Enterococcus hirae* the clustering occurs at the interface of adjacent *c* subunits or within the four helix bundle in *K* subunits respectively. For *Ilyobacter* the bound sodium ion is clustered within the residues of three helices. In this coordination model, side chain oxygens of Gln32 and Glu65 originate from the same subunit. Hydroxyl oxygen of Ser66 and backbone carbonyl oxygen of Val63 of the neighbouring subunit stabilise the sodium ion in the binding site (82). This supports former findings in which residues Gln32, Glu65, and Ser66 of *Propionigenium modestum* were identified by mutagenesis (83). Additional stabilising hydrogen bonds lock the ion within the binding side to prevent an uncontrolled transfer to subunit *a*. This in return makes conformational changes for protonation and deprotonation processes within the *a/c* interface necessary.

Curiously the atomic diameter which can be placed in the ion/proton binding site is similar for known ATP synthases (84). This gives the flexibility to transport different ions over a small range like sodium and lithium. It also explains why sodium ATP synthases can operate with protons as well as sodium ions and it outlines that subunit *c* determines the binding specificity (70, 84). For protons it was suggested that they are not transported as H^+ directly bound to the essential glutamate or aspartate. Instead they can form a hydronium ion with solvent water which gives the proton a diameter corresponding to cations like sodium or lithium. This hydronium ion induces circularisation of side chains within the binding site to form a crown ether (85).

With this background the ability of the *Ilyobacter* and *Propionigenium* ATP synthase to switch between sodium and proton translocation, can be explained (86). In this paper, the authors also describe a different inhibitory effect of DCCD over a pH range between proton and sodium translocating ATP synthases. DCCD is a very hydrophobic compound which binds to the acidic residue in the *c*-ring. In a first step DCCD accepts the proton from the binding site which results in an O-acyl urea intermediate. After a rearrangement, DCCD is covalently bound as N-acyl urea to the carboxylate (42, 87, 43). If a sodium ion is present in the binding site this reaction cannot occur and there wont be any inhibition detectable (88). The enzymes from *Ilyobacter* and *Propionigemnium* can alter between sodium and proton translocation depending on the physiological conditions. In the sodium mode the ion binding follows a bell shaped curve and the maximum activity is in a pH range from seven to nine. After switching to the proton mode the binding behaviour changes to a curve with a sharp peak at pH 6.5-7. This pH optimum corresponds to the pKa determined for the essential acidic residue in the unique hydrophobic environment for proton translocating enzymes such as in *E. coli* (81). H^+ ATP synthases were therefore expected to

have a similar binding profile with a sharp peak at a pH around the proposed pKa of seven. Interestingly, pure proton pumps show a broad bell shaped profile at pH 8-9 like the sodium pumps with their preferred ion. This suggests that in proton ATP synthases not a simple carboxylate protonation and deprotonation at glutamate or aspartate occurs but that instead the proton is coordinated as a hydronium in a crown ether. For sodium ATP synthases it is suggested that a network of hydrogen bonds avoids an uncontrolled binding of hydronium ions in sodium site. For the proton mode of sodium ATP synthase it is suggested that the proton is directly bound to the carboxylate and not coordinated (85, 86).

1.4.2. Subunit *a*

As mentioned before, no structural information is available about subunit *a* at present. A topographic mapping was mainly done in the lab of Fillingame (47, 48, 49, 89, 50, 51, 52, 53, 90, 55, 54). They used short range cross-links with Ag^+ or disulphide bridges to find possible interaction surfaces to other subunits of the membrane part. Silver ions were used as they need an aqueous environment and therefore may show residue networks accessible for ions and/or protons. The basis for this cross-linking is a deprotonation of the introduced cysteine to a thiolate. Thiolate formation is obtained the easiest way in an aqueous environment (91, 92). These cysteines are ideal candidates to find water accessible areas within a protein. In additional experiments, the accessibility for proposed contact surfaces was tested with the bulky probe NEM (N-ethylmaleimide). Those residues accessible for NEM lie only at the periphery and allow for cross-linking between subunit *a* and *c*. For Ag^+, access to all side chains is given and therewith possible aqueous channels could be determined.

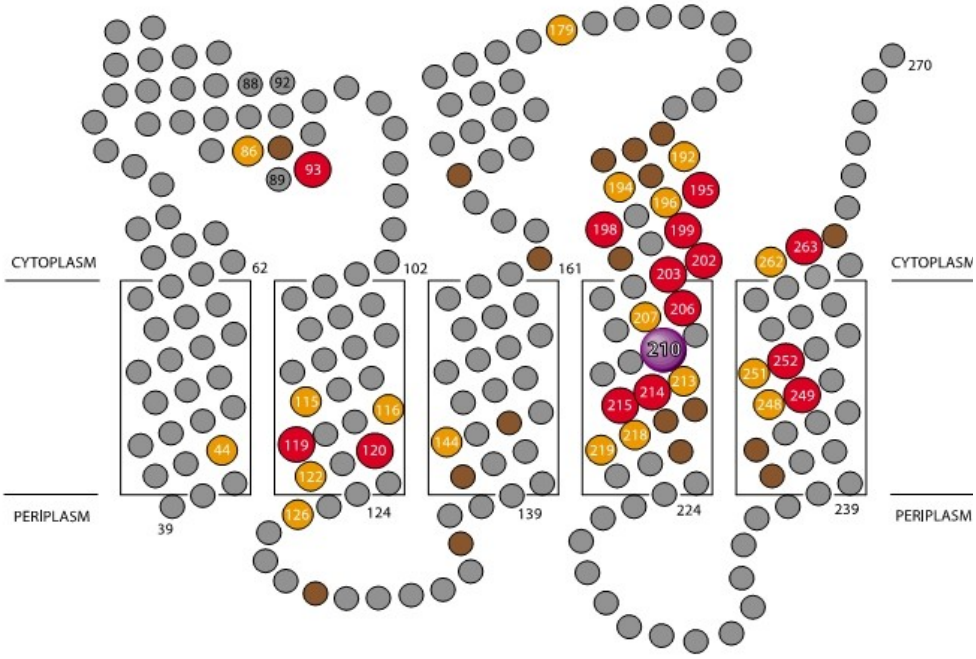

Figure 1.6: Subunit *a* from *E. coli* showing the proposed aqueous channels according to the strength of inhibition of proton translocation after cross-linking. (purple: essential Arg210; red: > 85% inhibition; orange: 66-85% inhibition; brown: 46-65% inhibition) (taken from Schwem and Fillingame, 2006; Moore *et al.*, 2008)

The topological map of subunit *a* from *E. coli* (Figure 1.6) shows those residues most sensitive for Ag^+ cross-links and the essential residue Arg210 (52, 90). The transmembrane helices two to five are expected to form a four helix bundle which places the residues most sensitive to silver ions in the centre of the bundle creating a polar cavity. This aqueous centre is proposed to be also accessible from both sides of the membrane. From the periplasm the entrance is given through residues 115, 116, 119, 120, 122, and 126 in helix two together with residues 213-215, 218, and 219 in helix four and 248, 249, 251, and 252 in helix five. The cytoplasmic half channel is proposed to involve residues 192, 194-196, 198, 199, 202, 203, 206, and 207 in helix four as well as 262 and 263 in helix five (51, 50, 90) and lies mainly on the peripheral side of these helices. Ser206 is proposed to be the check-point for the cytoplasmic half channel and is the exit for a proton/ion after a full revolution. Asn214 lies in the central region within the lipid bilayer and may therefore assist Arg210 in the process of protonation and deprotonation (48). Residues 140 and 144 in helix three are thought to pack close to the periplasmic side chains of helix two. Both helices are connected on the periplasmic side by a loop formed of residues 130 to 136 (53). The authors also suggest that helix one lies in a cleft between helices two and three. Even more interesting is the finding that

substitution of Asp44 in helix one results in a loss of passive proton translocation. Thus it was suggested that transmembrane helix four has a parallel orientation to the C terminal helix of subunit *c* in the *c*-ring so that *a*Arg210 can interact with *c*Asp61. The orientation of the inner and outer helices of subunit *c* in the ring is presented in Figure 1.2 for the theoretical model from *E. coli*. The importance of Arg210 for proton translocation was shown by mutagenesis (35, 47). It is also now widely accepted that Arg210 controls proton flux. This residue is also assumed to work as a barrier avoiding uncontrolled proton shuttling between the two proposed shifted half channels. Swivelling of the helices within the four helix bundle could allow for alternating access between the cytoplasmic and periplasmic half channels (51).

1.4.3. The *a/c* Interface

The interaction between subunits *a* and *c* is the basis for the proton translocation across the membrane. Both subunits work together in a concerted mechanism, and only if subunit *a* and *c* are combined, will rotation of the *c*-ring occur. Studies with electron microscopy revealed that more than one *c* subunit is within the interface and that subunits *b*, on the opposite flank of subunit *a*, support the rigid behaviour needed for the function (17). Stable complexes of subunit *a* and *c* could be isolated, but enzymatic activity was only possible after addition of subunit *b* or a minimum of about 40 membrane located amino acids (93). The interface has to be rigid so that an uncontrolled proton flux is avoided, but also has to be flexible to allow for a frictionless rotation. The position of the essential glutamate or aspartate in subunit *c* as well as the important arginine in subunit *a* are highly conserved throughout all species, and build the core of this interface. Short distance cross-linking experiments place helix four of subunit *a* in parallel with the outer helix of the monomers in the *c*-ring. The introduced cysteines gave positive cross-linking results only if residues were located on the surface of the helices in both subunits (49). The same method was used to determine the accessibility of the interface from the cytoplasm (54). The periplasmic channel was determined by Angevine *et al.* (53). They could show that water accessible residues, which could be cross-linked with Ag^+, are found in the interface. More than one subunit of the *c*-ring is expected to be within the interface. The arrangement of the binding site seen in the structure suggests that large conformational changes are unlikely (82). This is contradictory to possible movements within the interface proposed on the basis of the *E. coli* NMR structures. The two structures solved at pH 5.0

(39) and pH 8.0 (4) show the proposed protonated and deprotonated conformation respectively. To convert from one conformer into the other a clockwise rotation of 140° of the outer (C terminal) helix was suggested after re-interpretation of former results (4, 89). As arginine has a long side chain and the ion binding site of *Ilyobacter* is accessible from the periphery, it is maybe sufficient to change the rotamers in subunits *a* and *c* during the loading and unloading steps (33). The Dimroth lab (94, 95, 33) also obtained different results for the half channel concept proposed by the group of Fillingame. Dimroth *et al.* (72), working with the Na^+ translocating ATP synthase from *Ilyobacter tartaricus*, suggest only one half channel within the interface. The second one is proposed to be intrinsic in subunit *c*. Possible mechanisms of how both subunits work together and drive the rotation, will be described in more detail in the next section.

1.4.4. Rotor Movement Induced at the *a/c* Interface

Although no structural information is available for subunit *a*, on the basis of the cross-linking studies mentioned above, two hypotheses for a possible mechanism are proposed. An essential feature is that only a protonated or sodium occupied glutamate or aspartate in subunit *c* can leave the interface, and enter the membrane accompanied with ring movement (96, 25). After adding the essential arginine in subunit *a* to the system, the first models for possible mechanisms in the *a/c* interface were proposed (26).

Girvin et al. (39) and Rastogi and Girvin (4) used the *c* monomers from *Escherichia coli* ATP synthase to propose a mechanism. This model was further expanded by Fillingame *et al.* (89). All subunits of the *c*-ring are expected to be in the protonated state and therefore showing the outer helix in the straight pH 5 conformer (see Figure 1.5). Asp61 of subunit *c* is buried between the N and C terminal helices when protonated and moving within the lipid bilayer. *a*Arg210 competes with *c*Asp61 for the bound proton. When a *c* subunit comes into close proximity with the *a/c* interface it rotates for 140° clockwise to allow for access to the protonated Asp61 (*E. coli* numbering) (97). This is one adaptation to the Rastogi and Girvin model (4) who had proposed a counter clockwise rotation of 220°. *c*Asp61 is now pronounced and accessible. The hydrophobic environment around *c*Asp61 supports the protonation rather than deprotonation. The presence of *a*Arg210 changes the local pKa which favours a proton movement from subunit *c* to subunit *a*, and exit into the cytoplasm at *a*Ser206. After deprotonation, the outer helix of subunit *c* shows the

conformation as seen in the NMR structure at pH 8 (see Figure 1.5) with a pronounced kink around *c*Asp61. To allow for reprotonation of the charged *c*Asp61, a dramatic reorientation of the whole interface is expected. Helices four and five of subunit *a* move in such a way that the deprotonated subunit *c* can pass along and reach the protonation position near the periplasmic half channel. Helix four is expected to rotate counter clockwise while helix five shows a clockwise movement (98). Thereby contact to *a*Arg210 has to be avoided, to allow for a pKa high enough to bind a new proton. The electrochemical potential drives the reprotonation of the negatively charged *c*Asp61. To allow the newly protonated *c* subunit to leave the interface on one side helices four and five of subunit *a* move again in a concerted manner. On the other side of the *a/c* interface another loaded *c* subunit can enter again. This can be seen as a gear mesh where helices of subunit *a* push the reprotonated *c*Asp61 out of the interface. The outer helix of the adjacent *c* subunits rotate in their expected position. In the end the whole ring is rotated by one step or one subunit *c*. The mechanism uses the arginine as a ratchet to drive the ring. The direction is determined by the high energy penalty if a charged side chain in subunit *c* enters the membrane. To push the rotor out of its idling mode, an existent ΔpH seems to be sufficient and the function of a membrane potential could not be explained (99).

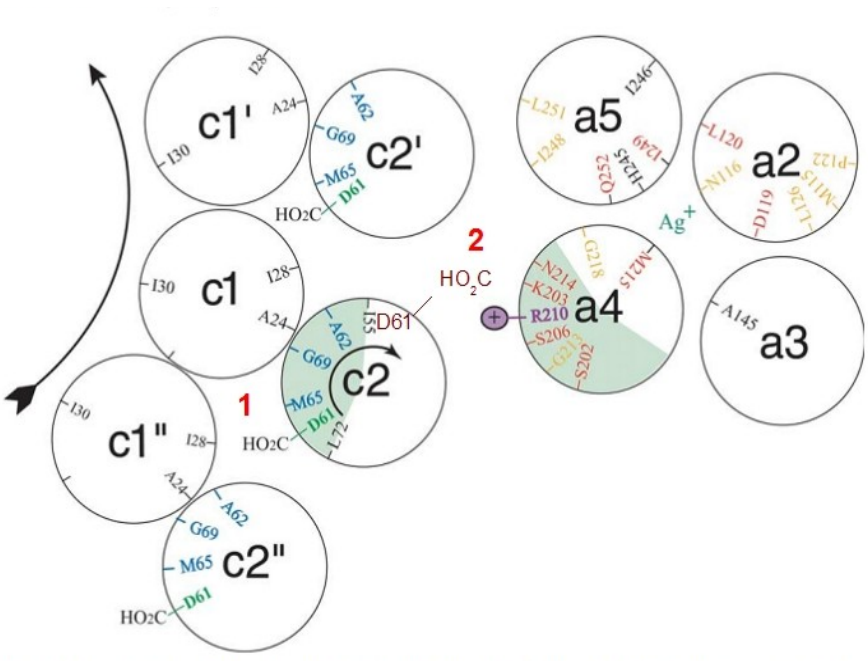

Figure 1.7: Three adjacent monomers of *c* subunits and the proposed four helix bundle of subunit *a* of *Escherichia coli* ATP synthase; Top view (from cytoplasm) on the *a/c* interface and proposed arrangement of the helices of the involved subunits. The numbers one and two in red give the position of Asp61 in the protonated (1) and deprotonated (2) state. The rotation of the c-ring is indicated counter clockwise and the ATP synthase is thought to be in synthesis mode (based on Fillingame *et al.*, 2003)

A very detailed mechanism was done on the basis of the PDB codes 1C17 and 1C0V, together with findings from Elston *et al.* (26), Rastogi and Girvin (4), Dmitriev *et al.* (100), Stock *et al.* (3), and Fillingame *et al.* (101). It shows interactions and movements between the two subunits as a result of molecular dynamics calculations for an *E. coli* model (102).

Dimroth, von Ballmoos and Meier evolved a different model for the rotation on the basis of the structure from *Ilyobacter tartaricus*. The essential arginine is seen as a switch that opens and closes, giving access to subunit *a* and the periplasmic channel or the binding site in subunit *c*. In the synthesis mode, *a*Arg226 and a sodium ion compete with their positive charges for the negative charge of the *c*Glu65. When a loaded *c* subunit enters the interface and comes into proximity of *a*Arg226, the sodium becomes repelled and exits the interface into the cytoplasm in a vertical manner. For the exit no aqueous half channel within subunit *a* is needed. Because of electrostatic interaction, the deprotonated *c*Glu65 is stabilised by a salt bridge with Arg226 in subunit *a*. If no membrane potential is present, then the rotor is trapped in an idling mode. An established membrane potential (cytoplasm negative and periplasm positive) pushes the rotor out of its stand-by mode into a directed motion. The stabilising salt-bridge between subunits *a* and *c* opens and the charged *c*Glu65 accepts a sodium ion when passing the periplasmic half channel in subunit *a*. Simultaneously, the next loaded *c* subunit enters the interface from the opposite side, to stabilise the free charge of the *a*Arg226. As sodium ions within the binding site prefer an aqueous environment, it is possible that the binding site is in an intermediate state with a bound water. This causes a vertical drop in the free energy between the empty and the adjacent loaded subunit. As a result the lateral membrane potential has a vertical component between an occupied and an empty binding site in the *c*-ring. Support for a vertical energy gradient is also given by the positions of the ion entrance and exit in the interface. They are shifted so that the *a*Arg226 in the stator tends to point towards the loaded incoming *c* subunits. The rotor charge after ion release instead points toward the periplasmic reservoir for ion uptake. This shows that the membrane potential besides its thermodynamical component also has a kinetic component (72). Compared to the model from the Fillingame lab, there is no dramatic movement within the subunits necessary, to give way for the ions. Subunit *a* gives rise only to the inlet channel from the periplasm, whereas the exit channel is part of subunit *c*. In the case of the two half channel model, a pH gradient is sufficient to push the rotor out of its idling mode and start a directed movement. The Dimroth lab instead applies a membrane potential as the key component, to kick start the rotation.

2. Purpose of this Study

CF_oF_1 from spinach chloroplasts is a proton pumping ATP synthase. The soluble part F_1, in which ATP synthesis takes place, was investigated in detail by several research groups. The protein structure is known to atomic detail and the different steps in the mechanism of ATP synthesis are already elucidated. The energy necessary for ATP synthesis is stored in a transmembrane proton gradient. This gradient is the driving force and is translated through mechanical rotation in the membrane part into structural changes in F_1 to form a chemical bond between ADP and inorganic phosphate.

The question is now how are the protons translocated in the membrane part F_o. Biochemical data such as ATP/proton ratio, pH dependency of the proton binding site, and response to inhibitors and toxins have not only been recorded for ATP synthase from chloroplast but also for other organisms. Stoichiometry data from several species show a conserved subunit composition as for F_1 except for subunit *c*, which is highly variable.

X-ray crystallography was chosen as it gives the possibility to investigate a large multisubunit complex such as ATP synthase from spinach. The focus was on the membrane part F_o. With different crystallisation experiments it was tried to crystallise the membrane part for structure solution. The attempt was to crystallise the complete membrane part as well as different combinations of subunits. Protonation and deprotonation has to occur in the active enzyme. It was tried to crystallise the *c*-ring with its binding sites in a protonated and deprotonated state by creating a low pH and high pH environment. Co-crystallisation of the CF_oF_1 complex with inhibitors was done to support biochemical findings, already published, with structural evidence. In addition, an already existing native data set of the membrane intrinsic rotor ring from F_oF_1 ATP synthase was further analysed and processed.

3. Materials and Methods

3.1. Materials

3.1.1. Biological Materials

Spinach grown in local green houses *Spinacia oleracea* cultivator *polka*

3.1.2. Technical equipment

Cluster	9 AMD dual-core Opteron nodes; one master node for queuing and monitoring and 8 computing nodes; operating system OpenSuse9.3; Sun Grid Engine batch queuing system

System Gold (126 NMP Solvent Module, 168 NM detector)	BeckmannCoulter
Biomek 3000 Laboratory Automation Workstation	BeckmannCoulter
Optima L-80 XP Ultracentrifuge	BeckmannCoulter
Avanti J-26 XP Centrifuge	BeckmannCoulter
table top centrifuge and Centrifuge 5810 R	Eppendorf
DU800 spectrometer	BeckmannCoulter
D8 (ApexII detector, 1 µS tube)	Bruker/Incoatec
Branson Sonifier 250	Branson
Blendor	Waring Commercial
Incubator Heraeus BK 600	Thermo Scientific
PCR thermocycler	Biometra professional
Anion exchange material: POROS® HQ20	Applied Biosystems

3.1.3. Chemicals

Acrylamid stock solution: 30% (w/v) acrylamide and 0.8% (w/v) N,N'-Methylenbisacrylamide	Roth
Adenosine 5'-diphosphate (ADP)	Boehringer Mannheim
Ammonium peroxodisulphate (APS)	Fluka
Adenosine 5'-triphosphate (ATP)	Sigma
Bovine Serum Albumin (BSA) standard 2 mg/ml	Interchim
BCA-Protein Assay Reagent	Pierce
Dithiothreitol (DTT)	Fluka
Cadmium chloride	Fluka
Cryo buffer	See 4.2.10
Crystallisation solutions	see appendix
Cyclohexylbutanoyl-N-hydroxyethylglucamide (10-HEGA®-C)	Anatrace
Dodecyl-β-D-maltoside (DDM)	Glycon
Lithium chloride	VWR
Mineral oil	Sigma Aldrich
Phenol	AppliChem
Phosphatidyl choline	Fluka
Phenylmethanesulphonyl fluoride (PMSF)	Sigma Aldrich
Sodium acetate	Merck
Sulphuric acid	VWR
Phloridzin	Sigma Aldrich
Phloretin	Sigma Aldrich
N,N'-Dicyclohexylcarbodiimide (DCCD)	Sigma Aldrich
Spermine	Sigma Aldirch

3.1.4. Consumables

Amicon Ultra Filtration Device – 15: 100 kDa MWCO; 4 and 15 ml	Millipore
Polyallomer tubes, thinwall, 38.5 ml	BeckmannCoulter

3.1.5. Materials for Crystallisation

24 wells Nextal plates	QIAGEN
60 and 72 wells Terasaki plates	Greiner
96 wells Imp@ct plates	Greiner
24 cell culture tissue plates	Greiner
Cover slips	Hartenstein
Microbridges	Hampton Research
CryoLoop™	Hampton Research
SPINE System for ESRF	Molecular Dimensions

3.2. Isolation and Purification of CF_oF_1 from Spinach Chloroplasts

The chloroplast ATP synthase was purified from frozen spinach *Spinacia oleracea* of the cultivator *polka*. The leave-veins were removed and the leaves were washed in distilled water. Portions of 500 g were stored at -20°C. The complete purification was carried out at 4°C or on ice.

3.2.1. Isolation of Thylakoid Membranes

The isolation of thylakoid membranes is based on the method of Strotmann *et al.* (103) and was modified by Groth and Schirwitz (104), to reduce contaminations of ribulose-1,5-bisphosphate carboxylase. About 1 kg of frozen spinach was homogenised with 2 L of buffer I in a Warring-Blendor. The suspension was filtered through cheese cloth (0.2 µm) and centrifuged for 20 min at 5700 x g (BeckmannCoulter Avanti J-26, rotor JA-10) at 4°C. The supernatant was discarded and

the pellet resolved in buffer II. A glass potter was used for better homogenisation of the suspension in every washing step. After centrifugation for 20 min at 5400 x g (BeckmannCoulter Avanti J-26, rotor JA-10) at 4°C, the chloroplast membrane was disrupted with buffer III. Finally the pellet was washed in buffer II again. After the last centrifugation, pellets were resolved in a minimal volume (500 – 750 µl depending on the pellet size) of resuspension buffer and intensively homogenised with a glass potter. Reduction of the complex was carried out in a final volume of 50 ml of resuspension buffer and a final concentration of 50 mM DTT, while stirring at 4°C in the dark for 15 min.

Buffer I		Buffer II	
300 mM	Sucrose	20 mM	NaPPi, pH 7.8
20 mM	Tricine, pH 7.4	2 mM	DTT
10 mM	NaPPi, pH 7.8	0.002% (w/v)	PMSF
2 mM	DTT		
0.002% (w/v)	PMSF		

Buffer III		Resuspension buffer	
20 mM	NaCl	400 mM	Sucrose
2 mM	DTT	20 mM	Tricine, pH 7.4
0.002% (w/v)	PMSF	5 mM	$MgCl_2$
		0.002% (w/v)	PMSF

3.2.2. Solubilisation of CF_oF_1

After resuspension of the pellets and reduction in the dark, the complex was solubilised in detergent micelles. 50 ml solubilisation buffer was added to the suspension and stirred again for 15 min in the dark. Solubilisation was accomplished by sonication with a Branson Sonifier Typ 250 for another 15 min on ice and stirring. The protein becomes isolated from the thylakoid membrane and integrates in mixed micelles of dodecyl maltoside and sodium cholate. Ultra centrifugation for one hour at 150000 x g and 4°C (BeckmannCoulter Optima L-80 XP, rotor Ti 70.1) separated the solubilised ATP synthase complex from remaining thylakoid membrane fragments. The supernatant with the soluble membrane protein was then treated in an ammonium sulphate precipitation step.

Solubilisation buffer	
400 mM	Sucrose
20 mM	Tricine, pH 7.4
5 mM	$MgCl_2$
1 mM	ATP
50 mM	DTT
0.002% (w/v)	PMSF
10% (v/v)	Ammonium sulphate
8% (w/v)	Glycine
20% (w/v)	Glycerol
1% (w/v)	Sodium cholate
2% (w/v)	Dodecyl maltoside

3.2.3. Fractionated Ammonium Sulphate Precipitation

In the first step, the ammonium sulphate concentration in the supernatant was slowly raised to 38% (v/v) with a saturated stock solution while stirring at 4°C for 15 min. Afterwards the suspension was centrifuged at 20000 x g for 15 min at 4°C (BeckmannCoulter Avanti J-26, rotor JA 25-50). The supernatant was used for a second precipitation step with a final ammonium sulphate concentration of 48% (v/v). The incubation time was 30 min. Centrifugation at 20000 x g for 15 min at 4°C (BeckmannCoulter Avanti J-26, rotor JA 25-50) was used to separate the precipitated CF_oF_1 complex. The pellet was resuspended with 230 µl of buffer A, homogenised with a glass potter and adjusted to a final volume of 10 ml. Before applying on a sucrose density gradient 20 µl PMSF (1%) and 50 µl DTT (1 M) were added.

Buffer A	
50 mM	Tricine, pH 7.8
5 mM	$MgCl_2$
5 mM	DTT
4% (w/v)	Glycine
10% (w/v)	Glycerol
0.1% (w/v)	Dodecyl maltoside
0.002% (w/v)	PMSF

3.2.4. Sucrose Density Gradient Centrifugation

The sucrose density gradient was composed as below and aliquots of 36 ml were filled in thin walled polyallomer tubes.

Sucrose density gradient	
600 mM	Sucrose
50 mM	Tricine, pH 8.0
5 mM	DTT
0.1% (w/v)	Dodecyl maltoside
0.002% (w/v)	PMSF

The a sucrose free gradient buffer (recipe above without sucrose) was used to resolve the pellets after ammonium sulphate precipitation and for adjusting the gradients for centrifugation. The gradients were stored at -20°C and slowly thawed at 4°C before use. This procedure causes the formation of a linear sucrose density gradient with the highest concentration on the bottom. The protein was carefully applied on six gradients and centrifuged for 22.5 hours at 100000 x g (BeckmannCoulter Optima L-80 XP, rotor SW28) and 4°C. Afterwards, the gradient showed a pattern as in figure 4.1. To collect fractions of 500 µl, the tubes were pierced from the bottom. Fractions taken from below an intensive green band contained the protein. The exact fractions were determined with SDS-PAGE.

3.2.5. Purification of CF_oF_1 by Anionic Exchange Chromatography

After identifying protein containing fractions on a silver stained SDS-PAGE, these fractions were pooled and further purified by anionic exchange chromatography. A column with the a diameter of 4.6 mm and a height of 100 mm was filled with POROS® HQ20 anionic exchange material (Applied Biosystems) and used with a BioCAD 700 E Perfusion Chromatography Workstation. The column was equilibrated with buffer A at a flux of 15 ml/min. 2 ml of the protein solution were applied on the column with a flux of 15 ml/min and eluted with a linear salt gradient from 0 to 1.5 M NaCl (buffer B). The intact complex eluted between 0.9 and 1 M NaCl and was collected in 500 µl fractions.

Buffer A		Buffer B	
50 mM	Tricine, pH 8.0	50 mM	Tricine, pH 8.0
4% (w/v)	Glycine	4% (w/v)	Glycine
10% (w/v)	Glycerol	10% (w/v)	Glycerol
5 mM	$MgCl_2$	5 mM	$MgCl_2$
5 mM	DTT	5 mM	DTT
0.002% (w/v)	PMSF	0.002% (w/v)	PMSF
0.1% (w/v)	Dodecyl maltoside	0.1% (w/v)	Dodecyl maltoside
		2 M	NaCl

This purification step separates “empty” and protein containing micelles and reduces the amount of impurities. The soluble part of the ATP synthase, CF_1, interacts with functional groups of the column material and can be eluted with a salt gradient. The “empty” micelles do not bind and leave the column (105).

The elution profile identified a maximum peak with one or two fractions containing all CF_oF_1 subunits. These fractions were pooled and concentrated to a volume of 50 to 150 µl in an Amicon ultra filtration devices (Milipore, exclusion size: 100 kDa). Afterwards, the buffer of the anion exchange step was replaced with one to be used in crystallisation. The recipe of this buffer was always dependent on the planned experiments and a list of these washing buffers can be found in Appendix 7.1. The protein concentration was determined with a BCA test.

3.2.6. SDS-Polyacrylamide-Gelelectrophoresis

Discontinuous SDS-PAGE was used to separate proteins according to their molecular weight (106). In combination with silver staining, SDS-PAGE served as a control tool in various steps during protein purification. After synchrotron measurements and when receiving crystals in new crystallisation conditions it was also used to determine the protein content of the crystals.
The gels were composed of a 5% acrylamide stacking gel and a 15% acrylamide separating gel.

Separation gel		Stacking gel	
15% (v/v)	Acrylamide	5% (v/v)	Acrylamide
0.4% (v/v)	Bisacrylamide	0.1% (v/v)	Bisacrylamide
0.1% (v/v)	TEMED	0.1% (v/v)	TEMED
0.1% (v/v)	APS	0.1% (v/v)	APS
in separation gel buffer		in stacking gel buffer	

Separation gel buffer (2.5x)		Stacking gel buffer (5x)	
1.85 M	Tris/H_3PO_4	0.3 M	Tris/H_3PO_4
0.25% (w/v)	SDS	0.5% (w/v)	SDS
pH 8.9		pH 6.8	

The gels had a width of 29.70 cm and a height of 21 cm and therefore were used for separation over night (12-15 hours) at 25 to 35 mA and 600 V.
Protein samples were mixed with a four fold sample buffer and denatured immediately. Heating at 95°C for six minutes as often done for soluble proteins was not applied. Additional denaturation with heat increases the tendency of membrane proteins to aggregate so that they cannot be separated in an SDS-PAGE.

Electrophoresis buffer	
0.25 M	Tris
1.92 M	Glycine
0.5% (w/v)	SDS

Sample buffer (4x)	
100 mM	Tris
100 mM	Borate
30 mM	DTT
5 mM	$MgCl_2$
25 mM	EDTA, pH 7.0
6% (w/v)	SDS
16% (w/v)	Sucrose
0.16% (w/v)	Bromphenoleblue

3.2.7. Silver Staining

After running SDS-PAGE the gel was stained with silver. Therewith proteins and/or their subunits can be detected according to their molecular weight. This method is very sensitive, and the lowest detection limit is 100 pg (107). For crystallisation, protein of high purity has to be achieved, which can efficiently be tested with this method. Furthermore the protein amount in a crystal is very low, so a method with a high sensitivity like silver staining is needed.

First, the gel was incubated in a fixation solution and then transferred in an incubator solution, 30 min each. Afterwards, the gel was washed three times for 10 min with distilled water. A staining solution containing silver nitrate was applied for 30 min. The staining solution was removed and the gel washed under rinsing water for a few seconds. A developer solution containing sodium carbonate was added, and after reaching the desired colour intensity, the reaction was stopped with citric acid.

Fixation solution	
30% (v/v)	Ethanol (technical)
10% (v/v)	Acetic acid (technical)

Incubator solution	
30% (v/v)	Ethanol (p.a.)
0.5% (w/v)	Sodium acetate
0.2% (w/v)	Sodium thiosulphate
0.5% (v/v)	Glutardialdehyde

Staining solution		Developer solution	
0.1% (w/v)	Silver nitrate	2.5% (w/v)	Sodium carbonate
0.01% (v/v)	Formaldehyde	0.01% (v/v)	Formaldehyde

Stopping solution	
2.3 M	Citric acid

3.2.8. Determination of Protein Concentration

Before determining the protein concentration, the sample was centrifuged for two minutes at 14000 x g at 4°C to eliminate aggregates which may have formed during overnight storage at 4°C. Volume and concentration of the purified CF_oF_1 complex were highly dependent on the washing buffer used. Therefore, the protein standard was chosen according to the protein buffer and was 0-10 mg/ml, 0-25 mg/ml or 0-50 mg/ml. For background correction, buffer was added to the protein standard. The protein was used in a 1:5 dilution.

The protein concentration was determined with a BCA protein assay (Pierce). This test kit is composed of two different solutions containing bicinchoninic acid. In the presence of proteins containing cysteines, tyrosines, and tryptophans the bicinchoninic acid reacts with Cu^{2+} ions in one of the solutions and forms a purple complex. The two components were mixed according to the manufacturer. A protein standard with BSA was made from a 2 mg/ml stock solution. Samples and standard were incubated at 37°C for 30 min. The green-cyan colour turned into purple, and the intensity of the colour gave the amount of protein. The intensity was determined at $\lambda = 562$ nm with a UV-Vis spectrometer (BeckmannCoulter DU800).

3.2.9. Determination of Detergent Concentration

The detergent content was determined after DuBois *et al.* (108) with modifications from Urbani and Warne (109). This assay is based on the reaction of the anomer C-atom of a sugar with sulphuric acid in the presence of phenol. Many detergents used in membrane protein purification have a sugar

part as soluble component. In the purification of CF_oF_1 dodecyl maltoside was used, so the sugar component is maltoside. A maltoside standard from 0 to 0.3% was used. The standard and the sample in a volume of 50 µl were mixed with 250 µl 5% (v/v) phenol. Then 600 µl concentrated sulphuric acid was added and mixed by turning upside down. After cooling the mixture 30 min, the absorption at 490 nm was determined with a photometer (BeckmannCoulter DU800).

3.3. Basics in Crystallography

Producing crystals suitable for structure determination with X-rays is still the crucial step in X-ray crystallography. If for the target protein homologues or related structures have been solved, it is very likely that the protein of interest crystallises under similar conditions. With such a starting point, it is relatively easy to find conditions, which give rise to crystals good enough for structure solution. In cases without any prior information, a lengthy search is required, to find appropriate conditions. It usually involves small scale initial crystallisation trials, to cover as much as possible of the general crystallisation space. With available robotic systems and commercial screens the period to receive first results can drastically be reduced.

To reduce the effort, it is always recommended to get as much background information about the protein of interest as possible. This means for example, where it is located within the cell, is it in the membrane or soluble, for which process is it designed for, what are its substrates and products. On this basis, the experiments can be designed more easily.

In general, crystal growth can be divided into two steps (110). First, is the formation of nuclei and second the growth of a crystal by enlarging the nucleus. These processes can be described in a phase diagram.

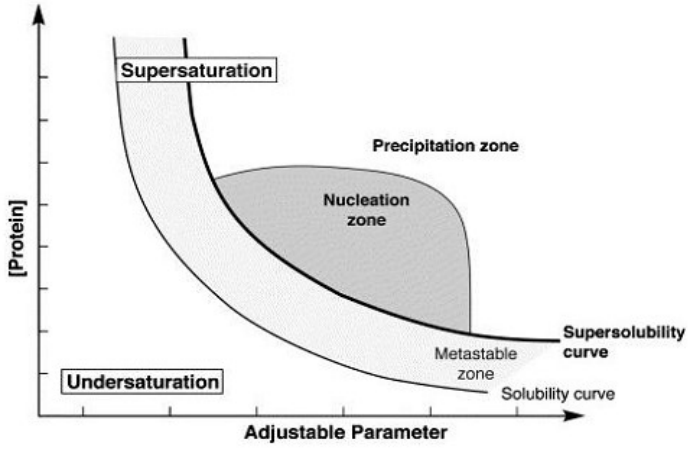

Figure 3.1: General phase diagram (taken from Chayen, 2005)

It is of high interest, to control the condition which give rise to nuclei and afterwards force crystal growth. The solubility curve describes the border line between the under- and supersaturated areas of a protein solution, which are in an equilibrium. The crystallisation process starts with an

undersaturated solution. There, neither nuclei formation nor crystal growth can occur. If the solution becomes concentrated over time, the equilibrium moves towards the nucleation zone where nuclei can form. These small aggregates of protein reduce the concentration of free protein molecules and the system moves into the metastable zone. In the metastable zone crystal growth can occur but nuclei formation is not possible. If conditions are chosen, which are too far from the solubility curve, the protein will form amorphous precipitate. The goal is now, to find the appropriate conditions to ensure nucleus formation so that the crystallisation environment moves in the metastable zone and crystal growth can occur.

Even with the knowledge of the native protein environment and a phase diagram, it is impossible to predict the exact crystallisation conditions. There are too many variables, which influence the whole crystallisation process, e.g. temperature, growth condition during protein production, humidity when setting up trials, vibrations while moving crystallisation plates. In the end it is still an empirical trial and error procedure to find the right combination of variables.

Any variable that helps to increase the protein concentration and forces the formation of nuclei can be used to bring a protein solution into supersaturation. Widely used components are:

- temperature
- pH
- salt concentration (low → salting in, high → salting out)
- addition of polymers (PEG)

Often more than one component has to be varied during the experiment and often, a combinations of variable changes will be used in the end. Usually, the precipitant is a polymer or high salt concentration.

3.3.1. Different Crystallisation Techniques

3.3.1.1. Batch/Microbatch Technique

In this technique, the protein solution and the precipitant solution are usually mixed in an equal amount. In the case of microbatch the whole plate is covered with mineral or silicon oil afterwards

(111, 112). The plates are stored at the temperature of interest. Originally, this batch technique was used without a covering layer and became less interesting when vapour diffusion techniques were developed. By the use of mineral and silicon oil it was possible to have influence on the crystallisation process after the initial mixing step (113). Silicon oil allows for far more water to evaporate from the drop compared to mineral oil, and thus changes in the protein concentration occur more quickly. Because of the hydrophobic behaviour of the covering layer it is impossible to use organic solvents or high PEG concentrations in the crystallisation trials, as they dissolve or interact with the oil. In general batch/microbatch is an easy to use set up and it can be combined with robotic equipment (114). No migration of detergent into the oil could be found so far, which makes the technique also suitable for membrane proteins.

3.3.1.2. Vapour Diffusion Technique

Hanging drop, sitting drop, and sandwich method are variations of the vapour diffusion technique. In the vapour diffusion technique, the protein solution is usually mixed in an equal amount with the precipitant solution. Additionally, a reservoir is present also containing the precipitant solution. As the precipitant solution in the reservoir has a higher concentration compared to the volume mixed with the protein solution both, the drop and the reservoir, tend to reach an equilibrium. When mixing protein and precipitant solution the starting drop is in undersaturated conditions and is placed over the reservoir to reach the equilibrium. The whole system is isolated to the surrounding environment by grease or rubber seal. This gives the possibility to grow crystals to an equilibrium state. As there is also an air volume present between the two solutions, it takes more time to reach supersaturated conditions in the drop compared to the batch/microbatch method. On the other hand this gives the possibility to influence the crystallisation speed by changing the ratio between reservoir and drop volume. Usually, the reservoir volume exceeds the drop volume by a factor of 100-500. The surface behaviour is different for hanging drop, sitting drop, and the sandwich method. For a protein of interest all methods may have to be tried.

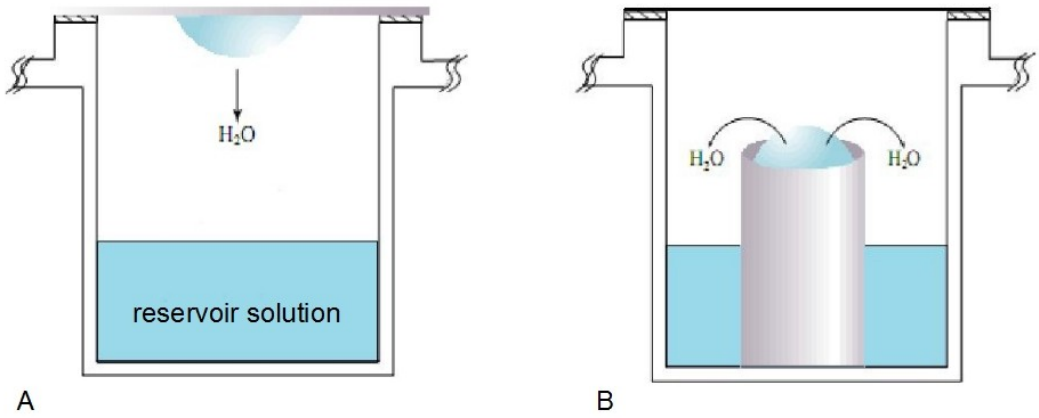

Figure 3.2: (A) Experimental setup for sitting drop. (B) Experimental setup for hanging drop. (adopted from www.hamptonresearch.com)

3.3.2. Choice of Crystallisation Conditions

In the case that some initial information for the target protein is available, e. g. because of known homologous structures from other species, the crystallisation space can be reduced. Similar working environments of proteins suggest similar crystallisation behaviour. In such a case it is often sufficient to make an incomplete factorial screen (115) and alter several variables in small steps around known conditions from homologous proteins.

If there is no information about the target protein available, the best start is to purchase commercial crystallisation kits, which usually are composed as sparse-matrix screens (116). This means, they include crystallisation conditions which have been successful in other cases and cover therefore a huge variety of solution compositions. If there are promising results, such as micro crystals, phase separation or even precipitation, these conditions can be used to set up a grid screen and optimise the composition of the crystallisation solution in a systematic way. This is usually done with self-composed screens by changing one or two parameters at the same time while keeping the others fixed.

To avoid the use of large amounts of chemicals and to screen as much of the crystallisation space as possible, the microbatch technique is the method of choice for initial screening. If it is combined

with a high throughput system a huge number of conditions can be screened within a few weeks.

3.3.3. Crystallisation of Membrane Proteins

Membrane proteins are a somewhat special case in crystallisation. Most commercial setups and equipment available, are designed for soluble proteins. The latter are usually easier to produce, purify and crystallise and can be analysed without big efforts in most laboratories.

Although membrane proteins make up about 30% of the total protein amount in a cell, little is known about their structures. Production of recombinant membrane protein in expression systems is difficult as they tend to aggregate because of hydrophobic patches on the protein surface. This results in formation of inclusion bodies within the cell. Even if they can be produced without problems, there is still the risk of aggregation during purification. Detergents are used to simulate a membrane environment and make the proteins soluble at the same time. Sometimes lipids, lost during purification, have to be given back to the protein, to stabilise the structure.

The crystallisation itself occurs in the same way as for soluble proteins. The protein can crystallise in 2D crystals so that detergent molecules simulate a membrane layer, in which the protein molecules are integrated. In 3D crystals several of these layers are stacked on top of each other (type I crystals). Alternatively the protein can be surrounded by a detergent micelle rather than a membrane-like sheet. In that case, crystallisation produces type II crystals. Another but less common application is lipidic cubic phase, in which the protein inserts into a lipid system (117). The precipitant then induces protein stacking within the membrane layer. A detergent concentration above the CMC must be achieved to ensure the formation of micelles or layers.

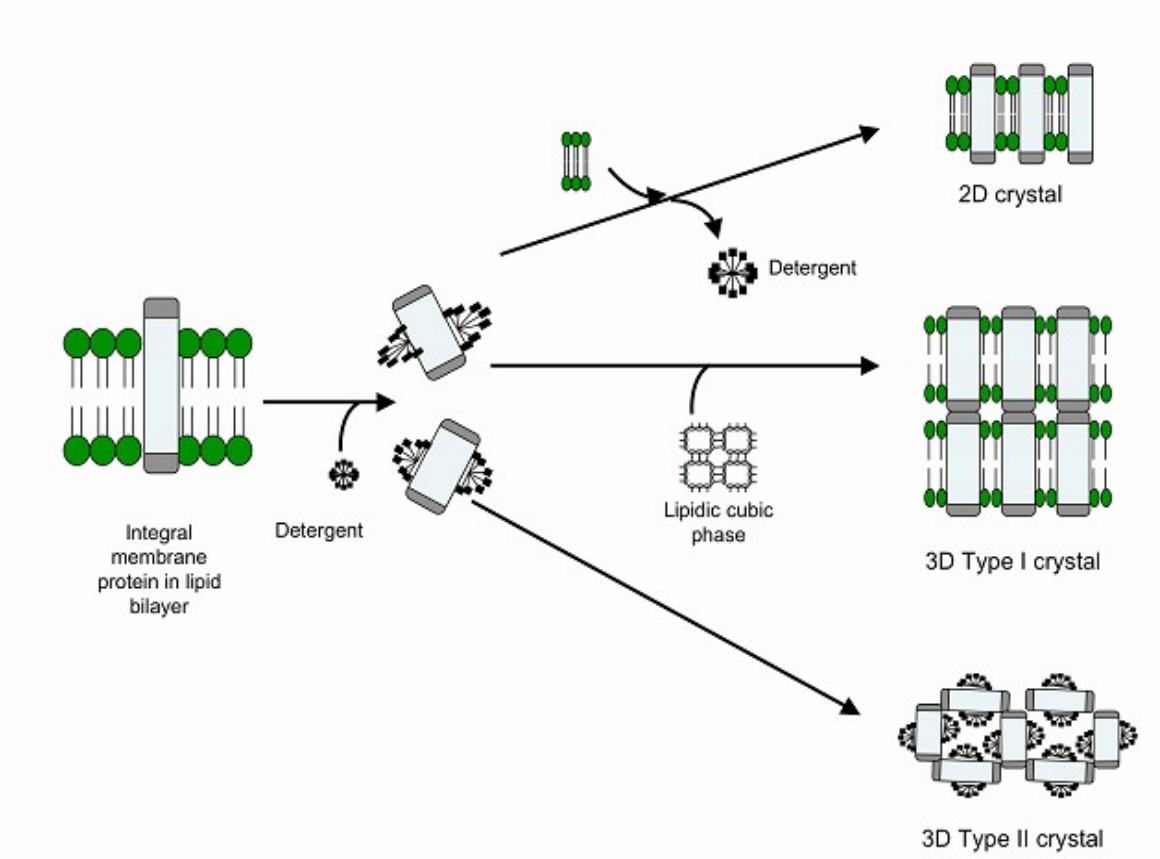

Figure 3.3: Possible crystal packing of membrane proteins (taken from Bergfors, 1999)

3.3.4. Analysis of Protein Crystals

Especially in the state of initial screening it is difficult to distinguish between salt and protein crystals. After having some experience with the target protein, information is available about the crystallisation behaviour and the shape of the crystals. But this can never be taken for granted, as changing the crystallisation technique for example has an influence on the crystal shape. So other methods have to be used to determine whether a crystal is derived from protein or salt.

3.3.4.1. Crystal Texture

A very simple way to test whether a crystal is a protein or a salt crystal is a breaking test with a needle or capillary. Protein crystals are very soft, especially if they are derived from PEG as precipitant. Not much pressure is necessary to distorted the packing and break then. The resulting scarp is rough and the crystals often show a woollen like texture. Salt crystals instead are very hard and hard to destroy.

3.3.4.2. SDS-Polyacrylamide Gelelectrophoresis

The method, which gives very detailed results is SDS-PAGE. A crystal is dissolved in sample buffer and loaded on a gel. The protein content of the crystal can be analysed after silver staining. Salt crystals dissolve in the buffer and the lane in the gel is empty after staining. It is very important to wash the crystals, e. g. in a cryo buffer. Precipitate present on the surface of a crystal can produce false positive results. It may contain different protein subunits or fragments compared to the crystal content.

3.3.5. Co-crystallisation and Use of Additives

Co-crystallisation is a very elegant way to introduce an anomalous scatterer or essential ligands and cofactors into a protein crystal. As these substances are built in during crystallisation there is little risk to cause distortion of the crystal lattice as may occur in post-crystallisation treatments. Especially ligands and cofactors can help to stabilise the protein and facilitate crystallisation in general. The following additives were tested in co-crystallisation:

Additive/Inhibitor	Concentration
ADP (pH 8.0)	40 µM, 1 mM, 2 mM, 3 mM, 4 mM
DCCD	50, 100, 150 µM
Phloretin	50, 100, 150 µM
Phloridzin	25 and 70 µM
Spermine	10 mM

3.3.6. Dehydration

With post-crystallisation treatment it is possible to manipulate crystals after their growth. Usually the idea is to improve the diffraction quality of the crystals or to prepare them for experimental phasing.

Protein crystals are usually traversed by solvent channels. So a crystal has a solvent content in the crystal between 30 and 70%. The main component of this solvent is water, which can cause several problems. A high solvent content in a crystal prevents a dense packing of the molecules, which allows for high flexibility of the molecules and reduces the diffraction quality. Numerous repeats of a molecule in the same orientation arranged in a regular manner in three dimensions with little distortion and misorder give rise to a good diffraction pattern. Solvent makes the crystals very fragile and so difficult to handle. Water as the main component tends to expand when flash frozen in liquid nitrogen and disrupts the ordered packing.

To dehydrate a crystal and reduce the amount of water, evaporation is the easiest application. This can be done by opening the well and expose the crystal to air. Another possibility is to use solutions with increasing concentrations of precipitant, whereas the other components stay constant. Small volumes with higher precipitant concentrations can be added directly into the drop containing the crystal. After equilibration, usually several minutes, the same volume as added before is then removed. This is repeated until the last precipitant concentration is added. Then the crystal is flash frozen and can be used for data collection.

It is also possible to transfer the crystal in solutions containing increasing concentrations of precipitant. The last solution should contain the buffer used as cryo protectant. This method is very quick. Unfortunately, if the changes in the buffer conditions are too harsh or the incubation times too long it is very likely that the crystals show cracks. This means that the water was removed or replaced by other buffer components too quickly and the crystal lattice could not rearrange. These crystals usually cannot be used for data collection or show only low resolution diffraction.

Alternatively the whole drop with the crystal is placed over new reservoirs containing increasing concentrations of precipitant. The drop is allowed to equilibrate over the new well for up to 12 hours. The exact equilibration time is different for every protein and the crystallisation conditions used. This method is more gentle but requires transfer of the crystal in a cryo buffer afterwards which can still cause distortion of the packing (118, 119).

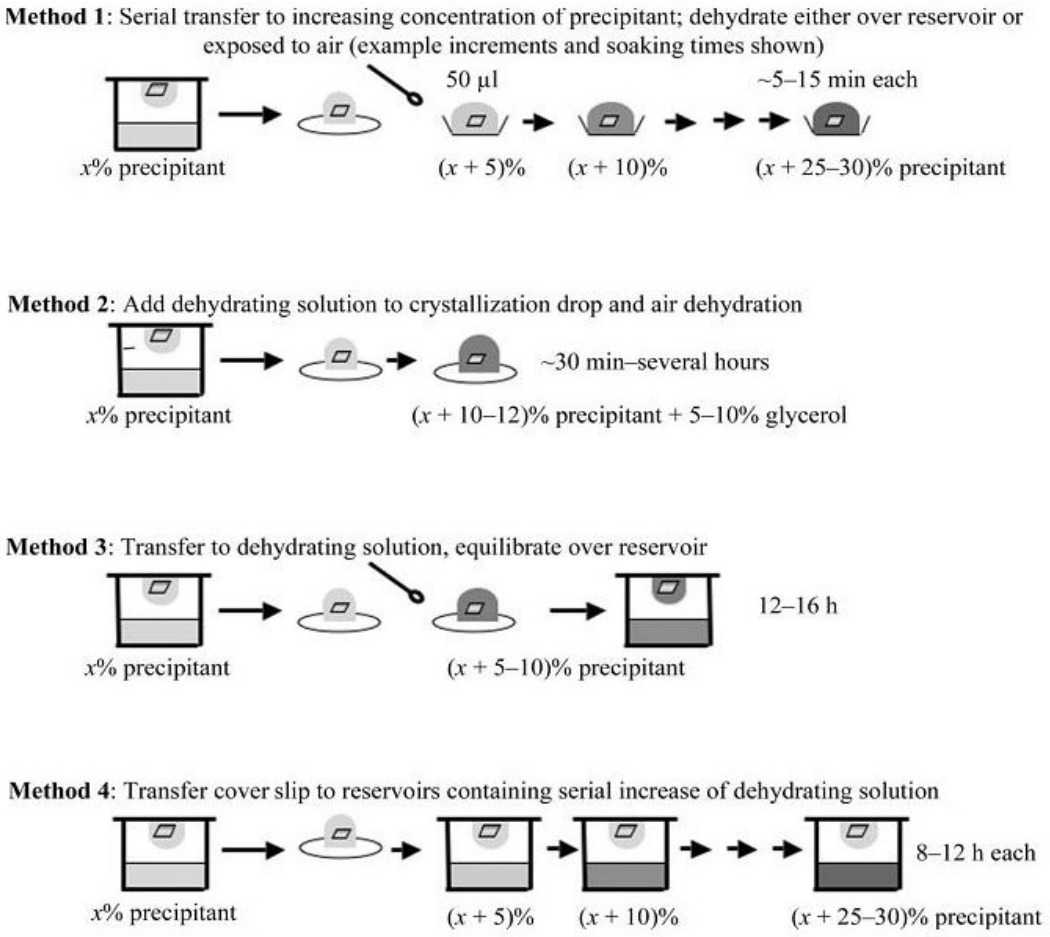

Figure 3.4: Different dehydration procedures (taken from Heras and Martin, 2005)

3.3.7. Cryo-protection

The function of a cryo buffer is to protect the crystal from uncontrolled dehydration, reduce radiation damage, and replace as much water as possible within a crystal lattice. Obviously it has to fulfil contradicting purposes. Bound crystal water is essential for crystal stability. On the other hand too much water within the crystal disrupts the ordered lattice during freezing in liquid nitrogen.
Another reason for the use of a cryo-protectant is the reduction of radiation damage. Third generation synchrotrons give the possibility of fast data collection as the beams used are highly

energetic. But as a consequence radiation damage is a growing problem. Thereby water within the crystal becomes ionised and the creation of $^{\bullet}OH^{-}$ radicals occurs. The radicals react with the protein and modify side chains or disrupt bonds. In the end, this destroys a crystal lattice and reduces the diffraction quality of a crystal. This can be seen towards the end of data collection in a loss of resolution (120, 121).
Standard cryo buffers are PEG400, Paratone N or ethylene glycol. If these are not appropriate for a given crystal, a screening for suitable cryo buffers has to be carried out. Cryo buffers tested with the CF_oF_1 complex are discussed in the Results 4.2.10.

3.3.8. Storage and Transport of Crystals

The maximum storage time within an incubator is protein specific and can be in the range of a few weeks up to several years. There is only little risk of dehydration through an oil or rubber seal. Instead it is more likely that modification of the protein occur because of enzymes, bacteria or fungi, as the preparation is usually not carried out under sterile conditions. Even the use of chemicals like azide and PMSF can't avoid modifications as they lose their activity over the time.
The transport of crystals is usually done in the frozen state in liquid nitrogen. Especially since the implementation of the SPINE system at the synchrotrons in Europe and the use of sample changers it is more convenient to transport frozen crystals. Therefore they are collected from the crystallisation plate with nylon or litho loops, washed and cryo protected, and then flash frozen in liquid nitrogen. To avoid uncontrolled movement they are covered with crystals caps. If use of a sample changer is planned, they are put in special baskets. For testing of cryo buffers at the beamline fresh crystals are needed so the transport of the whole plates is also possible, as long as uncontrolled movement and vibration are avoided.

Figure 3.5: Components of SPINE system; (A) Cap and vial for crystal harvesting and storage in liquid nitrogen. (B) Basket for use in a sample changer. (taken from www.esrf.eu)

3.4. Crystallographic Theory

3.4.1. Crystal Packing

Crystals in general are built up of repeating identical blocks, namely the unit cell. The unit cell is defined by the lattice constants a, b, c and the angles α, β, γ. Stacking the unit cell in the same orientation in three dimensional translations creates the crystal lattice. The unit cell itself contains smaller building blocks without any symmetry elements, namely the asymmetric unit (asu). Several of them related by symmetry operations such as mirror planes, inversion centres, rotation axis and screw axis form a unit cell. As all biomolecules have at least one chirality centre (L-amino acids) only rotation and screw axes can be found as symmetry elements. When applying these symmetry operations the following seven crystal classes are possible:

Crystal system	Minimum symmetry requirement	Conventional choice of axes	Constrains on interaxial angles and axial length
Triclinic	None	No constraints	None
Monoclinic	One 2-fold axis	b parallel to 2-fold a and c perpendicular to 2-fold axis	α and γ = 90°
Orthorhombic	Three perpendicular 2-fold axes	a, b, and c parallel to 2-fold axis	α, β, and γ all 90°
Trigonal	One 3-fold axis	c parallel to 3-fold axis a and b perpendicular to 3-fold axis	β = 120°, α and γ = 90° a and b equal length
Tetragonal	One 4-fold axis	c parallel to 4-fold axis a and b perpendicular to 4-fold axis	α, β, and γ all 90° a and b equal length
Hexagonal	One 6-fold axis	c parallel to 6-fold axis a and b perpendicular to 6-fold axis	β = 120°, α and γ = 90° a and b equal length
Cubic	Four 3-fold axes	a, b, and c related by 3-fold axis	α, β, and γ all 90° a, b, and c equal length

Table 3.1: Seven crystal classes (taken from Blow, 2006)

The system of seven crystal classes is made of primitive unit cells. In some cases this is not sufficient to describe the lattice. So fourteen more complex forms of unit cells were created, the Bravais lattices. The combination of primitive unit cells, Bravais lattices and possible point group symmetry operations in the molecules within the unit cell results in a final choice of 230 possible space groups. As mentioned before chirality in biomolecules causes the lack of inversion centres and mirror planes, which reduces the number of possible space groups to 65. The space group of the complete crystal lattice is determined by the sum of the symmetry operations within the unit cell.

3.4.2. Working with X-rays

To show atomic structures of macromolecules, such as proteins, the characteristic of crystals to diffract electromagnetic waves is used. To see the interesting details like bonds between atoms, the use of waves, which correspond in wavelength to the distances between atoms, is necessary. For X-rays this means 1 to 2 Å. The applied X-rays interact with the matter in the crystal in three different ways:

- Absorption

  Absorption is an unavoidable byproduct of diffraction experiments. Some energy of the X-ray beam is absorbed by the crystal. The high energetic beam interacts for example with water present in the crystal and produces $^{\bullet}OH^{-}$ radicals which damage the protein and disrupt the structure. Absorption is used in diffraction experiments with anomalous scatterer.
- Incoherent diffraction

  This is also called the Compton effect. It is inelastic diffraction, which is caused by clashes between photons of the X-ray and the electrons of the atoms in the crystal lattice. As a result, the electrons emit radiation with a longer wavelength than the incoming beam. The emitted waves do not interfere with each other and only cause background radiation.
- Coherent diffraction

  This elastic diffraction is also called Thomson radiation. The incoming X-ray beam causes the electrons of the atoms within a crystal to vibrate. As result the electrons emit X-rays, which have the same wavelength as the incoming beam but have a different phase instead. This radiation can cause constructive interference and produces sharp spots recorded in a diffraction pattern.

3.4.2.1. Working with Waves

Waves can be described in a mathematical manner as a sine curve. Such a curve is characterised by different parameters. The wavelength λ defines the distance between two wave maxima. The amplitude A gives the height of a wave maximum, whereas the phase Φ defines the position of the wave maximum at a point x = 0 and a time t = 0. A wave moves with a certain velocity and its frequency 1/λ is dependent on the wavelength. So in a geometric manner a wave can be described as:

$$W = A\cos\left[\left(\frac{2\pi x}{\lambda}\right)+\Phi\right] \qquad (3.1)$$

With the help of complex numbers a wave is separated into two components, namely amplitude and phase. This is shown in an Argand diagram.

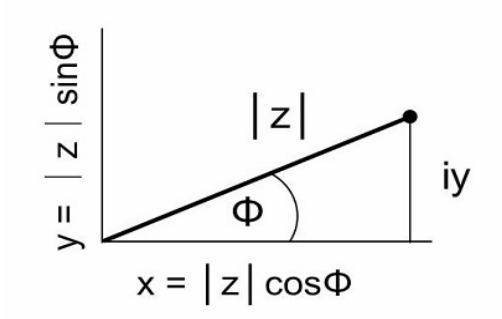

Figure 3.6: Argand diagram (taken from Blow, 2006)

Z is a complex number composed of a real part (x axis) and an imaginary part (y axis; iy). |z| represents the magnitude A of a wave and Φ is the corresponding phase. The geometrical construction in the Argand diagram can be written as:

$$z = x + iy = |z|e^{i\Phi} = |z|(\cos\Phi + i\sin\Phi) \qquad (3.2)$$

The consideration of the wavelength λ and the wave propagation together with equation (3.1) results in:

$$W = A\mathrm{e}^{\left[i\left(\frac{2\pi x}{\lambda}+\Phi\right)\right]} \qquad (3.3)$$

3.4.2.2. Interference of Waves, Laue Equation and Miller Indices

If the incoming beam has a known angle of incidence μ then the diffracted angle is defined as well. A crystal lattice can be considered as a three dimensional sieve with a well defined difference in step width n (n = 1, 2, 3...), which corresponds to the distance between the atoms or atom layers within the crystal. The layers interact with waves and can therefore be defined as $n\lambda$ (n = 1, 2, 3...). As a consequence of this interaction, the diffracted beam produces a Laue cone around every atom with a defined angle υ.

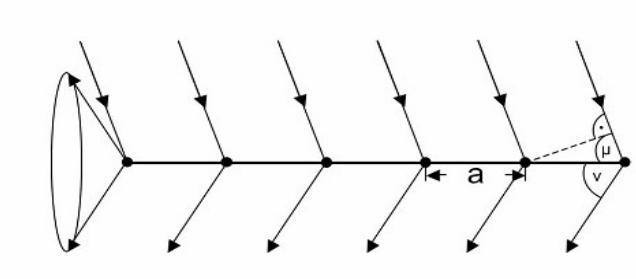

Figure 3.7: Formation of a Laue cone around an atom (taken from Massa, 2005)

In a three dimensional lattice like a crystal the describing equations are

$$\begin{aligned} a\cos\mu_a + a\cos\nu_a &= n\lambda \\ a\cos\mu_b + a\cos\nu_b &= n\lambda \\ a\cos\mu_c + a\cos\nu_c &= n\lambda \end{aligned} \qquad (3.4)$$

As the intercept has to be between angles of all three dimensions it is obvious that this is a very rare event. But if it happens and the incoming beam and the diffracted beam have the same angle then the whole process is a reflection at a plane. The constructive interference produces a reflection, which can be recorded.

The atoms in a three dimensional crystal lattice are ordered in planes and are assumed to serve as mirrors. Plane positions in the crystal are defined by Miller indices *h*, *k*, *l*. The distance between planes is given as *d*. All planes separated with the same *d* belong to the same group of planes.

3.4.2.3. Bragg's Equation and Reciprocal Lattice

On the basis of constructive interference and a plane system within a crystal, the Laue term (3.4) can be described in a different way, the Bragg equation. If incoming and diffracted beam have the same angles, and if θ is chosen to fulfil the Laue term in three dimensions, this results in the Bragg equation:

$$2\,d_{hkl}\sin\theta = \lambda \qquad (3.5)$$

Figure 3.9 gives a geometrical description of the Bragg equation.

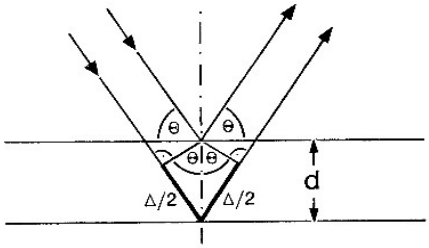

Figure 3.8: Geometrical form of Bragg equation (taken from Massa, 2005)

The result of a reflection event at a crystal plane *hkl* in the crystal is a corresponding point in the reciprocal lattice shown as a spot in a diffraction pattern. The connection between a real crystal and the reciprocal lattice is given through the unit cell. A point within the unit cell is described as a vector *d* or alternatively as an atom in a plane of the unit cell with a distance *d* to the next plane of the same plane group. In a real lattice of a crystal the plane defined by *hkl* intersects with the edges of the unit cell *a*, *b*, *c*. The resulting intersection points can be written as fractions in a real lattice.

$$\frac{1}{d^2}=\frac{h^2}{a^2}+\frac{k^2}{b^2}+\frac{l^2}{c^2} \quad (3.6)$$ or in a reciprocal lattice $$d^{2'}=a^{2'}+b^{2'}+c^{2'} \quad (3.7)$$

At the end of the diffraction vector *d'* lies a reciprocal lattice point ,which is recorded as a reflection *h*, *k*, *l* with an intensity I_{hkl} that can be indexed.

3.4.2.4. Ewald Construction

The Ewald construction is a geometrical explanation how a reflection in the reciprocal lattice is created on the basis of a real lattice in a crystal and Bragg's equation.

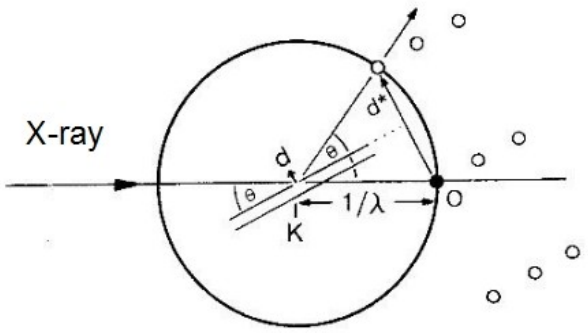

Figure 3.9: Ewald construction; *X-ray* is the incoming beam; *K* the crystal with the distance *d* between the crystal planes whereas *d** is the distance between the planes in the reciprocal lattice; *O* gives the origin of the reciprocal lattice; the radius is determined through the frequency *1/λ*; *θ* gives the diffraction or Bragg angle (taken from Massa, 2005)

The plane system separated by the distance *d* in the crystal *K* is the centre of a circle (two dimensions) or a sphere (three dimensions). The radius is given as the frequency of the radiation $1/\lambda$. If the incoming beam *X-ray* interacts with the crystal planes, and the Laue term as well as Bragg's equation are fulfilled, then the angles *θ* of incoming and diffracted beam are identical. For the diffracted beam this results in an intersection with the surface of a sphere in the case of a three dimensional lattice. The intersection point correlates with a point in the reciprocal lattice and causes a reflection in a diffraction pattern. The angle between the diffracted beam and the extension of the incoming beam is *2θ*. The point where the incoming beam leaves the sphere after crossing, is the

origin of the reciprocal lattice *O*. The distance between the origin in reciprocal space and the intersection point of the diffracted beam with the sphere surface is the reciprocal distance *d** and is related to the distance *d* between crystal planes of the same group in real space. Extension of the real crystal plane causing the reflection at the intersection point, results in a perpendicular intersection with *d**. The resulting right-angled triangle has the radius $1/\lambda$ as hypotenuse with θ opposite one catheti. Following Pythagoras this can be written as:

$$\sin\theta = (d^*/2)/(1/\lambda) \qquad (3.8)$$

3.4.2.5. Waves, Complex Numbers and Fourier Transformation

In a crystal the unit cells are organised in a repetitive way in three dimensions. This can be interpreted as a harmonic wave in three dimensions. The unit cells are seen as a Fourier series. And as said before, a wave can be written as a complex number with a real and an imaginary part. In a direct Fourier transformation the electron density within a unit cell can be calculated from amplitude and phase. With atom positions given in Cartesian coordinates a Fourier summation over all *h*, *k*, *l* within a unit cell can be written, which results in an electron density $\rho(x, y, z)$.

$$\rho(x, y, z) = \frac{1}{V} \sum_{hkl} F_{hkl} e^{[-2\pi i(hx+ky+lz)]} \qquad (3.9)$$

F_{hkl} corresponds to $|z| \; e^{i\Phi}$ in the Argand diagram and $e^{[-2\pi i(hx+ky+lz)]}$ is the Fourier transformation itself. Together both terms describe a wave as a complex number. The calculations are done in three dimensions, which makes the consideration of the unit cell volume given as *V,* necessary.

An inverse Fourier transformation of the electron density allows for determination of the phase, which is in contrast to the amplitude, not known from measurements. The corresponding structure factors F_{hkl} are calculated with a Fourier integral.

$$F_{hkl} = V \int \rho(x, y, z) e^{[2\pi i(hx+ky+lz)]} dV \qquad (3.10)$$

A closer look at the spots of a diffraction pattern or the electron density itself, reveals a smeared out

shape that follows a Gaussian function. This is because of disorder in crystal packing as well as thermal vibrations of the atoms.

$$F_{hkl} = \sum_{N} f_i \, e^{[-2\pi i(hx+ky+lz)]} \, e^{\left[-B_i\left(\frac{\sin^2\theta}{\lambda^2}\right)\right]} \qquad (3.11)$$

N is the number of all atoms within the unit cell and f_i is the atomic scattering factor and gives the contribution of a particular atom to the structure factor. The B factor or Debye-Waller factor describes thermal and crystal lattice disorder and is defined as $e^{\left[-B_i\left(\frac{\sin^2\theta}{\lambda^2}\right)\right]}$ with $B = 8\pi^2 u^2$.

The mean-square displacement of an atom i is given with u^2. In the ideal case of isotropic behaviour this parameter is identical in every direction x, y, z for an atom in the unit cell. The B factor term as well as the atomic scattering factor vary with the resolution and therefore with the distance d between the crystal planes and the corresponding diffraction angle θ. A high B factor causes a decrease of the amplitude which is mostly pronounced at high resolution.

3.4.3. The Phase Problem and Possible Solutions

In a diffraction experiment only the amplitude of a diffracted beam can be determined through the intensity of a reflection in a diffraction pattern. To have a complete wave description, information about the phase of the diffracted beam is also needed. This dilemma is named the phase problem.

3.4.3.1. Patterson Function

With the help of the Patterson function a Patterson map can be created, which can be used to find a crystal structure in a diffraction pattern and circumvent the phase problem. The square of the amplitude is calculated from the intensities of reflections as follows:

$$I_{hkl} = A_{hkl}^2 = |F(hkl)|^2 \qquad (3.12)$$

A sum over all intensities in a diffraction pattern, including constructive and destructive interference

as a result of scattering, gives information about the three dimensional distribution of the atoms within the unit cell. The interatomic vectors in the Patterson map are indicated with *u, v, w* and are based on the unit cell edges *a*, *b*, *c*. They are completely independent from atom coordinates *x*, *y*, *z*.

$$P_{uvw} = \frac{1}{V} \sum_{hkl} |F_{hkl}|^2 \cos[2\pi(hu + kv + lw)] \qquad (3.13)$$

or alternatively written as

$$P(\vec{u}) = \int_{\vec{r}_1} \rho(\vec{r}_1)\, \rho(\vec{r}_1 + \vec{u})\, d\vec{r}_1 \qquad (3.14)$$

with a changing endpoint for $\vec{r}_1$ within the unit cell and a constant $\vec{u}$. The only prerequisite is the presence of centrosymmetric reflections. An absolute origin, as for a reciprocal lattice, is not necessary. The origin will be created out of all self-vectors of each atom as well as the cross-vectors, which result from atom interactions. The highest maximum in the map is set as origin. This allows for a differentiation between heavy and light atoms. Additionally the general look and appearance of maxima within a Patterson map can be compared for related molecules.

3.4.3.2. Molecular Replacement

Molecular replacement uses an existing structure of a homologous or similar protein or at least parts of a known structure as a search mask to find consensuses in the phases of an unknown crystal structure. This process can be divided in substeps:

- finding the angular orientation of a model in the crystal structure of interest
- finding the origin position of the model within the unknown structure
- creating a hypothetical structure of interest which includes the search model used

The whole process needs the rotation of the model around three axes with the angles φ, ψ, κ and then translations along three axes *x*, *y*, *z*. To accelerate model positioning, one six dimensional search is divided into two three dimensional searches. The basis for both searches in a three dimensional space are the Patterson maps created from the model and the structure of interest.

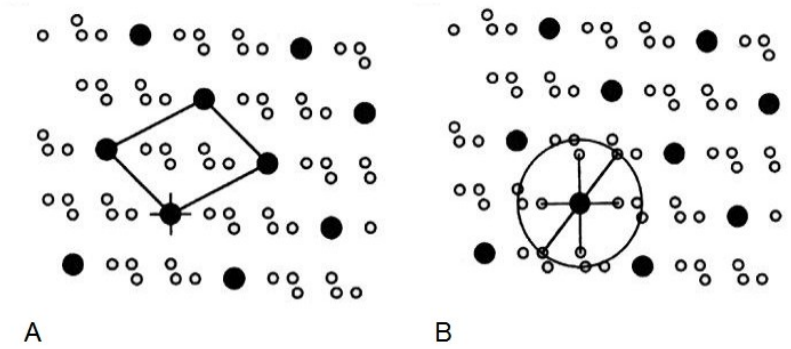

Figure 3.10: (A) shows a Patterson map from a molecule of interest. A triple-weight vector can be found in the origin (indicated with a cross) and in the other lattice points. This results in a cell, which includes six single-weight vectors. (B) shows the rotated Patterson function of a model molecule M superimposed on six vectors of the Patterson of the target structure. All of these vectors lie in a circle, which gives the maximum dimensions of M. (taken from Blow, 2006)

Positioning the model in the Patterson map starts with a rotation function. The maximum peak in a Patterson map is created by zero-length vectors and determines the origin. In a first attempt this point has to be found for the maps of the model and the unknown structure. At this point of coincidence both maps are placed on top of each other and are then rotated in a sphere to find the orientation with the highest likelihood between both. The sphere used gives also the maximum dimensions of the models. Additional peaks can still be found within or outside the sphere and show differences between the two structures. If symmetry is present in the target structure but not in the search model then the search is more complicated and the additional molecules cause noise signal. By reducing the radius of the search sphere the noise can be reduced.

If the rotation step was successful and gave one or more possible solutions, the translation step can be started. The origin of both, the lattice of the target and of the model, is identical if symmetry mates are only related by translation. If rotational symmetry is found in the structure of interest, then the origin of the lattice of the target protein has to be placed in relation to the rotation axes. This avoids collision between symmetry mates after they have been found with the help of cross-vectors.

After the model is positioned in the asymmetric unit of the target structure a first estimation of the phases for the unknown structure can be done. The phase angles $(\alpha_{hkl})_{calc}$ are used from the model and they have to be related to the structure factors $|F_{hkl}|_{obs}$ of the new structure.

$$F(hkl)=|F_{obs}(hkl)|e^{[i\alpha_{calc}(hkl)]} \qquad (3.15)$$

The first term gives the measured structure amplitudes and the second term the phase angles calculated from the model. This means at the same time that the new structure is biased by the model. To eliminate weak signals from atoms still belonging to the model but not present in the new structure, and to see which, signals are unique for the new model, a difference map is calculated.

$$\rho_{diff}(xyz)=\frac{1}{V}\sum_{hkl}(|F_{obs}(hkl)|-|F_{calc}(hkl)|)e^{[i\alpha_{calc}(hkl)]}e^{[-2\pi i(hx+ky+lz)]} \qquad (3.16)$$

The phases of the unknown structure are only estimated from the model. They have to be improved by further model building.

3.4.4. Data Collection and Processing

3.4.4.1. Data Collection and Integration

Data set collection and screening of native *c*-ring crystals as well as crystals co-crystallised with inhibitors was done on beamlines ID14-1, ID14-4, ID23-1, and ID23-2 at ESRF (Grenoble) as well as BW7B, X11, and X12 at EMBL (Hamburg). Additional screenings were done on a home source (Bruker). iMOSFLM/mosflm (122) was used for data integration followed by scaling and merging with Scala (123).

3.4.4.2. Construction of Search Models for Molecular Replacement

For molecular replacement, models of transmembrane *c*-rings from *E. coli* and *Ilyobacter tartaricus* were used as well as self-created models, which were produced by shell scripting. Models produced by the scripts were based on existing information from other organisms and results from other techniques. The number of subunits for the spinach *c*-ring complex was available, as monomers could be counted in cryo-EM images (5). From an NMR structure it was known that a monomer consists of two anti-parallel α-helices in a hairpin structure (39). Structural alignments gave an

identity of 60% (http://toolkit.tuebingen.mpg.de/hhpred) between *Ilyobacter tartaricus* (PDB code: 1YCE) and spinach chloroplasts. So the *Ilyobacter c*-monomer was the basis for model screening.
Initial trials were done with a poly-Ala model, which was created with PDBset (124) from the CCP4 suite. The self-written shell scripts were run on linux as operating system. This gave the possibility to use several programs of the CCP4 suite for model creation, molecular replacement, and refinement. In the first step the monomer, either as poly-Ala or later with most of the spinach side chains, was orientated in three dimensional space. This was done with varying polar angles omega, phi, and kappa. Because of tight packing of 14 monomers in a ring the search space was restricted and only small angle ranges were used. Afterwards the orientated monomer was placed on the origin and according to the chosen diameter a ring with 14 subunits was created. The multimeric models thus created were used as search models in molecular replacement. First runs on a cluster gave no results with MOLREP (125). In the following experiment the starting orientation of the monomer was changed in COOT (126) before running the scripts. Different angle and radii combinations were again computed on a cluster.
CHAINSAW (127) from the CCP4 suite was used to produce a "mixed" monomer. All conserved residues between *Ilyobacter* and spinach were present and every other side chain was cut back to Cγ. Additional residues of the *Ilyobacter* sequence were aligned to gaps in the spinach sequence were eliminated from the model. The CHAINSAW-model was used to build a full length multimer. All models were used in molecular replacement with MOLREP (125) followed by rigid body refinement and ten cycles in Refmac5 (128) using default settings. After refinement the models were ranked according to their R_{free}. The one with the lowest R_{free} created with the poly-Ala monomer was used for subsequent subunit exchange with PHASER (129). In a second attempt the mixed monomer created with CHAINSAW (127) was used for a repeated run of the shell scripts with the successful poly-Ala settings. This later run gave the starting model for further model building and refinement.

3.4.4.3. Further Model Building and Refinement

Further model building was carried out in COOT (126) using NCS as 14 identical subunits are present in the *c*-ring. Density modification was applied with the program dm (130) from the CCP4 suite. Refmac5 was used for refinement. Tight NCS restraints were used as well as tight restraint parameters for bond angles and bond lengths. For thermal movements TLS (131) was applied. Different TLS groups of seven pairs and 14 monomers were tried but in the end the complete ring was taken as one group (http://skuld.bmsc.washington.edu/~tlsmd/).

3.4.4.4. Validation and Visualisation

The model was validated with PROCHECK (132) and Whatcheck (133). Images were produced using PyMOL (134). Electrostatic surface was calculated with the Adaptive Poisson-Boltzmann Solver (APBS) plugin for PyMOL (135). The necessary input file was created with PDB2PQR (136).

3.4.4.5. Structure Deposition

The native structure of the *c*-ring from F_oF_1 ATP synthase from spinach chloroplasts was deposited in the protein data bank (www.pdb.org) with the access code 2W5J.

4. Results

4.1. Purification

4.1.1. Isolation of CF_oF_1 from Thylakoid Membranes

As mentioned in chapter 3.2, the purification of thylakoid membranes followed the method described in Strotmann *et al.* (103) with some modifications. After treatment with a solubilisation buffer and sonication the thylakoid membranes are present in a mixture containing 2% dodecyl maltoside and 1% sodium cholate. The detergent mixture partly simulates a membrane and allows for extraction of membrane proteins from their natural environment and their incorporation in micelles. The whole ATP synthase, including membrane integrated F_o, becomes soluble as proteo-micelles. After ultra centrifugation and fractionated ammonium sulphate precipitation CF_oF_1 containing proteo-micelles were separated from contaminations according to their specific density. Figure 4.1 shows a sucrose density gradient after at least 22 h in an ultra centrifuge. Below a green band CF_oF_1 proteo-micelles have accumulated.

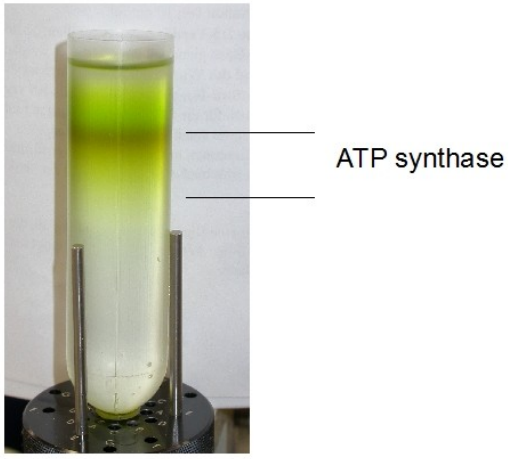

Figure 4.1: Sucrose density gradient after 22.5 h in an ultra centrifuge. The bars indicate the position of ATP synthase

SDS-PAGE (Figure 4.2) was used to identify the protein composition of fractions collected from the sucrose density gradient. Those fractions containing all CF_oF_1 subunits and only minimal contaminations, were pooled and further purified in anion exchange chromatography on a HQ20 anion exchange column.

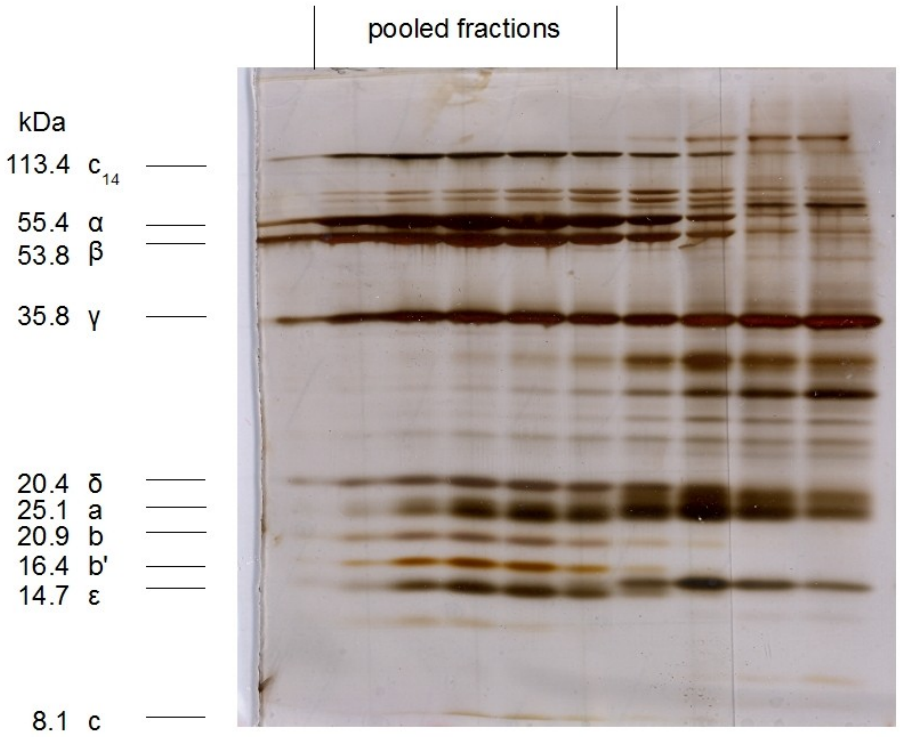

Figure 4.2: Fractions of a sucrose density gradient analysed on a 15% SDS-PAGE

The CF_1 part of the ATP synthase, as not covered by a detergent micelle, interacts with functional groups, polyethyleneimine, on the column matrix of poly(styrene-divinylbenzene) flow-through particles. Elution with a salt gradient yielded a final volume between 10 and 20 ml. Concentration and subsequent buffer exchange resulted in a final volume between 50 and 150 µl of CF_oF_1 in the washing buffer desired for crystallisation trials.

4.1.2. Washing Buffer

Several washing buffers have been tested to find such conditions, which keep the protein complex most stable for experiments and storage but still facilitate crystallisation. A list of washing buffers (WB) used can be found in the Appendix 7.1. Buffers one to eight, and 14 stabilised the protein but showed great differences in the crystallisation experiments. Washing buffer one is composed of 100 mM sodium citrate (pH 5.5), 10% (w/v) glycerol, 4% (w/v) glycine, 2 mM magnesium chloride, 0.02 % (w/v) azide, 0.002% (w/v) PMSF, and 0.1% (w/v) dodecyl maltoside. WB one and two differ only in the detergent concentration with 0.1% (w/v) and 0.01% (w/v) respectively. Buffer three has the same composition as buffer one, except twice the concentration of magnesium chloride. 25 mM tricine (pH 8.0) replaces 100 mM sodium citrate (pH 5.5) of WB one in buffer four. Buffer five and eight differ only in the concentration of the buffer component with 35 mM and 25 mM respectively. Both use bis-tris-propane (pH 6.5) as buffer component and 35 mM 10-HEGA-C as detergent in contrast to WB one. The detergent concentration was reduced from 0.1% (w/v) dodecyl maltoside in buffer one to 0.01% (v/w) in WB six and seven. In both buffers 100 mM sodium acetate (pH 4.6) is used as buffer component. WB6 also lacks 1 mM EDTA (pH 7.0). Washing buffers four and 11 were composed to create a basic (pH 8.0) or an acidic (pH 4.6) environment for CF_oF_1. These compositions were done on the basis of a pKa of about seven for the essential acidic residue Glu61 of the *c*-ring (81) and the pH profile of the chloroplast ATP synthase proton binding site (86). A pH of eight is proposed to facilitate the deprotonated state of the proton binding site and a pH of 4.6 the protonated state. Buffer 11 kept the protein stable only, if the final volume was at least 100 µl. Washing buffer 12 is derived from buffer four and contains additionally 0.1% (w/v) phosphatidyl choline (PC). The aim for the use of PC was to restore lipids, which had been removed during purification and may be essential for CF_oF_1 stability. Washing buffer 15 was composed on the basis of buffer eight and 11. It combines an acidic environment (pH 4.6) and C-HEGA-10 as detergent. The influence of the absence of glycerol was tested with washing buffer 16. In both buffers, WB 15 and 16, the protein started to precipitate during the concentration step and was lost completely after storage over night at 4°C. An alternative for glycerol was tested in buffer 14. 10% (w/v) sucrose replace 10% (w/v) glycerol while the remaining components are kept according to buffer 11.

CF_oF_1 is stable over a broad pH range, pH 4.6 to eight, and also tolerates several buffer components in different concentrations. The detergent concentration can be varied without any loss in stability.

Glycerol or sucrose are essential for protein stability. Present lipids avoid high protein concentration resulting in a maximum protein concentration of 3.5 mg/ml.

4.1.3. Detergent Content

The detergent concentration in the concentrated protein solution was determined by a colourimetric assay. The method used was based on DuBois *et al.* (108) with modifications as described in Urbani and Warne (109). This assay was done for dodecyl maltoside in WB 11 and C-HEGA-10 in WB eight.

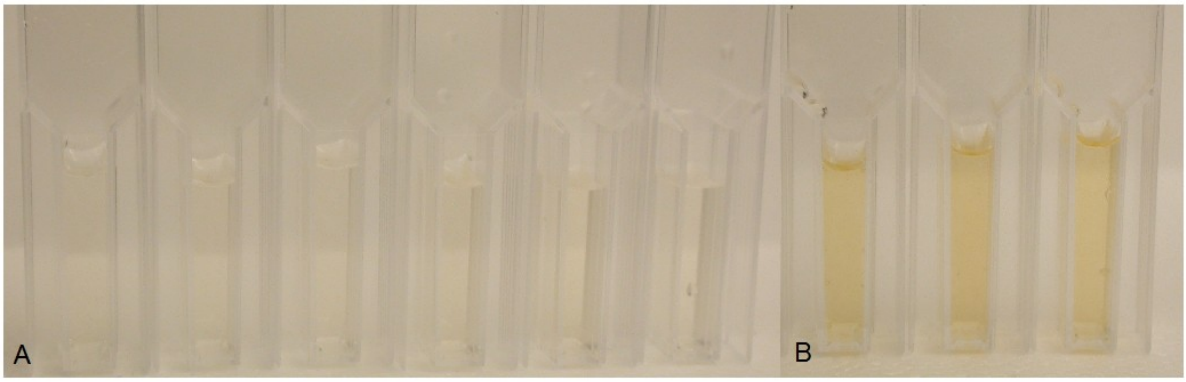

Figure 4.3: Detergents determination for washing buffer eight; (A) standard series; (B) samples taken after concentration step

Washing buffer eight contains C-HEGA-10 as detergent. Figure 4.3 (A) shows one standard series for C-HEGA-10. Any chosen concentration range produced the same result. No detergent was detectable. The slight colour originates from other buffer components and present the background. Three samples of CF_oF_1 in washing buffer eight (dilution 1:10) are given in Figure 4.3 (B). They have a clear orange colour, which is more intense than expected from the background found in the standard series.

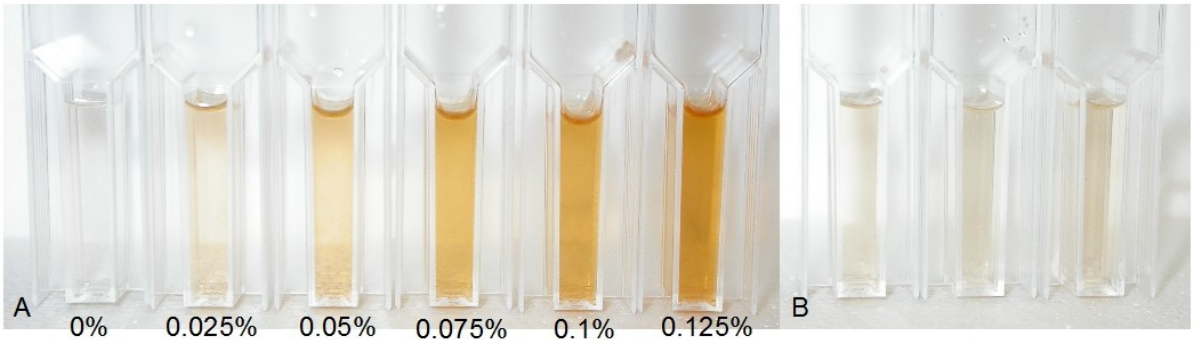

Figure 4.4: Detergents determination for washing buffer 11; (A) standard series containing 0-0.125% (w/v) dodecyl maltoside; (B) samples taken after concentration step

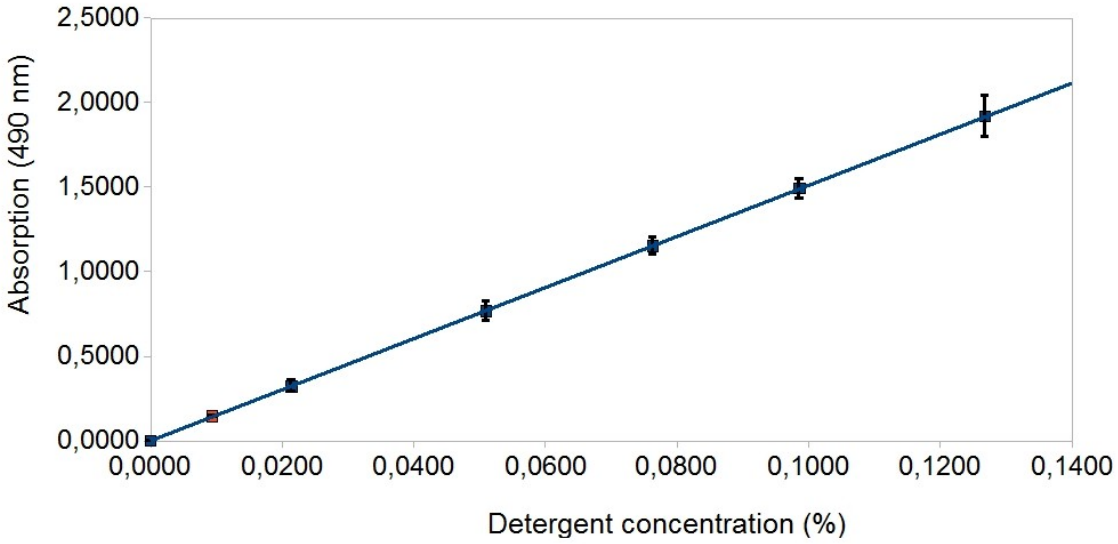

Figure 4.5: Diagram corresponding to standard series in Figure 4.4 (A); samples of Figure 4.4 (B) are indicated as red square

Contrary to C-HEGA-10, dodecyl maltoside contains maltose, a disaccharide of two glucose molecules. Present anomer carbon atoms can be determined in this colourimetric assay. For the samples in a dilution of 1:50 a concentration of 0.0094% (w/v) was estimated by this assay. This gives a final detergent concentration of 0.47% (w/v).

4.2. Crystallisation

4.2.1. Influence of the Washing Buffer on the Crystallisation Process and Diffraction

Trials with washing buffer 1, 2, and 3, which only differ in detergent concentration and double concentration for magnesium chloride for the latter on, did not produce crystals. Precipitate appeared immediately upon mixing of protein solution and crystallisation buffer. No crystals were detectable after a couple of weeks or months. Extension of the incubation time to about one year did not facilitate crystal appearance either.

Washing buffer four produced the first crystals suitable for diffraction experiments. The crystals were grown in three dimensions with lengths from 10 to 80 µm. They grew either in a compact form or as hexagonal plates.

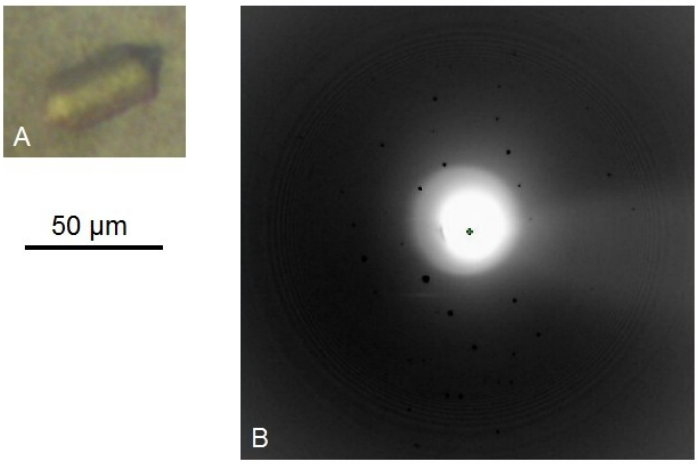

Figure 4.6: (A) Crystal grown from 10 mg/ml CF_oF_1 in WB 4 with a crystallisation buffer composed of 31% PEG 400, 110 mM $CdCl_2$, 95 mM sodium acetate (pH 4.6/HAc) plus 2 mM ADP (pH 8.0) at 15°C; dimensions 50 x 20 µm; (B) zoomed diffraction image; spots at a maximum resolution of 7.4 Å; detector: MAR image plate (X11)

SDS-PAGE (15%) of this crystal did not reveal protein bands although the gel staining was very intensively.

Replacing 25 mM tricine (pH 8.0) and 0.1% (w/v) dodecyl maltoside from WB four against 35 mM bis-tris-propane (pH 6.5) and 35 mM C-HEGA-10 in WB five did not result in crystal formation within a couple of weeks or months. Extension of the incubation time to about one year, revealed huge crystal plates with a square shape and dimensions of about 300 µm x 150 µm x 20 µm.

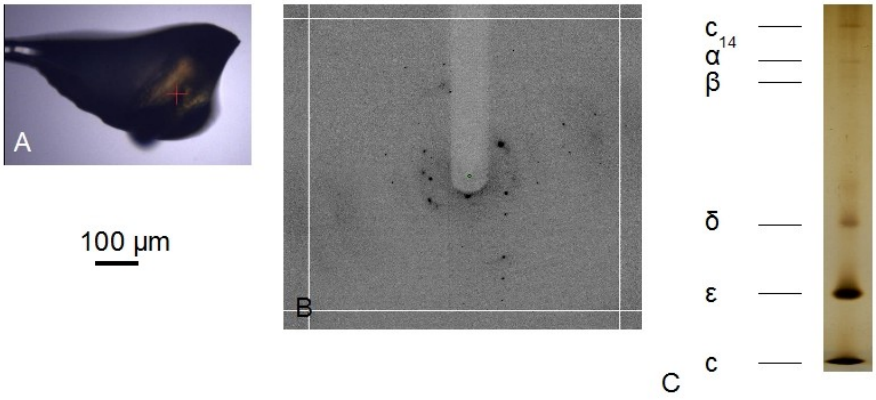

Figure 4.7: (A) Crystal grown from 10 mg/ml CF_oF_1 in WB 5 with a crystallisation buffer composed of 30% PEG 400, 100 mM $CdCl_2$, 100 mM sodium acetate (pH 4.6/HAc) plus 2 mM ADP (pH 8.0) at 15°C;dimension: 300 x 150 x 20 µm; (B) zoomed diffraction image; spots at a maximum resolution of 9.2 Å; detector: ADSC-Q315r (ID23-1); (C) corresponding 15% SDS-PAGE of the crystal (A)

These huge plates diffracted to a maximum resolution of about 9.0 Å with a X-ray beam attenuated to 5%. A SDS-PAGE of a crystal grown in these conditions identified subunits *α*, *β*, *δ*, *ε*, and *c* as monomer and 14mer.

The exchange of 100 mM sodium citrate (pH 5.5) in WB two against 100 mM sodium acetate (pH 4.6) in WB six did not result in the formation of protein crystals. Precipitate appeared directly upon mixing but even after 1.5 months no crystals were detectable. After more than one year a phase separation could be seen in these trials. The origin of this phase separation is not clear as it also appeared in control trials without CF_oF_1 after one year.

Washing buffer seven did not produce any crystals of CF_oF_1 as well. This buffer is based on WB six with the addition of 1 mM EDTA (pH 7.0). Upon mixing the protein solution with crystallisation buffer the precipitate appeared as usual but no crystals formed. Even after more than one year no crystals were present and no phase separation or salt crystals were obtained.

After no more than two weeks, crystals appeared in trials using washing buffer eight. They are numerous and small compared to those produced with washing buffer four. The two buffers

differentiate from each other in the buffer component and the detergent, 25 mM bis-tris-propane (pH 6.5) and 35 mM C-HEGA-10 in WB eight versus 25 mM tricine (pH 8.0) and 0.1% (w/v) dodecyl maltoside in WB four. The crystals are large enough for diffraction measurements. Dimensions are between 10 µm and 20 µm and the crystals had cubic-like shape. Some single crystals formed between the micro crystals and reached dimensions between 50 and 100 µm after one or more months.

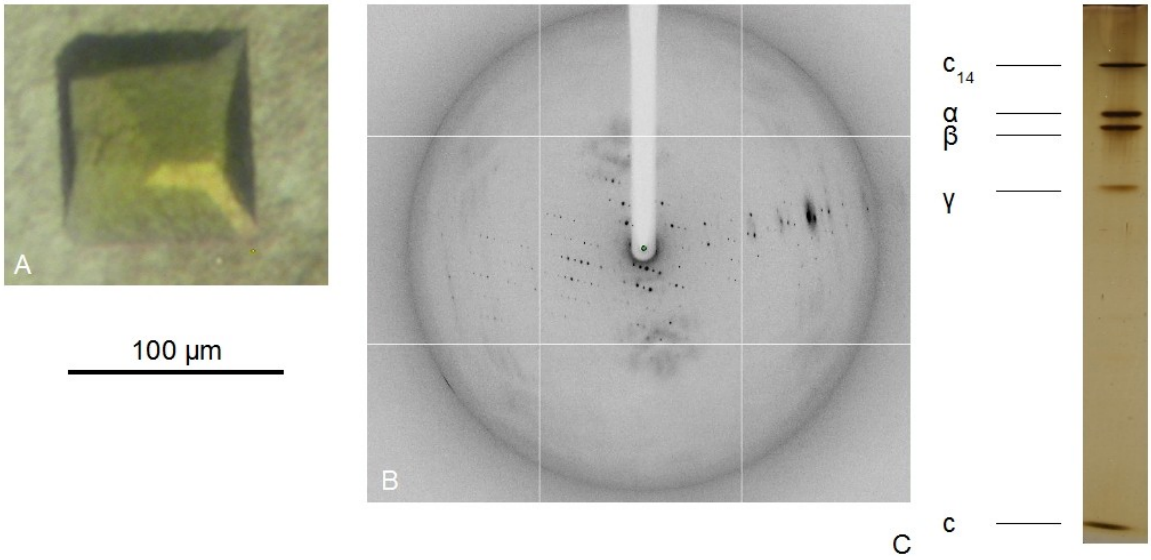

Figure 4.8: (A) Crystal grown from 5 mg/ml CF_oF_1 in WB 8 with a crystallisation buffer composed of 30% (v/v) PEG 400, 100 mM $CdCl_2$, 100 mM $LiCl_2$, 100 mM sodium acetate (pH 4.6/HCl) plus 4 mM ADP (pH 8.0) at 15°C; dimensions: 80 x 80 x 80 µm; (B) diffraction image; spots at a maximum resolution of 3.8 Å; detector: ADSC-Q315r (ID23-1); (C) corresponding 15% SDS-PAGE of the crystal (A)

Figure 4.8 shows a protein crystal and corresponding diffraction image as well as SDS-PAGE grown in crystallisation trial with WB eight. This crystal diffracted to a maximum resolution of 3.8 Å. The SDS-PAGE revealed subunits *α*, *β*, and *γ* of CF_1 and subunit *c* as monomer and 14mer.

Washing buffer 11 was used for intensive screening experiments like washing buffer four. As outlined in 4.1.2. Each of these two buffers provides an environment for CF_oF_1 that either supports the protonated or deprotonated state of the proton binding site in the *c*-ring. In WB 11 25 mM sodium acetate (pH 4.6) replaces 25 mM tricine (pH 8.0) in WP four. Protein crystals grown in the presence of the former buffer (see Figure 4.9 (A)) diffracted to a maximum resolution of 3.3 Å. The corresponding SDS-PAGE reveals subunit *c* as well as very small and thin bands for subunits *α* and *β*.

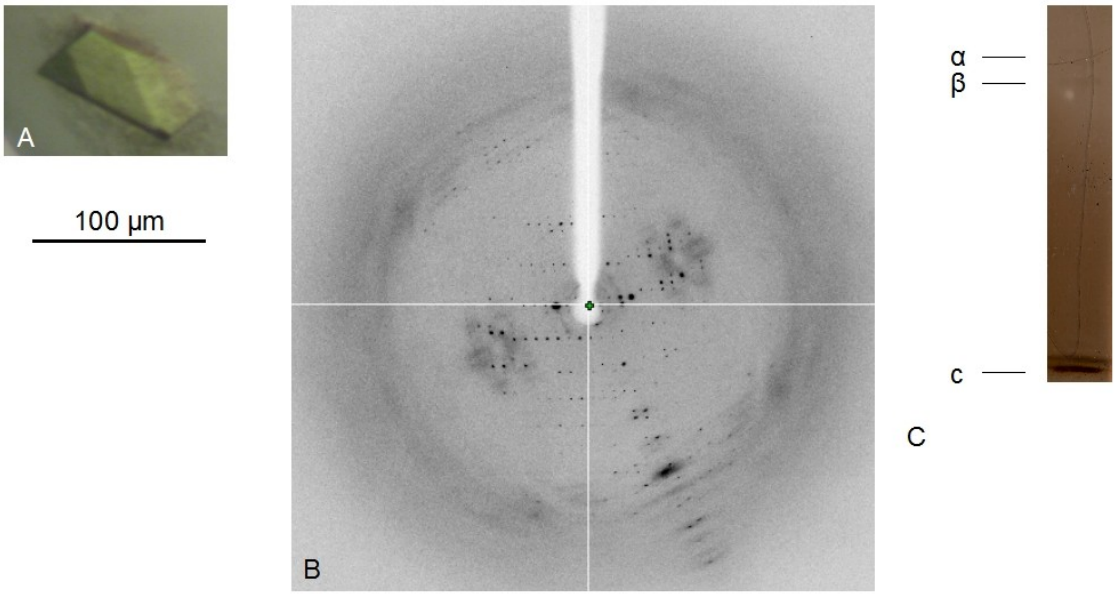

Figure 4.9: (A) Crystal grown from 6 mg/ml CF_oF_1 in WB 11 with a crystallisation buffer composed of 30% (v/v) PEG 400, 100 mM $CdCl_2$, 100 mM sodium acetate (pH 4.6/HCl) plus 4 mM ADP (pH 8.0) at 15°C; dimensions: 70 x 40 x 30 µm; (B) diffraction image; spots at a maximum resolution of 3.3 Å; detector: MAR-MOSAIC (ID23-2, micro focus); (C) corresponding 15% SDS-PAGE of the crystal in (A)

Except additional 0.1% (w/v) phosphatidyl choline (PC) washing buffer 12 had the same composition as buffer four. WB 12 could not be used to achieve the desired CF_oF_1 concentration of at least 6 mg/ml. Consequently WB 12 was combined with WB four. The CF_oF_1 complex was concentrated in buffer four and then diluted to a protein concentration of 6 mg/ml with buffer 12. This resulted in a phosphatidyl choline concentration of 0.03% (w/v). Upon mixing with crystallisation buffer precipitation was observed. Prolonged incubation time of about one year, did not result in crystal formation.

Washing buffer 14 discerns from WB 11 in that way that glycerol 10% (w/v) in WB 11 is replaced by sucrose 10% (w/v). Protein crystals appeared after two weeks with dimensions of about 50 µm. The crystals grew in a mixture of single crystals and micro crystals. Compared to WB 11 amorphous crystals appeared in the presence of WB 14, which had overgrown the protein crystals within a couple of days.

CF_oF_1 in washing buffers eight and 11 resulted in diffracting protein crystals of similar quality. Data sets of protein crystals grown in the presence of each of the two buffers are compared in 4.2.11. Consequently washing buffer 15 was created on the basis of WB eight and 11. 25 mM sodium

acetate (pH 4.6) was taken from WB 11 and the detergent C-HEGA-10 (35 mM) as in WB eight. Such a composed buffer forced the protein to precipitate during the concentration step. Complete precipitation was achieved after over night storage at 4°C.

For detailed screening of crystallisation buffers, additives, and inhibitors WB four and WB 11 were used in first instance. The results of these screenings were then applied to trials with CF_oF_1 in WB eight, as formed protein crystals showed less anisotropy than buffers four and 11.

4.2.2. Analysis of Precipitate

Analysis of protein crystals grown from CFoF1 in various buffer combinations show different subunit composition on a SDS-PAGE. The precipitate was also analysed on a SDS-PAGE as it may be present on the crystal surface and give a false positive result. In addition crystals washed in crystallisation buffer was run on a gel for comparison.

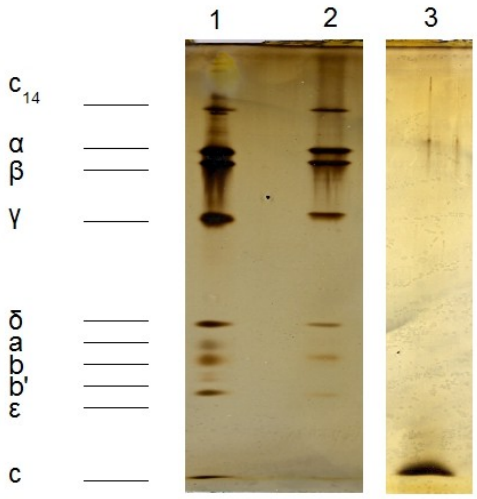

Figure 4.10: SDS-PAGE (15%) to analyse precipitate; (1) CF_oF_1 standard; (2) precipitate; (3) washed crystal

A crystal after washing shows only subunit c on a SDS-PAGE (3), whereas precipitate contains almost any other subunit (2).

4.2.3. Effect of Protein Concentration

Protein concentrations from 2-10 mg/ml were tested. Concentrations higher than 6 mg/ml produced high quantities of small crystals with dimensions between 10 and 20 µm. Protein concentrations less than 6 mg/ml produced mainly single crystals with dimensions between 50 and 100 µm. Less than 10 crystals grew in each well. They were easy to harvest with nylon loops and were used for diffraction experiments. Surrounding precipitate was not removed in all experiments. For washing buffer four and 11 the standard concentration for experiments was set to 6 mg/ml and for washing buffer eight to 5 mg/ml.

4.2.4. Effect of Temperature

Temperatures of 4°C, 10°C, 15°C, and 20°C were generally used for crystallisation. Additionally, a temperature gradient was tested for washing buffer 11 in hanging drop and microbatch. Transfers between 4° and 20°C as well as between 10°C and 15°C were tested.
Experiments done at 4°C and 10°C did not produce crystals. A temperature of 15°C produced protein crystals in four days for washing buffer four, eight, and 11. At 20°C the protein crystals appeared as quick as at 15°C, but were usually larger and more amorphous. The temperature gradient done for CF_oF_1 in washing buffer 11 lead to formation of three dimensional protein crystals in a temperature range from 16°C to 18°C. At higher temperatures, the crystals were amorphous and salt crystals formed as well. Trials at lower temperatures showed only precipitate. Transfers between different temperatures had no effect on the crystallisation process. A temperature of 15 °C was set as standard as it widely used for protein crystallisation.

4.2.5. Effect of Crystallisation Buffers

A list of crystallisation buffers tested, can be found in the Appendix 7.2. Crystallisation buffers resulting in crystal formation are mentioned here and in Chapter 4.2.6. The remaining buffers in the list were not successfully tested. The standard crystallisation buffer in combination with washing

buffers four and 11 contained 30% (v/v) PEG 400, 100 mM $CdCl_2$, and 100 mM sodium acetate (pH 4.6/HCl). For WB eight 100 mM $LiCl_2$ were added to the standard buffer. If lithium chloride was missing in buffer eight, no crystals appeared. Additional lithium chloride in buffers four and 11 avoided the formation of protein crystals.

An incomplete factorial screen was set up on the basis of the standard crystallisation buffer. The pH of the crystallisation buffer was kept constant whereas concentrations of PEG 400, cadmium chloride, and sodium acetate were varied in a small range. All three changed variables were combined with each other. Within the chosen ranges, 28-32%(v/v) PEG 400, 90-110 mM cadmium chloride, and 90-110 mM sodium acetate, no combination was identified that significantly improved the crystallisation process.

Very important is the acid or base used for adjustment of the pH. The use of acetic acid for pH adjustment instead of hydrochloric acid resulted in protein crystals with amorphous shape. The incubation time was at least two weeks and the reproducibility was low. Using hydrochloric acid resulted in protein crystal formation within four days. Five to ten single crystals grew per well, showed a regular shape, and dimensions between 50 and 100 µm. The reproducibility was high.

Commercial screens were used in combination with a pipetting robot to accelerate the screening procedure. However, none of the tested crystallisation buffers (see Appendix 7.2) produced crystals. Commercial screens were used in micro batch and sitting drop trials only.

4.2.6. Additives and Inhibitors

A standard additive to stabilise the CF_oF_1 holo-enzyme is ADP. ADP was included in all trials and was tested in concentrations of 20 µM and 1-4 mM.

For washing buffer four a concentration of 4 mM ADP resulted in appearance of 10 to 20 single protein crystals per well after 14 days. The crystal dimensions were between 10 and 30 µm. Over some time, the crystals grew to maximum edge dimensions of about 80 µm. ADP concentrations of 20 µM did not result in formation of protein crystals. In a concentration between 1 to 3 mM the incubation time was extended up to two months. For crystallisation trials of CF_oF_1 in washing buffer four the standard ADP concentration was set to 4 mM.

The standard ADP concentration found in combination with WB four was used in the starting trials of CF_oF_1 in WB 11. In the first attempts addition of 4 mM ADP in washing buffer 11 resulted in

protein crystals with dimensions of 20 to 50 µm, which appeared after 4 days. In lower ADP concentrations a few single crystals, usually less than five per well, could be grown. They reached a similar size as in the presence of 4 mM ADP, but only over several months. For washing buffer 11 the standard ADP concentration was also set to 4 mM.

For CF_oF_1 in washing buffer eight starting trials were set up with 4 mM ADP. Protein crystals appeared after four days in a large amount of microcrystals. Lowering the ADP concentration to 3 mM lead to the appearance of a mixture of single crystals and microcrystals. The crystals still appeared after 4 days with dimensions of 100 µm for the single crystals. An ADP concentration of 3 mM was set as standard for crystallisation trials of CF_oF_1 in washing buffer eight.

An ADP concentration of 4 mM could be used over a protein concentration range from 2 to 10 mg/ml. In control trials with a pH range from 2.0 to 6.5, ADP was precipitating. The precipitation was more pronounced and appeared quicker at lower pH values. This suggests that precipitation upon mixing of crystallisation buffer and protein solution is not only caused by the protein itself.

Spermine was tried with CF_oF_1 in washing buffers four, eight, and 11 in combination with the corresponding standard crystallisation buffer. Furthermore, spermine was combined with the inhibitors DCCD, phloretin, and phloridzin. Protein crystals grown of any of these conditions generally had a regular and three dimensional shape. Spermine assured the appearance of crystals after a few days but had no effect on the diffraction quality.

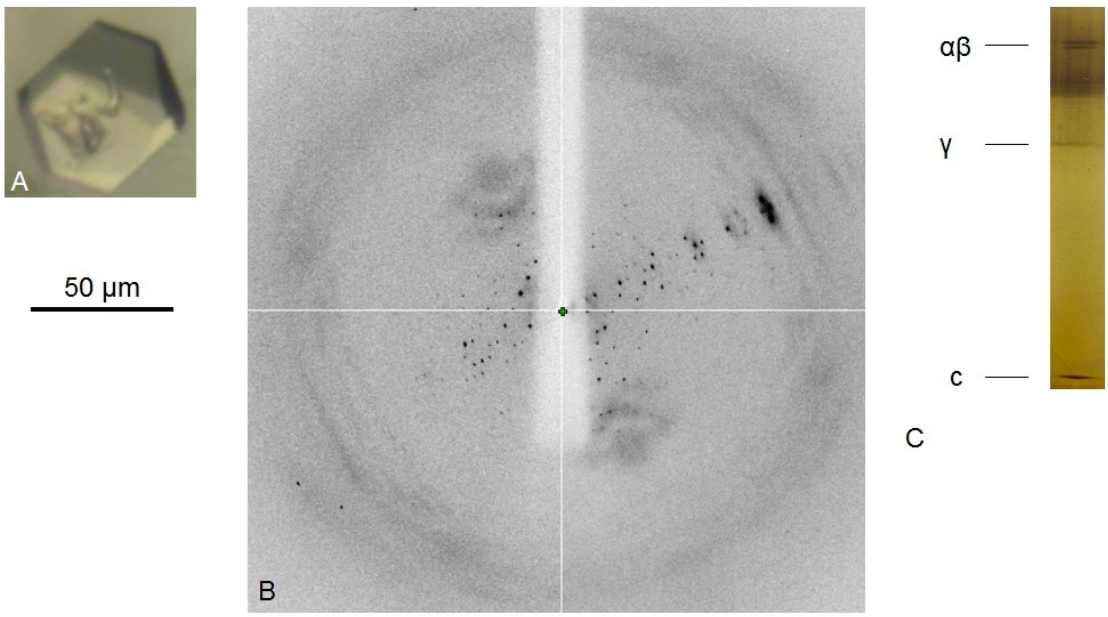

Figure 4.11: (A) Crystal grown from 6 mg/ml CF_oF_1 in WB 11 with a crystallisation buffer composed of 30% (v/v) PEG 400, 100 mM $CdCl_2$, 100 mM sodium acetate (pH 4.6/HAc) plus 4 mM ADP (pH 8.0), 10 mM spermine at 15°C; dimensions: 50 x 60 µm; (B) diffraction image; spots at a maximum resolution of 5.0 Å; detector: MAR-MOSAIC (ID32-2); (C) corresponding 15% SDS-PAGE of the crystal in (A)

The crystal in Figure 4.11(A) was grown in the presence of 10 mM spermine. Its analysis with diffraction image and SDS-PAGE revealed a maximum resolution of 5.0 Å and a subunit composition of α, β, and γ of CF_1 as well as *c* of CF_o.

DCCD (N,N'-dicyclocarbodiimide) is known as a specific inhibitor for the transmembrane *c*-ring of proton translocating F-ATPases. The molecule is very hydrophobic and can therefore diffuse through the membrane very easily. When it comes into proximity of a glutamate or aspartate at the proton binding site in the *c*-ring, it accepts the proton if present. After an intermediate state, DCCD binds covalently to the glutamate or aspartate in the binding site, which completely inhibits the enzyme. Concentrations of 25, 50, 100, and 150 µM were tested with CF_oF_1 in different washing buffers and in combination with other additives and inhibitors. Generally, the protein crystals tend to have a more amorphous shape and have a yellow colour compared to those grown under native conditions. Both characteristics were most pronounced after a long incubation time of several months.

For CF_oF_1 in washing buffer four and 11 protein crystals in presence of DCCD appeared as quickly

as native crystals but tend to be slightly smaller in the beginning. Over time, they increased in size and were as large as native protein crystals. Washing buffers four and 11 were tested at concentrations of 50, 100, and 150 mM DCCD. Most successful were the trials in the presence of 50 mM DCCD. Five to 10 single crystals appeared after four days like in native trials and had a defined shape. Increased concentrations of DCCD yielded high amounts of micro crystals with an amorphous shape.

For trials of CF_oF_1 in washing buffer eight the initial DCCD concentration was set to 150 µM on the basis of the results for buffers four and 11. But the crystals appeared as micro crystals with amorphous shape so that the DCCD concentration was reduced to 50 µM for trials with buffer eight.

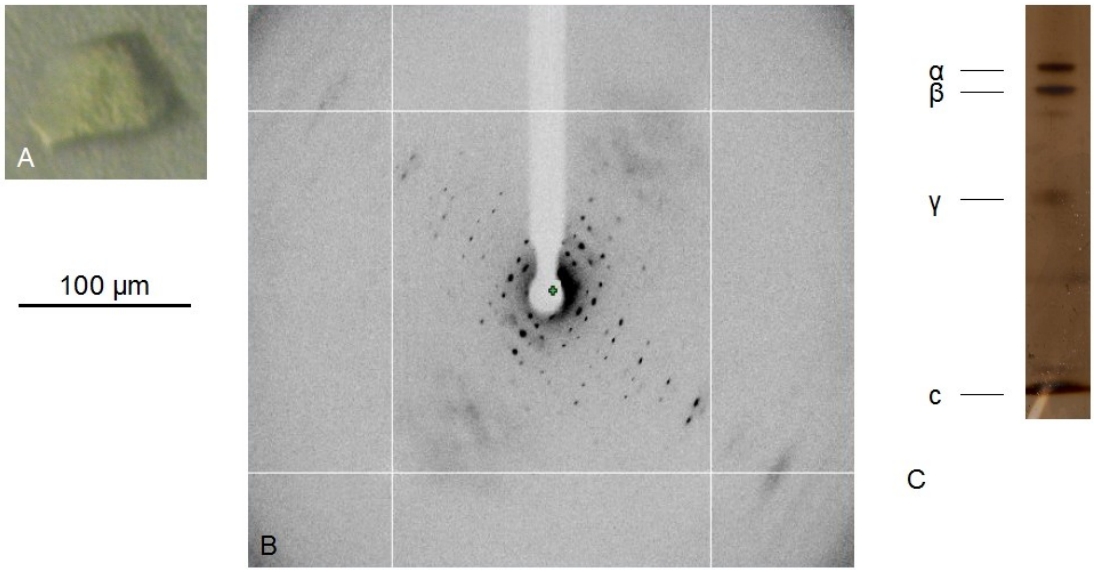

Figure 4.12: (A) Crystal grown from 6 mg/ml in WB 11 with a crystallisation buffer composed of 30% (v/v) PEG 400, 100 mM $CdCl_2$, 100 mM sodium acetate (pH 4.6/HCl) plus 4 mM ADP (pH 8.0), 50 µM DCCD at 15°C; dimensions: 70 x 40 µm; (B) diffraction image; spots at a maximum resolution of 4.8 Å; detector: ADSC-Q315r (ID14-4); (C) corresponding 15% SDS-PAGE of crystal (A)

Figure 4.12(A) shows a protein crystal grown in the presence of 50 µM DCCD. The corresponding diffraction images shows a maximum resolution of 4.8 Å and the SDS-PAGE reveals a subunits *α*, *β*, *γ*, and *c*. A data set was taken of a crystal grown of washing buffer 11 in combination with 30% (v/v) PEG 400, 100 mM $CdCl_2$, 100 mM sodium acetate (pH 4.6/HCl) with either 50 or 150 µM DCCD. Additionally a data set was taken with a combination of 50 µM DCCD and 10 mM spermine and identical buffer combination as mentioned above. As the example in Figure 4.12

shows, the SDS-PAGE reveals subunits α, β, and γ from F_1 and subunit *c* from F_o as crystal content. Phloridzin and phloretin are proposed to be inhibitors for ATP synthase. Phloretin was used at concentrations of 50, 100, and 150 µM and in combination with CF_oF_1 in washing buffer 11. Only diffraction images taken from protein crystals grown in the presence of 50 and 150 µM phloretin could be indexed. A data set was taken from a protein crystal grown in 150 µM phloretin. Phloridzin, the glucose derivative of phloretin, was only used in a concentration of 70 µM for CF_oF_1 in WB four and 11. In all trials in the presence of phloretin or phloridzin protein crystals appeared after four days. This result was independent of the inhibitor concentration used. Higher concentrations of phloretin produced a larger number of slightly smaller protein crystals. For 50 µM phloretin and 70 µM phloridzin the crystals had dimensions of about 50 µm.

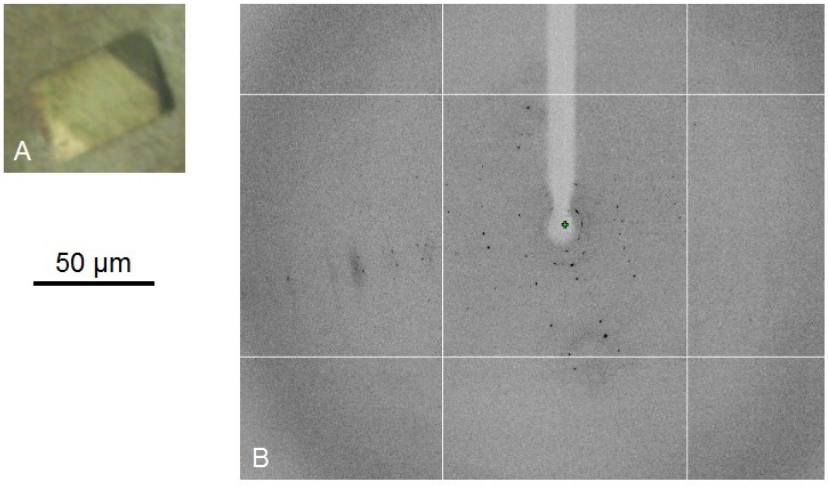

Figure 4.13: (A) Crystal grown from 6 mg/ml CF_oF_1 in WB 11 with a crystallisation buffer composed of 30% (v/v) PEG 400, 100 mM $CdCl_2$, 100 mM sodium acetate (pH 4.6/HCl) plus 4 mM ADP (pH 8.0), 50 µM phloretin at 15°C; dimensions: 50 x 30 µm; (B) diffraction image; spots at a maximum resolution of 3.8 Å; detector: ADSC-Q315r (ID14-4);

For both, phloretin and phloridzin, protein crystals were grown from CF_oF_1 in WB eight. In a first attempt only 150 µM phloretin and 70 µM phloridzin were tested. In both cases a large amount of micro crystals appeared after four days. Consequently, the experiment was repeated with 50 µM phloretin and 25 µM phloridzin. Protein crystals still appeared after four days but next to the micro crystals also bigger single crystals were found, with dimensions of about 30 µm. A data set was taken from a protein crystal grown from CF_oF_1 in WB eight and 25 µM phloridzin. Spots in diffraction images taken from a protein crystal grown in the presence of phloretin or phloridzin

were generally finer and sharper than in images taken from native crystals. For the crystal in Figure 4.14 subunits α, β, and γ from CF_1 and subunit *c*, as monomer or 14mer from subunit F_o are identified on a SDS-PAGE as crystal content.

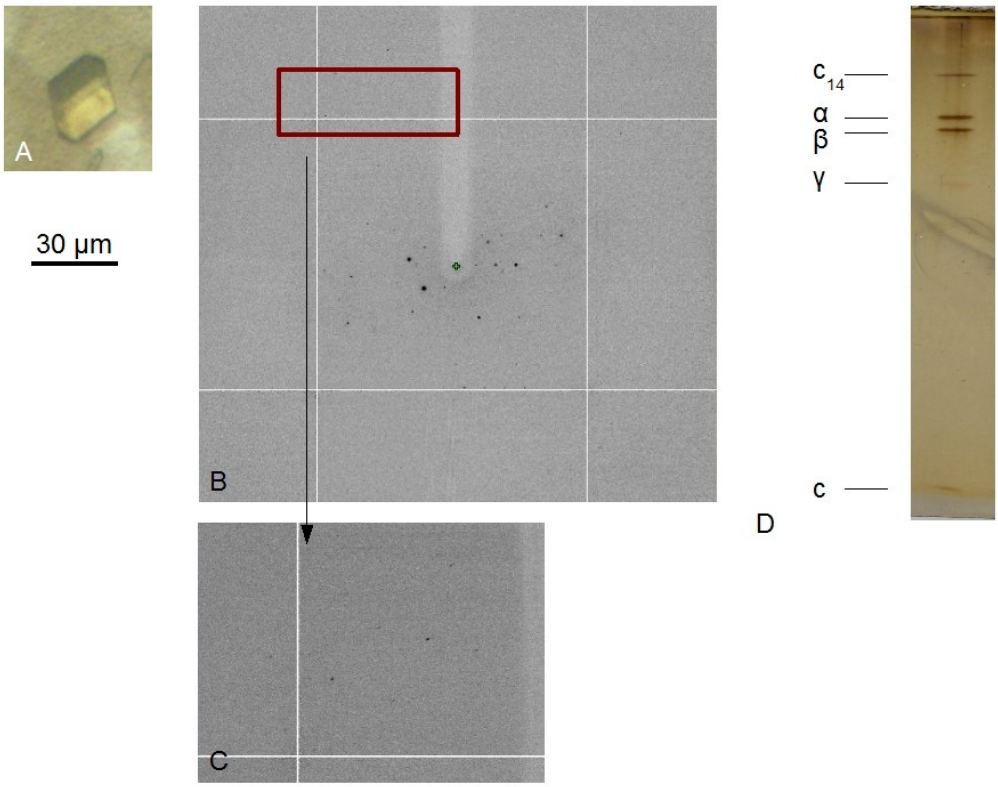

Figure 4.14: (A) Crystal grown from 6 mg/ml in WB 11 with a crystallisation buffer composed of 30% (v/v) PEG 400, 100 mM $CdCl_2$, 100 mM sodium acetate (pH 4.6/HCl) plus 4 mM ADP (pH 8.0), 70 µM phloridzin, at15°C; dimensions: 30 x 30 µm; (B) diffraction image; spots at a maximum resolution of 4.4 Å; (C) zoomed area with sharp and fine spots; detector: ADSC-Q315r (ID14-4); (D) corresponding 15% SDS-PAGE of the crystal in (A)

4.2.7. Cation Screening

This screening was set up to search for another suitable di- or trivalent cation, which may improve the crystallisation of the *c*-ring compared to cadmium chloride. The crystallisation results for CF_oF_1 in WB four and 11 are presented here, but only for the latter one diffraction data are available. The additive used was 4 mM ADP (pH 8.0) in all trials.

Results for washing buffer four:

Table 4.1: Magenta labels indicate crystals suitable for diffraction analysis

Salt	Crystallisation result (mM)			
	50	100	150	200
$CrCl_2$	-	-	+	+
$CuSO_4$	+	+	+	+
$CoCl_2$	-	+	-	-
$LiSO_4$	-	-	-	-
$ZnCl_2$	-	+	+	+
$CerCl_2$	+	+	+	+
$MgSO_4$	-	-	-	-
Fe^{3+}-III-Cl_3	-	-	-	+
$MnCl_2$	-	-	-	-
$Mg(CH_3COO^-)_2$	-	-	-	-
Fe^{2+}-II-Cl_2	-	+	+	
$Li(CH_3COO^-)_2$	-	-	-	-
$CuCl_2$	+	+	-	+
$NiSO_4$	+	+	+	+
$HgCl_2$	-			
Fe^{2+}-II-SO_4	-	-	-	-

A pH of 8.0 in washing buffer four creates a basic environment and favours the deprotonated conformation of the *c*-monomers. The indication as suitable for diffraction analysis means that the protein crystals grew with dimensions between 10 and 30 µm, which can easily be used in diffraction experiments. Crystals appeared within four days, except those grown in a crystallisation buffer containing iron III chloride, for which a incubation time of about four weeks was necessary. All protein crystals had the same shape as crystals grown in standard conditions, except those grown in the presence of either cerium chloride or iron III chloride. Corresponding pictures of these protein crystals grown either in the presence of cerium chloride or iron III chloride can be found below. *c*-ring crystals in the presence of chrome chloride or cobalt chloride only appeared for CF_oF_1 in washing buffer four. It seems that these divalent cations are more likely to produce *c*-ring crystals if CF_oF_1 is provided in a basic washing buffer.

Results for washing buffer 11:

Table 4.2: Magenta labels indicate crystals suitable for diffraction analysis

Salt	Crystallisation result (mM)				a	b	c	α	β	γ	Resolu-
	50	100	150	200	(Å)	(Å)	(Å)	(°)	(°)	(°)	tion (Å)
$CrCl_2$	-	-	-	-	-	-	-	-	-	-	-
$CuSO_4$	-	+	+	+	157.3	101.2	130.7	90	109.7	90	3.3
$CoCl_2$	-	-	-	-	-	-	-	-	-	-	-
$LiSO_4$	-	-	-	+	-	-	-	-	-	-	-
$ZnCl_2$	-	-	+	+	-	-	-	-	-	-	-
$CeCl_2$	+	+	+	-	Indexing not possible						20
$MgSO_4$	-	-	-	+	-	-	-	-	-	-	-
Fe^{3+}-III-Cl_3	-	-	+	+	-	-	-	-	-	-	-
$MnCl_2$	-	-	-	+	-	-	-	-	-	-	-
$Mg(CH_3COO^-)_2$	-	-	-	+	-	-	-	-	-	-	-
Fe^{2+}-II-Cl_2	-	+	+		-	-	-	-	-	-	-
$Li(CH_3COO^-)_2$	-	-	-	+	-	-	-	-	-	-	-
$CuCl_2$	+	-	-	+							
$NiSO_4$	+	-	+	-	Indexing not possible						20
$HgCl_2$	-				-	-	-	-	-	-	-
Fe^{2+}-II-SO_4	-	-	-	+	-	-	-	-	-	-	-

Washing buffer 11 with sodium acetate and a pH of 4.6 provides a acidic environment, which facilitates the protonation of the c-ring. Crystals of the c-ring grown from this washing buffer in combination with the standard crystallisation buffer but different cations appeared after four days, except for present iron III chloride with about four weeks incubation time. In the presence of cerium chloride as well as iron III chloride a new form for *c*-ring crystals was found (see Figure 4.18(B)). The magenta label indicates crystallisation results for protein crystals having dimensions between 10 and 30 µm. Some of the crystals were tested in diffraction experiments. Diffraction images collected for *c*-ring crystals grown in the presence of nickel sulphate or cerium chloride revealed a maximum resolution of 20 Å. However, indexing was not possible so no information about unit cell dimensions is available. Diffraction images collected for *c*-ring crystals in the presence of copper sulphate revealed very fine and sharp spots with a maximum resolution of 3.3 Å. The reference image shown in Figure 4.16 and the collected data set will be discussed in more detail in Chapter 4.2.12.

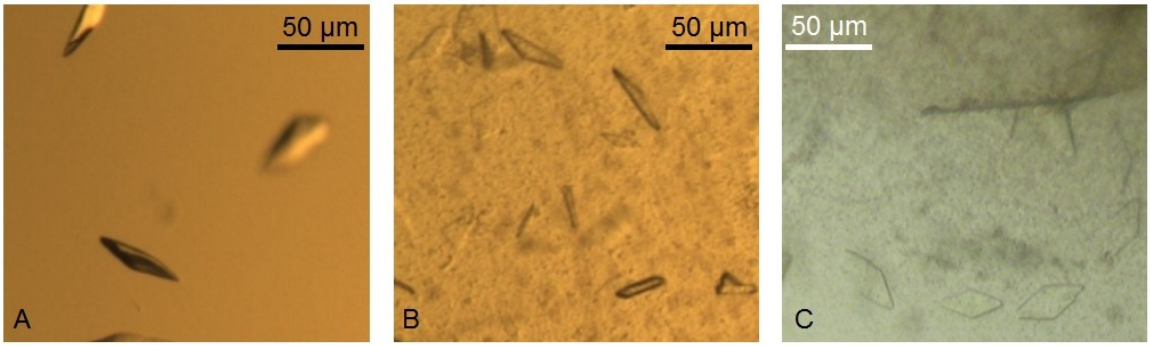

Figure 4.15: (A) Crystals grown from 6 mg/ml CF_oF_1 in WB 4 with a crystallisation buffer composed of 30% (v/v) PEG 400, 100 mM Fe^{3+}-III-Cl_3, 100 mM sodium acetate (pH 4.6/HCl) plus 4 mM ADP (pH 8.0) at 15°C; (B) Crystals grown from 6 mg/ml CF_oF_1 in WB 11 with a crystallisation buffer composed of 30% (v/v) PEG 400, 100 mM Fe^{3+}-III-Cl_3, 100 mM sodium acetate (pH 4.6/HCl) plus 4 mM ADP (pH 8.0) at 15°C; (C) Crystals grown from 6 mg/ml CF_oF_1 in WB 11 with a crystallisation buffer composed of 30% (v/v) PEG 400, 100 mM $CeCl_2$, 100 mM sodium acetate (pH 4.6/HCl) plus 4 mM ADP (pH 8.0), 15°C; (A) - (C) crystal dimensions: 20 x 50 µm

c-ring crystals grown from CF_oF_1 in washing buffer four in combination with cerium chloride in the crystallisation buffer looked identical to those presented for a combination with washing buffer 11 in Figure 4.15 (C).

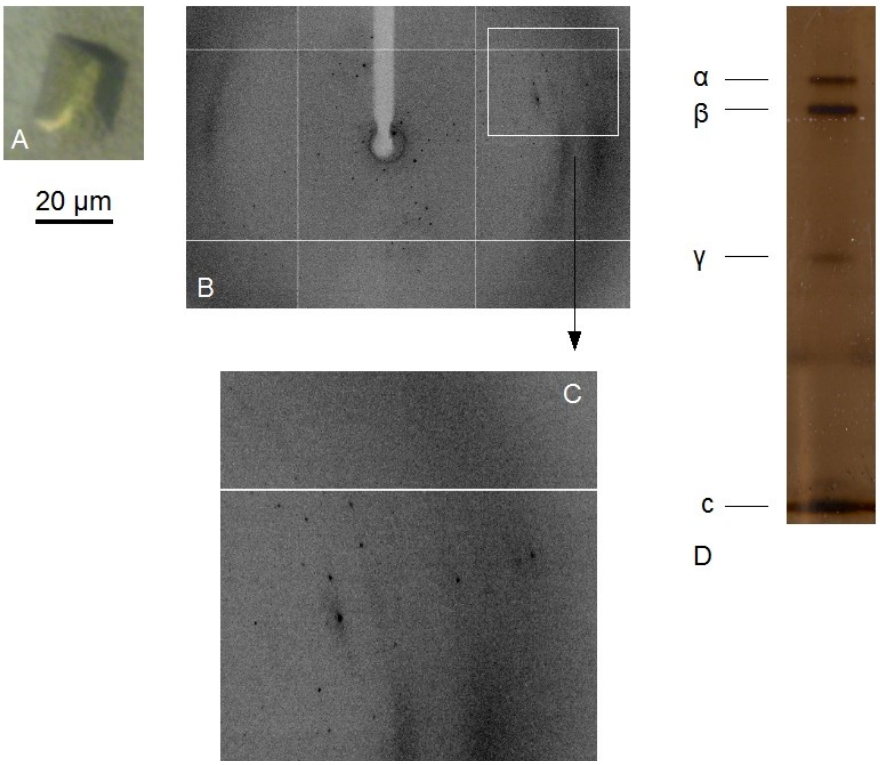

Figure 4.16: (A) Crystal grown from 6 mg/ml CF_oF_1 in WB 11 with a crystallisation buffer composed of 30% (v/v) PEG 400, 100 mM $CuSO_4$, 100 mM sodium acetate (pH 4.6/HCl) plus 4 mM ADP (pH 8.0) at 15°C; (B) diffraction image; spots at a maximum resolution of 3.3 Å; detector: ADSC-Q315r (ID14-4); (C) zoomed area with sharp and fine spots; (D) corresponding 15% SDS-PAGE of the crystal in (A)

4.2.8. Effect of the Crystallisation Method

Sitting drop experiments were set up by hand, with and without micro bridges, and additionally with a pipetting robot. In the hanging drop setup, trials were always done by hand, either with cover slips and grease in tissue culture plates (Greiner) or in Nextal® Easy Xtal plates (QIAGEN). The microbatch method was done as combination of pipetting robot and 96wells Imp@ct plates (Greiner) or by hand in 60/72wells Terasaki plates. Except for the setup using the robot all each method applied resulted in protein crystals. The results given are for washing buffer 11 with standard crystallisation buffer (30% (v/v) PEG 400, 100 mM $CdCl_2$, 100 mM sodium acetate (pH 4.6/HCl)) and 4 mM ADP (pH 8.0).

Experiments with the microbatch method usually needed long incubation times. Protein crystals

appeared after several months and had dimensions of 10 to 50 µm. In combination with the pipetting robot no protein crystals formed.

In sitting drop experiments the crystals appeared after about two weeks if micro bridges were used. The micro bridges were combined with 24 well tissue culture plates (Greiner), and grease was used to seal the setup. Protein crystals grown in the micro bridge setup had only low reproducibility but still reached dimensions of 10 to 50 µm. If sitting drop was combined with the pipetting robot, no crystal growth was observed.

The first trials with hanging drop used 24 well tissue culture plates (Greiner), glass cover slips, and grease as seal. Crystals appeared after about one week, only slightly quicker than with the sitting drop method. The reproducibility was again very low like in the sitting drop method. A significant improvement of the crystallisation process could be seen with the use of Nextal® Easy Xtal plates. Protein crystals appeared after four days and with dimensions of 50 µm. The reproducibility was very high and almost every trial resulted in five to ten crystals per well. In a standard trial the reservoir contained 400 µl and the drop consisted of 3 µl protein solution and 3 µl crystallisation buffer. Hanging drop in Nextal® plates was the standard method used for screening of buffer conditions and additives. After an incubation time of about two weeks dimensions of about 100 µm could be achieved whereas in experiments with microbatch and sitting drop method no significant dimension increase could be recorded.

4.2.9. Effect of Drop and Reservoir Volume

Different volumes for the protein-crystallisation buffer mixture and for the reservoir were tested. Crystallisation buffer and protein were always mixed in equal amounts to a final volume of 2, 4, 5, and 6 µl. Crystals appeared in every volume but they differed in size and number.

For CF_oF_1 in washing buffer four and 11 at standard conditions, crystals grew in a volume of 2, 4 or 5 µl. Maximum dimensions of about 30 µm were obtained in volumes of 2 and 4µl. Protein crystals grown in a final drop volume of 5 µl had slightly bigger dimensions of about 50 µm. With a volume of 6 µl the crystals showed dimensions between 50 and 80 µm. The protein crystals appeared after four days in any drop volume. In smaller volumes, 2 and 4 µl, numerous crystals appeared, but only five to ten single crystals grew in volumes of 5 and 6 µl. Crystallisation trials with CF_oF_1 in washing buffer eight were directly started with a final volume of 6 µl. Combinations with drop volumes of 2

and 4 µl together with reservoir volumes of 300, 400, 500, 600, and 700 µl were tested. A reservoir size from 300 to 500 µl didn't effect the crystal growth significantly. The crystals appeared after a couple of days with dimensions of 30 to 50 µm. Using a reservoir volume of 600 or 700 µl didn't produce crystals at all. Both volumes, 600 and 700 µl, were combined with 2 and 4 µl protein-crystallisation buffer mixtures and with CF_oF_1 in washing buffer four and 11. In none of the trials was crystal growth observed.

Sitting drop setups using a pipetting robot had a reservoir volume of 70 µl and a drop size of 2 µl. No crystals grew in the automated setup. For sitting drop experiments done with micro bridges the volume for the reservoir was kept constantly at 400 µl, which had given the best results in hanging drop trials. Drop sizes of 2 and 4 µl were tested. The resulting crystals were smaller as for the same volume combinations in the hanging drop experiment. Maximum dimensions were about 30 µm and only a couple of crystals per well appeared after four days.

In the microbatch method drop volumes of 2, 4, and 5 µl were tested. Limitation was given by the well volume. Tests were done for CF_oF_1 in washing buffers four and 11. The drop volume didn't show any effect on the crystal size. Different drop volumes had no effect on the incubation time of about two months for the appearance of the first crystals. Crystals grown after a couple of months were generally smaller than for the other methods. This was independent of the drop volume chosen for the protein-crystallisation buffer mixture. Maximum dimensions reached in the microbatch method were 30 µm.

4.2.10. Dehydration Experiments

The aim of dehydration experiments was to receive a tighter packing within the crystal lattice by reducing the water content. Protein crystals are traversed by aqueous channels, which form as a result of unit cell stacking. The experiments were done for crystals grown from CF_oF_1 in washing buffer 4 and 11 in combination with standard crystallisation buffer. In first trials a protein crystal was taken from the drop and transferred to a dehydration buffer, which had the same composition as the crystallisation buffer except a higher PEG 400 concentration. PEG 400 is small enough to diffuse freely within the aqueous channels and partly replace the water molecules. The crystal lattice was disrupted with this procedure as indicated by visible cracks throughout the crystals.

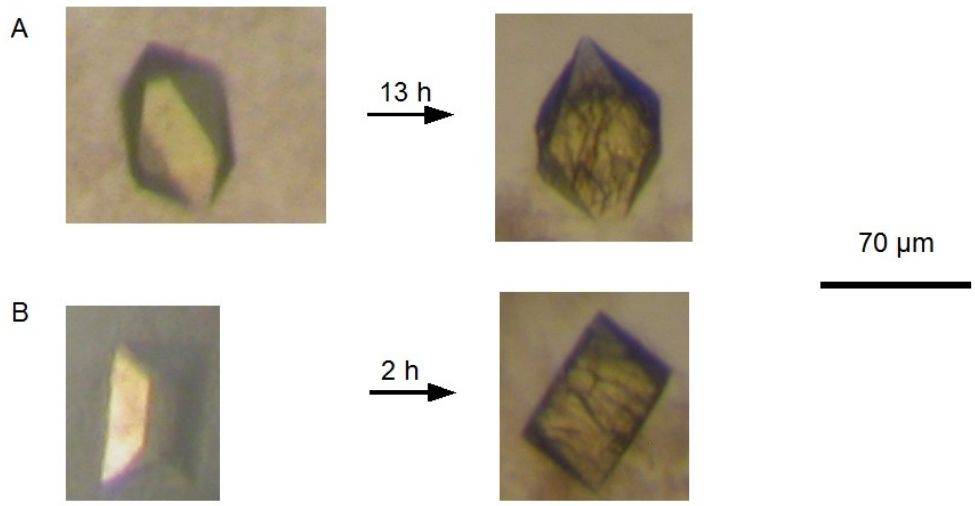

Figure 4.17: (A) Crystal grown from 6 mg/ml CF_oF_1 in WB 11 with a crystallisation buffer composed of 30% (v/v) PEG 400, 100 mM $CdCl_2$, 100 mM sodium acetate (pH 4.6/HCl) plus 4 mM ADP (pH 8.0) at 15°C; incubated for 13 h in a drop containing 40% (v/v) PEG 400 at 20°C; (B) Crystal grown from 6 mg/ml CF_oF_1 in WB 11 with a crystallisation buffer composed of 30% (v/v) PEG 400, 100 mM $CdCl_2$, 100 mM sodium acetate (pH 4.6/HCl) plus 4 mM ADP (pH 8.0) at 15°C; for 2 h in a drop with pure crystallisation buffer at 20°C

Alternatively not a single crystal was transferred into the dehydration buffer, instead the complete drop containing the crystal was transferred over a well filled with a dehydration buffer. The reservoir contained 400 µl of crystallisation buffer with increasing PEG 400 concentrations. Every 12 hours the drop was moved to a well with a 5% higher PEG 400 concentration. After the last step the drop had shrunk reasonably and the crystals didn't show any cracks. The precipitate dehydrated as well and showed to be highly viscous. As a result the crystal couldn't be separated from the precipitate. Additionally amorphous salt and protein crystals grew which made crystal harvesting more difficult.

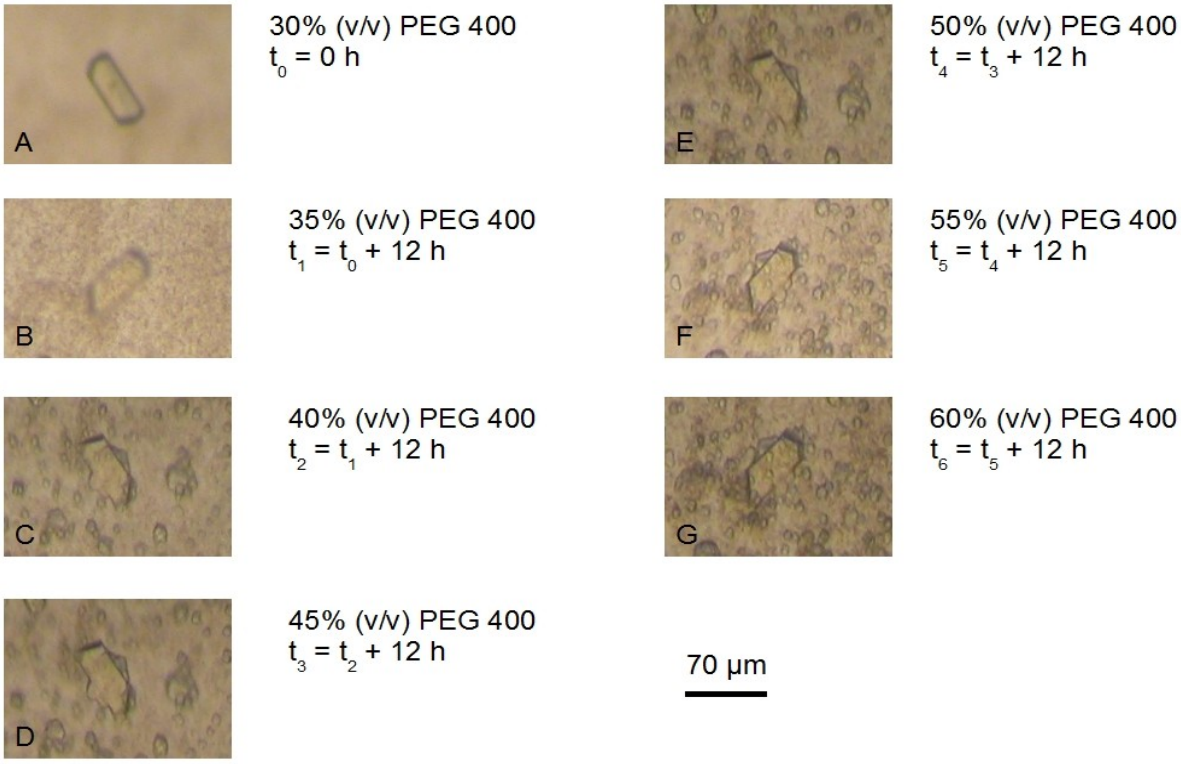

Figure 4.18: Crystal grown in WB 11; 6 mg/ml, 4 mM ADP (pH 8.0), 15°C; 30% (v/v) PEG 400, 100 mM $CdCl_2$, 100 mM sodium acetate (pH 4.6/HCl); percentages (v/v) give the increasing concentrations of PEG 400 other components are kept constant corresponding to standard crystallisation buffer; changes were always done after 12 h

4.2.11. Effect of Cryo Buffers and Annealing

A detailed screening for cryo buffers was done at beamline X12 at EMBL (Hamburg). The standard crystallisation buffer contains 30% (v/v) PEG 400. In the protein buffer 10% (w/v) glycerol is present. So in general no additional cryoprotection should be necessary. Normally crystals are harvested with a nylon loop and are directly flash frozen in liquid nitrogen or in the cryo stream. This reduces mechanical stress and therefore the risk of increased mosaicity. To test if the use of a cryo buffer would improve the diffraction quality of *c*-ring crystals, this screening was set up.

In the first trial, different concentrations of glycerol (10%-30% (w/v)) were added to the standard crystallisation buffer. Empty nylon loops were dipped in the buffer mixture to be covered with a thin layer of the solution. The crystal was harvested and then dipped in 10 µl of the cryo buffer. The

crystal stayed in the drop only for a couple of seconds and was directly mounted on the goniometer and frozen in the cryo stream. To see whether a certain cryoprotectant improved diffraction, crystals grown under standard conditions were used. In the presence of 10 to 22% (w/v) of glycerol the spots in the diffraction images were always broad and unclear with a maximum resolution of 10 Å. Attempts to index the reference images with iMOSFLM/mosflm (122) failed. If 24%, 26%, 28% or 30% (w/v) glycerol was added, the spots didn't look different from the lower concentrations, but indexing was possible and the maximum resolution was 5 Å. Compared to crystals frozen directly from the crystallisation drop without a cryo buffer there was no improvement in the diffraction quality.

A next trial was to apply annealing to crystals cryoprotected in 30%, 32%, and 50% (w/v) glycerol added to the standard crystallisation buffer. The initial experiments were done for 30% (w/v) glycerol only. Single annealing steps were used to thaw and freeze the crystal-containing drop in the loop. This didn't cause any changes in the diffraction quality. As a result the number of annealing steps was increased to create a sequence of thawing and freezing. The general scheme was blocking the cryo stream for 3 s and allow the drop within the nylon loop to thaw. This was repeated three times separated by a 5 s pause so that the drop could freeze again.

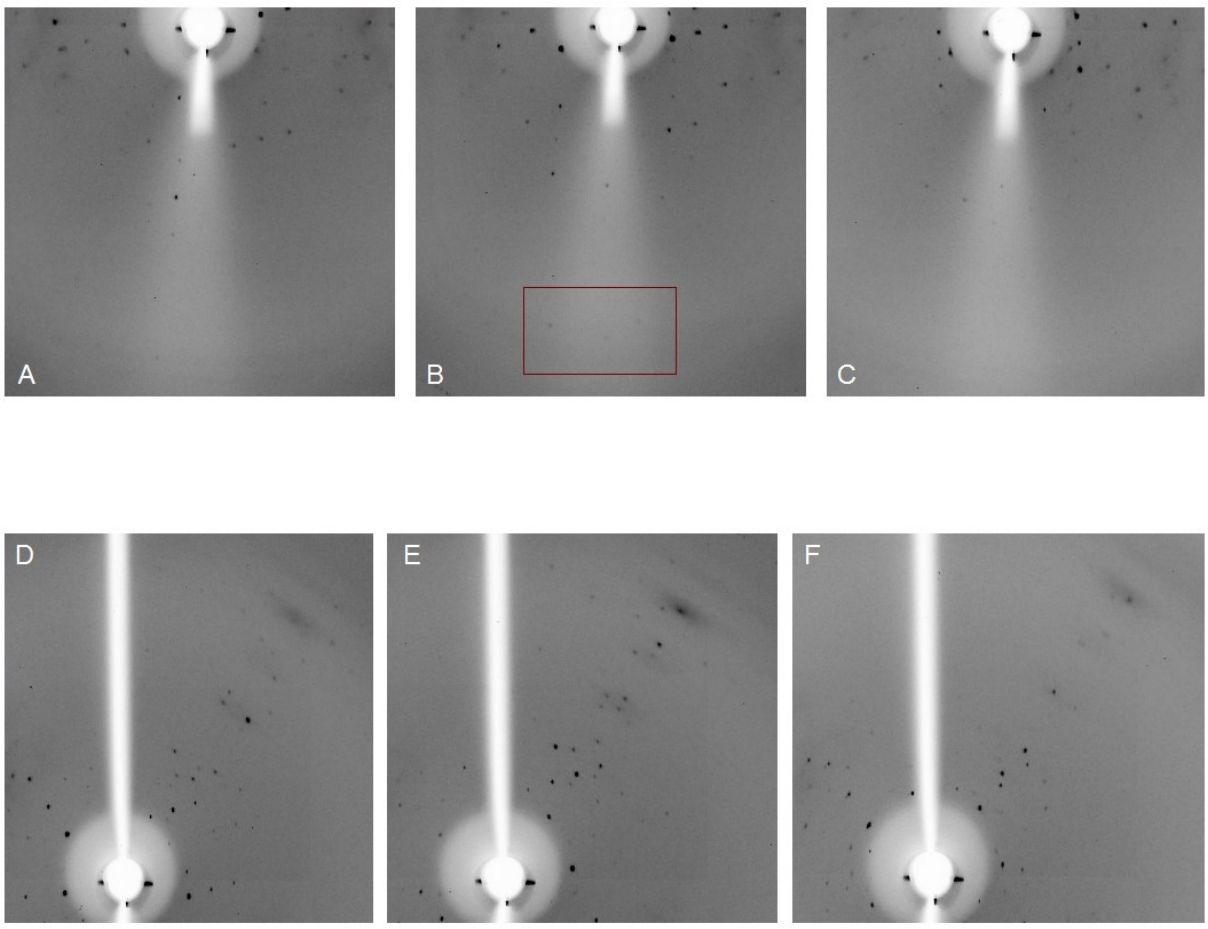

Figure 4.19: (A) and (D) pre-annealing; (B) and (E) once annealing scheme; (C) and (F) two more rounds of annealing and additionally thawing for 10 s and again for 30 s; images (D), (E), and (F) are taken 90° apart from (A), (B), and (C); exposure time: 2s; $\Delta\varphi$= 1°; detector: MAR CCD

For a crystal cryoprotected with 30% (w/v) glycerol one cycle of thawing and freezing supported the appearance of additional spots at a higher resolution of 5 Å. The starting resolution was 8 Å. Two more cycles of annealing followed by 10 s and 30 s of annealing diminished resolution to 9 Å. The improvement and the following decline in diffraction quality were not only observed for a single angle but also in images taken 90° apart.

In the next experiments, the glycerol concentration was increased to 32% and 50% (w/v). Applying the same scheme of thawing and freezing didn't improve the diffraction quality further compared to the experiments with 30% (w/v) glycerol. The spots did not improve in sharpness and no higher resolution was achieved. An additional annealing for 10 s also didn't result in changes in the diffraction images.

As mentioned in Materials and Methods 3.3.7, the function of a cryo buffer is to protect the crystal from ice formation within the lattice, radiation damage, and dehydration before flash freezing. So 15 and 30% (w/v) glycerol in standard crystallisation buffer or the buffer on its own were combined with paraffin oil. The use of 15% (w/v) glycerol with standard crystallisation buffer and paraffin oil as covering layer, did not improve the diffraction quality of *c*-ring crystals. Besides being weak and broad, the best spots could only be seen at about 11 Å. The same result was found for a combination with 30% (w/v) glycerol. A crystal cryoprotected in this buffer showed broad and diffuse spots in a diffraction image. An additional annealing step of 10 s did not result in changes of the diffraction pattern. Only a suitable resolution of 10 Å was obtained. Using the pure standard crystallisation buffer as cryo protectant with an additional cover layer of paraffin oil, the crystal showed almost no diffraction at all.

In the following experiments, several combinations of glycerol and other known cryoprotectants were tested. The different buffers are listed below.

	Solution combination
1	30% (v/v) glycerol, 15.2% (v/v) PEG 400
2	18% (v/v) glycerol, 4% (v/v) isopropanol
3	18% (v/v) glycerol, 4% (v/v) ethylene glycol
4	30% (v/v) glycerol, 40% (v/v) PEG 400; 3 times 3 s annealing with 5 s breaks, 2 sessions

Table 4.3: Cryo buffer composition

A crystal cryoprotected in combinations one or two (Table 4.3) did not improve in diffraction quality. The spots were weak and broad and crystals diffracted to a maximum resolution of about 8 or 9 Å. For number three (Table 4.3), improved at least the strength of the spots on a diffraction image of a crystal. The spots were stronger and clearly seen on the background. The cryo buffer presented in number four (Table 4.3) did not improve in the diffraction quality in the first diffraction images taken from a *c*-ring crystal. But after applying one series of annealing the spots became clear and strong. Some reference images are presented below.

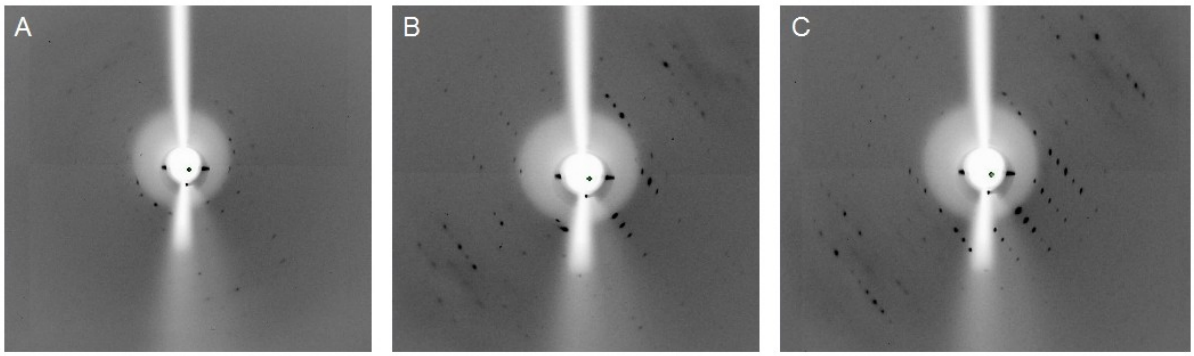

Figure 4.20: (A) 30% (w/v) glycerol, 40% (v/v) PEG 400, pre-annealing; (B) first annealing cycle; (C) second annealing cycle; The crystal was produced with standard settings; exposure time: 2s; Δφ= 1°; detector: MAR CCD

	Solution combination
5	15% (w/v) sucrose in standard crystallisation buffer; 3 times 3 s annealing with 5 s breaks
6	15% (v/v) ethylene glycol
7	10% (v/v) PEG 1500
8	5% (v/v) PEG 1500, 30% glycerol; 3 times 3 s annealing with 5 s breaks (2 sessions)
9	15% (v/v) ethylene glycol, 30% (v/v) glycerol
10	30% (v/v) glycerol, 7.5% (w/v) sucrose; 3 times 3 s annealing with 5 s breaks (2 sessions); again through cryo buffer
11	30% (v/v) PEG 400, 100 mM $CdCl_2$, 100 mM sodium acetate (pH 4.6/HCl); pre-frozen

Table 4.4: Cryo buffer composition

In combination five (Table 4.4) sucrose1 5% (w/v) was added to the standard crystallisation buffer. Such a cryoprotected crystal showed the same diffraction as with combination one (Table 4.4). The spots were weak and broad and the maximum resolution was 9 Å. Applied annealing steps did not improve the diffraction quality any further. Crystals cryoprotected in ethylene glycol and PEG 1500, combinations six and seven (Table 4.4) showed no improved resolution on diffraction images. The resolution was maximal at 9 or 10 Å. Generally the spots were very weak and broad. Crystals in cryo buffer combination number eight (Table 4.4) with PEG 1500 and glycerol showed only broad spots and weak diffraction. After a first session of annealing the spots improved to be stronger and sharper. A second session, turned the spots again into a weak and diffuse appearance with a maximum resolution of 8.5 Å. Crystals cryoprotected in a combination of ethylene glycol

and glycerol (combination nine, Table 4.4) showed no improvement in diffraction quality. Only a maximum resolution of 9 Å was achieved and the spots were weak and broad. 30% (w/v) glycerol and 7.5%(w/v) sucrose were combined (combination ten, Table 4.4) for cryo protection of a protein crystal and a first session of annealing was applied. This resulted in a diffraction image with sharp and distinct spots, of which only a few showed diffuse tails. After a second annealing round the spots improved further in intensity but not in resolution which was 8 Å. Taking down the crystal from the goniometer and placing again into the cryo buffer destroyed the crystal.

Although none of the cryo buffers tested improved the diffraction quality of crystals derived form CF_oF_1 crystal annealing did help to improve the signal to noise ratio so that spots are better pronounced on the background. As a control experiment some crystals from the same plate grown under the same conditions were pre-frozen and analysed with an X ray beam. They showed the known diffraction quality and had a maximum resolution of 3.8 Å.

4.2.12. Data Sets

Several data sets have been collected for CF_oF_1 crystallised in different combinations of washing buffers, crystallisation buffers, additives, and inhibitors. The following tables give the data sets with highest resolution achieved. They were all taken at beamlines of the ESRF, Grenoble. Given are experimental settings, indexing and processing results.

The crystals showed a highly anisotropic diffraction in several consecutive images over a small angle area, where also maximal resolution was observed. This is given with the line “max. resolution”. The mosaicity was always calculated for the first image automatically by the indexing software, which is listed as well as fixed mosaicity used for processing of a particular data set. The line “attenuation” gives the percentage of the beam used for data collection.

Table 4.5: Data sets; Standard HAc: standard crystallisation buffer (30% (v/v) PEG 400, 100 mM $CdCl_2$, 100 mM sodium acetat (pH 4.6) adjusted with acetic acid; Standard HCl: standard crystallisation buffer (30% (v/v) PEG 400, 100 mM $CdCl_2$, 100 mM sodium acetate (pH 4.6) adjusted with hydrochloric acid; 100 mM $CuSO_4$: standard crystallisation buffer but 100 mM $CdCl_2$ replaced by 100 mM $CuSO_4$, pH adjusted with hydrochloric acid; in brackets values in highest resolution shell

data set	20080509_6657	20080509_6955	20080509_6670	20080509_6672	20080509_6694	20080509_6671	20081112_6950
washing buffer	4	11	11	11	11	11	11
additive	4 mM ADP	4 mM ADP	4 mM ADP, 50 µM DCCD	4 mM ADP, 70 µM phloridzin	4 mM ADP, 10 mM spermine	4 mM ADP, 50 µM DCCD, 10 mM spermine	4 mM ADP
crystallisation buffer	Standard HAc	Standard HAc	Standard HAc	Standard HAc	Standard HAc	Standard HAc	100 mM $CuSO_4$
wavelength (nm)	0.872	0.919	0.919	0.919	0.919	0.919	0.979
detector distance (mm)	371.4	660.4	660.4	660.4	660.4	660.4	459.3
resolution after processing (Å)	27.83-8.80 (9.28-8.80)	22.14-7.00 (7.38-7.00)	29.60-7.00 (7.38-7.00)	-	26.88-8.50 (8.96-8.50)	27.20-8.60 (9.07-8.60)	21.82-6.90 (7.27-6.90)
a (Å)	150.7	153.7	131.1	137.3	148.7	141.1	157.2
b (Å)	99.5	100.0	105.2	148.6	102.5	106.7	101.2
c (Å)	130.7	130.4	146.4	164.7	131.2	129.9	130.9
α (°)	90	90	90	103.8	90	90	90
β (°)	107.9	108.8	108.7	112.2	108.5	107.7	109.8
γ (°)	90	90	90	104.8	90	90	90
space group	C2	C2	P2	P1	C2	C2	C2
lattice	mC	mC	mP	aP	mC	mC	mC
mosaicity (first image) (°)	0.85	0.73	0.69	0.88	0.76	0.93	0.25
mosaicity for processing (°)	0.9	1.3	1.5	-	1.4	1.3	1.0
max. resolution	5.0	5.0	4.9	4.4	4.9	5.0	3.3
beamline	23-2	23-1	23-1	23-1	23-1	23-1	14-4
exposure time (s)	2.0	1.0	1.0	1.0	1.0	1.0	1.0
rotation angle (°)	1.0	1.0	1.0	1.0	1.0	1.0	1.0
attenuation	100%	30%	30%	50%	30%	100%	5%
number of reflections	5121	8642	16679	-	4087	4512	10844
number of unique reflections	1492	2912	9970	-	1622	1558	3219
I/σ(I)	1.2 (2.2)	4.1 (2.3)	-	-	2.0 (1.8)	2.3 (2.1)	9.0 (2.2)
completeness (%)	98.5 (98.5)	97.0 (99.5)	85.3 (87.4)	-	94.8 (94.8)	96.1 (99.6)	98.3 (99.4)
multiplicity	3.4 (3.6)	3.0 (3.1)	1.7 (1.7)	-	2.5 (2.6)	2.9 (3.0)	3.4 (3.3)
Rmerge (%)	9.9 (25.4)	7.3 (29.8)	-	-	13.7 (29.0)	14.3 (25.1)	4.1 (27.7)

All data sets with the identifier 20080509 were taken on ID23-2 or ID23-1. They all show very low resolution and a rather small total number of reflections after processing. Data set 20080509_6657 was taken of a crystal grown in a combination of WB four (25 mM tricine (pH 8.0)) and standard crystallisation buffer. For pH adjustment acetic acid had been used. A relatively long exposure time

of 2 s was used. Additionally the beam was not attenuated. Together with the high anisotropic diffraction behaviour of the crystal, there is a tremendous loss of resolution in all images following a rotation of about 90°. The decrease in resolution can be seen very clearly throughout the processing procedure and is accompanied by an increase of unit cell dimensions as well as a small number of reflections. In the end, this crystal could only be processed to a resolution of 8.8 Å.

The crystal, of which data set 20080509_6955 was taken was grown from CFoF1 washing buffer 11 (25 mM sodium acetate (pH 4.6)). The crystallisation buffer itself was the same as for crystal 20080509_6657. The improvement to a maximal resolution of 7.0 Å after processing may be addressed to the different washing buffer with a pH of 4.6 rather than 8.0. Throughout data processing there were still big changes in unit cell detectable. Loss of diffraction quality and resolution over time can directly be seen in the images although the beam was used with 30% of its intensity.

Data sets 20080509_6670 and 20080509_6672 were both indexed in different space groups than the expected C2. The former one was found to be in P2 whereas the latter was indexed as P1. In both cases, further data reduction was not possible. Even the change to the mainly found space group C2, failed in further data processing. The presence of the inhibitors DCCD and phloridzin may be the reason for the different space groups.

The crystals, of which data sets 20080509_6694 and 20080509_6671 were taken, grew in the presence of spermine or spermine and the inhibitor DCCD respectively. Data set 20080509_6694 was collected with an attenuated beam of 30% whereas for 20080509_6671 no attenuation was applied. They both show again an increasing unit cell with a loss of resolution during processing. In the end, they could be analysed up to a resolution of 8.5 Å and 8.6 Å respectively.

All data sets with the identifier 20080509 show increasing unit cell dimensions and loss of resolution during data processing. The images were collected on ID23-2, a micro focus beamline with a very intensive beam. Even an attenuation of 30% still enables enough X-rays to hit the crystal and cause sever radiation damage within 90° of rotation.

For all data sets with the identifier 20091112 the corresponding *c*-ring crystals have been grown in crystallisation buffers adjusted in their pH value with hydrochloride acid. The use of hydrochloric acid instead of acetic acid not only accelerated the crystallisation process, but also improved the diffraction quality. A decrease in resolution and diffraction quality is now dependent on the presence of additives, inhibitor or the exchange of the buffer and/or salt component. Replacing $CdCl_2$ with copper sulphate as part of the cation screen, also gave rise to crystals and a data set,

20081112_6950, was collected on ID14-4. Compared to the images collected for crystals grown under standard conditions, the spots were smaller and sharper in the diffraction pattern of a *c* ring crystal grown in the presence of copper sulphate. This data set could be processed to a final resolution of 6.9 Å.

Table 4.6: Data sets; Standard HAc: standard crystallisation buffer (30% (v/v) PEG 400, 100 mM $CdCl_2$, 100 mM sodium acetat (pH 4.6) adjusted with acetic acid; Standard HCl: standard crystallisation buffer (30% (v/v) PEG 400, 100 mM $CdCl_2$, 100 mM sodium acetat (pH 4.6) adjusted with hydrochloric acid; 100 mM $CuSO_4$: standard crystallisation buffer but 100 mM $CdCl_2$ replaced by 100 mM $CuSO_4$, pH adjusted with hydrochloric acid; in brackets values in highest resolution shell; processing results for data set 20090302_4192 are listed in table 4.7

data set	20081112_6985	20081112_6968	20081112_6979	20081112_6957	20090302_4192
washing buffer	11	11	11	11	8
additive	4 mM ADP	4 mM ADP, 70 µM phloridzin	4 mM ADP, 150 µM phloretin	4 mM ADP, 150 µM DCCD	4 mM ADP, 25 µM phloridzin
crystallisation buffer	Standard HCl	Standard HCl	Standard HCl	Standard HCl	Standard + 100 mM LiCl2
wavelength (nm)	0.933	0.979	0.979	0.979	
detector distance (mm)	301.0	459.3	459.3	459.3	
resolution after processing (Å)	15.81-5.00 (5.27-5.00)	15.18-4.80 (5.06-4.80)	15.18-4.80 (5.06-4.80)	25.30-8.00 (8.43-8.00)	
a (Å)	148.5	154.8	153.3	156.8	
b (Å)	98.8	100.8	100.0	101.8	
c (Å)	129.5	130.8	130.2	131.5	
α (°)	90	90	90	90	
β (°)	107.8	109.2	108.8	109.4	
γ (°)	90	90	90	90	
space group	C2	C2	C2	C2	
lattice	mC	mC	mC	mC	mC
mosaicity (first image) (°)	0.79	0.94	0.24	0.32	
mosaicity (for processing) (°)	0.9	1.2	0.9	1.2	
max. resolution (Å)	3.4	4.1	3.6	5.0	2.8
beamline	14-1	14-4	14-4	14-4	23-1
exposure time (s)	1.0	1.0	1.0	1.0	
rotation angle (°)	1.0	1.0	1.0	1.0	
attenuation	5%	5%	5%	5%	50%
number of reflections	24429	31540	31175	6591	
number of unique reflections	7753	9287	9109	2000	
I/σ(I)	5.2 (2.8)	8.0 (2.2)	7.7 (2.2)	1.9 (2.1)	
completeness (%)	98.8 (98.8)	98.3 (98.3)	98.6 (98.6)	92.8 (92.8)	
multiplicity	3.2 (3.2)	3.4 (3.5)	3.4 (3.5)	3.3 (3.0)	
Rmerge (%)	7.5 (27.0)	6.9 (32.5)	7.1 (32.7)	12.9 (26.9)	

Data set 20081112_6985 was processed to 5.0 Å resolution. Data integration proceeded very quickly as there were no serious problems because of radiation damage. These results can be compared to those of data set 20080509_6955. Besides knowing about the sensitivity of the crystals to X-rays the crystal quality was improved as well as a result using hydrochloric acid for pH adjustment. This is underlined by a decrease in unit cell dimensions and the mosaicity. Changes in these three parameters are a result of higher order and tighter packing of unit cells within the crystal.

One data set was taken with phloridzin (20081112_6968) and another with phloretin (20081112_6979). Phloridzin is a glucose derivative of phloretin. Both data sets show almost the same processing results and both have a final resolution at 4.8 Å. The resolution for both data sets does not differ significantly from the resolution determined for the native data set 20081112_6985. The unit cell dimensions are slightly larger instead.

Alternatively, the inhibitor DCCD was tested. The data set (20081112_6957) could also be processed, but reached only a final resolution of 8.0 Å. During the data integration step, more crystal slippage could be observed compared to data sets taken from native crystals or those with phloridzin or phloretin. The unit cell dimensions correspond rather to those determined for the data sets collected for co-crystals with phloridzin and phloretin than for the native data set (20081112_6985).

Data set 20090302 was taken from a crystal grown at the same conditions producing the crystal for native structure. The experiments differ only in the presence or absence of the inhibitor phloridzin. The washing buffer used was number eight in both cases. The differences to the previously tested buffers number four and 11 are the buffer component, 25 mM bis-tris-propane versus 25 mM tricine or sodium acetate, pH 6.5 versus 8.0 and 4.6, and detergent, 35 mM C-HEGA-10 versus 0.1% (w/v) dodecyl maltoside. The crystallisation buffer differed as well. In combination with washing buffer 8 additional 100 mM lithium chloride had to be added to the crystallisation set up. The resulting data set could be processed to a resolution of 4.25 Å compared to 3.8 Å obtained with the native. This will be further discussed in relation to the native data set in 4.2.13.

4.2.13. Structure Solution

The structure was solved with a data set collected in a previous PhD work (136), which has the highest resolution obtained so far. Data collection was carried out at beamline ID14-2, ESRF, Grenoble. Table 4.7 gives the processing and experimental details for this native data set. Furthermore the scaling and merging results of data set 20090302_4192 (see Table 4.6) are presented.

Table 4.7: Comparison of native data set and one obtained from a co-crystal with phloridzin

	native	25 µM phloridzin
wavelength (nm)	0.933	0.976
detector distance (mm)	330	530.8
resolution after processing (Å)	28.28-3.8	13.44-4.25
space group	C2	C2
a (Å)	128.60	151.11
b (Å)	89.99	96.77
c (Å)	124.89	129.02
αβγ (°)	90 104.70 90	90 106.5 90
completeness (%)	92.2 (93.4)	99.2 (99.2)
Rmerge (%)	6.9 (20.1)	8.1 (34.2)
multiplicity	2.6 (2.5)	3.4 (3.5)
number of reflections (after merging/scaling)	132804	150623
number of unique reflections	12636	12624
I/σ (I)	4.1 (3.3)	4.7 (2.1)
Δφ (°)	0.5	1.0
exposure time (s)	2.0	1.0
mosaicity (°)	1.3	1.2

The native structure was solved by molecular replacement. In first trials with MOLREP (125) monomer search molecules derived from the structures of *Ilyobacter tartaricus* (PDB code: 1YCE) and *Escherichia coli* (PDB codes: 1C17, 1C0V) as well as the complete rings gave no results. From electron microscopy studies (5) it was known that the transmembrane ring from spinach chloroplasts is composed of 14 monomers of subunit *c*. A structural alignment revealed 60% sequence identity with Ilyobacter (http://toolkit.tuebingen.mpg.de/hhpred). Consequently a

monomer taken from the *c*-ring structure of *Ilyobacter tartaricus* was used to create a multimer search model with shell scripting.

The first 14mer model was created on the basis of a monomer from 1YCE, which was mutated to poly-Ala and cut at residue 71, adjacent to the kink seen in the structure for *Ilyobacter*. Any chosen combination of angles and diameter didn't produce a suitable model for MR. Further inspection of the monomer lead to a change in the starting orientation of the monomer.

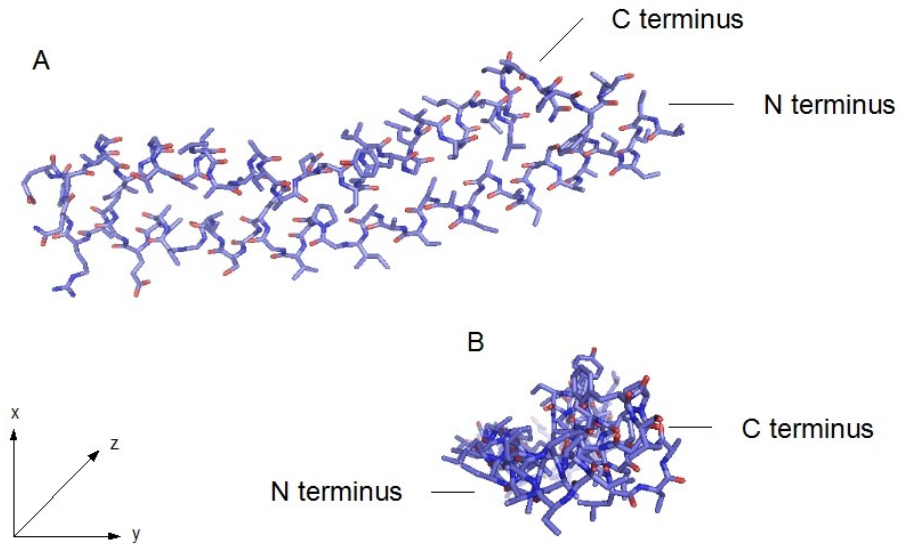

Figure 4.21: (A) starting orientation along y-axes wasn't successful in MR; (B) starting orientation along z-axes produced first suitable poly-Ala model; Both monomers are shown with complete spinach side chains

The shell scripts were run again with the poly-Ala monomer but in a new starting orientation and was successful for the variable combination omega = 2.5°, phi = 11.0°, kappa = 4.0°, and diameter = 22.4 Å. After running MOLREP (125) all created models were refined in 10 cycles with Refmac5 (128) applying rigid body refinement followed by restrained refinement with NCS. All refined models were listed according to their R_{free} values.

Table 4.8: Refinement results for the initial poly-Ala model after re-orientation in COOT

Rfactor	42.45
Rfree	48.46
-LL	84244
-LLfree	4485.9
rmsBOND	0.0101
zBOND	0.522
rmsANGL	1.166
zANGL	0.494

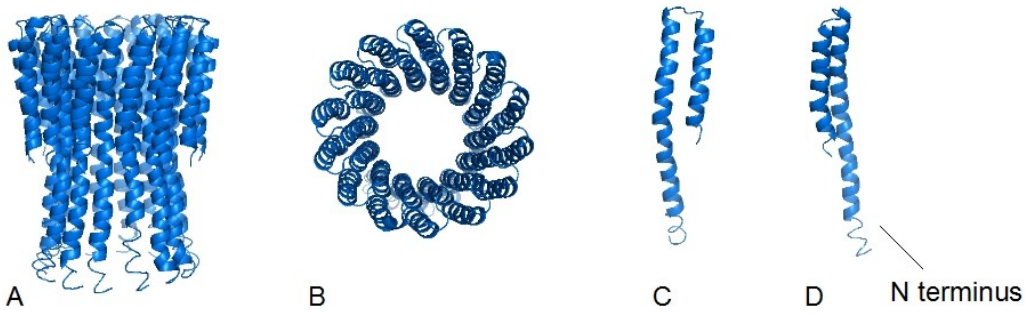

Figure 4.22: (A) front view of poly-Ala multimer created from a poly-Ala monomer cut at amino acid 71; (B) top view of (A); (C) front view and (D) side view of the used monomer

To check if molecular replacement would still be successful after manipulations, some of the subunits were deleted from the ring by a random choice whereas the general orientation of the ring was kept fix. The monomers were used as poly-Ala with different length of the C terminus as well as monomers having the spinach sequence, which was created with CHAINSAW. Generally all monomers created could be used to fill the gaps of randomly deleted subunits in the 14mer. Although refinement cycles were carried out after several monomer replacements, and additional solvent flattening was done with DM (CCP4 suite), the resulting multimers showed a chaotic shape. Figure 4.23 gives some examples.

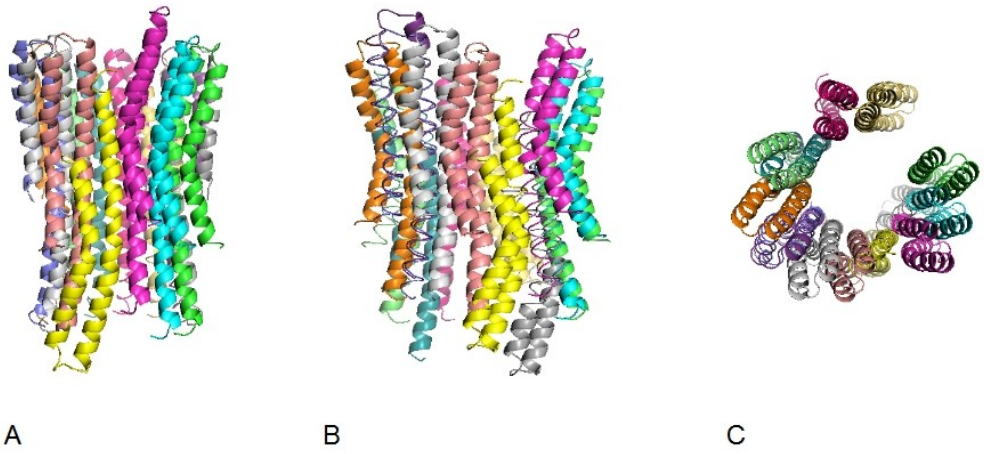

Figure 4.23: (A) and (B) side views of multimers after replacement of several subunits; (C) top view of a "chaotic multimer"

These chaotic may result from an irregular density distribution. Although 14fold NCS applied for density improvement, some of the monomer positions in the ring were not clearly defined. The next attempt was to start a consecutive replacement of the poly-Ala monomers with monomers carrying the spinach sequence only. One chain after the other was replaced without a random choice. After each exchange step 10 cycles in Refmac5 (128) were done with default parameters but applying 14-fold NCS restraints. The resulting 14mer was showed to carry the spinach sequence in each monomer and the overall structure was symmetrical. To improve the electron density, solvent flattening was applied with the program DM from the CCP4 suite. Additional refinement steps with varying combinations for backbone and side chain restraints could not lower the R_{free} significantly. The R_{free} decreased from 48% from the poly-Ala model to only 46% after all monomers had been replaced. After several refinement cycles R_{factor} and R_{free} started to diverge. This could also be seen in an increase of bond distances and angles or visually in COOT (126) as broken side chains and back bone.

The next step was to apply not only solvent flattening to the electron density, but also to use the 14-fold NCS to improve the map. The necessary rotation matrices and Euler angles for DM were produced by superpositioning one monomer within the ring on the 13 remaining subunits. Several runs of density modification and solvent flattening as well as NCS averaging were applied with different monomers as reference chain. NCS averaging for the density was used with the approximation that all 14 subunits within the ring are identical. The stepwise exchange of poly-Ala

monomers against those with the spinach sequence was repeated as mentioned above, but with the improved density and without a random choice. The replacement was successful and a regular 14mer was created. After replacing the monomers, the R_{free} of 48% for the poly-Ala 14mer was reduced to 46% as in the previous example. The additional modifications of the electron density allowed for a further decrease of the R_{free} to 41%. The restraints for backbone and side chains were varied again and combined in different ways but did not improve the R_{free} further. Visual inspection of the multimer revealed again broken protein backbone and side chains. Additionally the monomer showed some differences between the structure alignment used for manipulations in CHAINSAW (127) and the sequence found in the monomer.

As a result, the monomer creation was repeated and all errors such as frame shifts and sequence gaps were eliminated. The underlying sequence of the monomer was from spinach with 47 of 81 residues present with all atoms, which corresponds to a completeness of 58%. The other residues were present with C_γ only, which is a relic from creating a "mixed" model with CHAINSAW. This monomer was now used to repeat the cluster run, which had produced the first poly-Ala model (see Figure 4.22). The scripts were run with the appropriate settings of variables and produced a 14mer, which had now a starting R_{free} of 41.38%, reasonable values for bond lengths and angles, and showed no broken protein backbone and side chains in visual inspection. The refinement results after the model creation are listed below.

Table 4.9: Refinement results for the repeated poly-Ala model with a monomer carrying a mixed sequence as produced from CHAINSAW

Rfactor	33.56
Rfree	41.38
-LL	69349
-LLfree	3676.6
rmsBOND	0.0125
zBOND	0.554
rmsANGL	1.401
zANGL	0.623

The corresponding structure is shown in Figure 4.24.

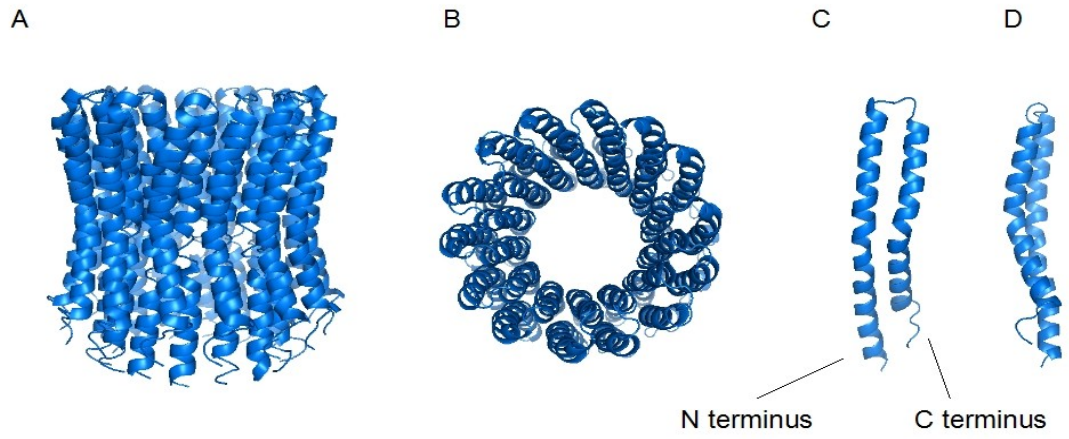

Figure 4.24: (A) front view of 14mer containing 47 of 81 residues with all atoms; (B) top view of (A); (C) front view and (D) side view of the used monomer

This model was now used for further model building, as more than 40% of the side chains were still missing.

4.2.14. Model Building and Refinement

A first trial was to apply density modification with the better positioned starting model. This did not improve the refinement results at all. In a second attempt TLS (131) was used in refinement and each subunit was chosen as a TLS group as recommended in the result from TLS-MD (http://skuld.bmsc.washington.edu/~tlsmd/index.html). However this did not help either. The next step was to set different NCS restraints and vary them in their weightings. Setting restraints tight for backbone and side chains, using all residues of a monomer, and defining one chain as master chain for the remaining subunits gave the first significant change of the refinement results. Although R_{free} and R-factor were still high they stopped diverging. Additionally, first model building was carried out in COOT (126). Upon visual inspection, side chains were completed if electron density was present. As mentioned before, only 58% of the residues were identical between the *Ilyobacter* sequence and spinach and consequently the only 58% of the side chains were present with all atoms.

Before continuing with model building, settings for refinement were optimised. The overall weighting term was decreased to 0.005 and later changed to 0.0075. This means that the weight for the refinement restraints is set to a fixed value in the likelihood search, so that the model has a higher weight than the measured data. This is reasonable as only low resolution data are available.

Bulk water was scaled in the Babinet way and the B-factors for water were set to 200. These settings resulted in a first R_{free} below 40%.

The number of TLS groups was varied. Dimers of c-subunits were constructed and seven TLS groups were used. Alternatively each monomer was defined as single TLS groups. The best result was achieved with a single TLS group over the complete ring. A new upload of the TLS file in each refinement run gave additional improvement of the R_{free}.

Geometrical restraints were also edited and changed to higher and tighter weighting terms. The overall weighting terms for B-factors and NCS positions were both changed from 1.0 to 3.0. And for bond angles the restraint value was set to 1.2 from an initial value of 1.0. An overall weighting term of 0.0075, with a single TLS group, and one master chain for 14-fold NCS were also used for refinement.

After defining refinement parameters further model building was continued in COOT (126). Applying the available NCS tool allowed the creation of 14 identical subunits with a higher accuracy. After some changes in one monomer, e.g. adding side chains and fitting rotamers into the $2F_o$-F_c density, these modifications were applied to the remaining monomers in the ring with the NCS tool in COOT. This was followed by several cycles of refinement. 20 cycles restrained refinement without TLS was applied. The resulting output file was used in second refinement step with 20 cycles of TLS refinement followed by 50 cycles of restrained refinement. Refinement steps without TLS were used to avoid too high B-factors and to reduce none-positive definite U problems (u = atomic displacement parameter).

Side chains without clear density and terminal amino acids Met1, Asn2, Phe80, and Val81 were removed, which improved the refinement further to the final values listed below.

Table 4.10: Refinement statistics of the published structure (PDB code: 2w5j)

Rfactor	31.67
Rfree	33.52
-LL	74678
-LLfree	3945.5
rmsBOND	0.0132
zBOND	0.579
rmsANGL	1.284
zANGL	0.559
Number of residues (with incomplete side chains)	1092 (182)
Rms NCS (Å)	0.001
Ramachandran Plot (Procheck)	
favoured	767 (72.1%)
allowed	258 (24.2%)
outlier	39 (3.7%)
Solvent content	66%
Matthews coefficient	3.64
B-factor (overall)	84.10

The resulting model is presented below.

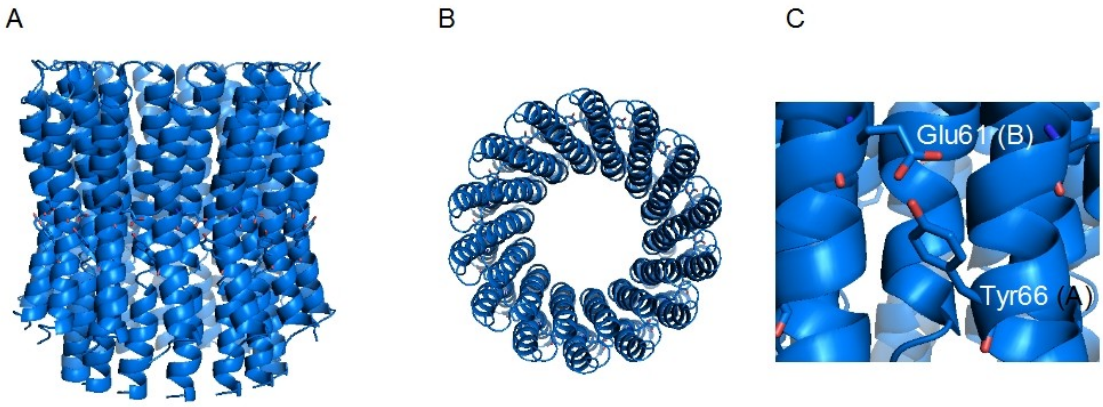

Figure 4.25: (A) front view of the final model released as 2W5J; (B) top view of (A); (C) proton binding site in the transmembrane ring of F_oF_1 ATP synthase from spinach chloroplasts

In order to verify the results, especially for the binding site, and to demonstrate that the structure is not biased from the *Ilyobacter* model an omit map was calculated. Therefore residues Glu61 and Tyr66 in the binding site have been deleted from the final model. Additionally, the command noise in PDBset as part of the CCP4 suite was used with a value of 0.2 for the variable NOISE. This value corresponds to a maximum displacement of the model by 0.2 Å and results in a randomisation of the structure which is shown by R_{free} increasing to 45%. After refinement of the model lacking residues 61 and 66 there was still positive density visible, which could be assigned to the binding site residues in an overlay of model and density as seen in the omit map below.

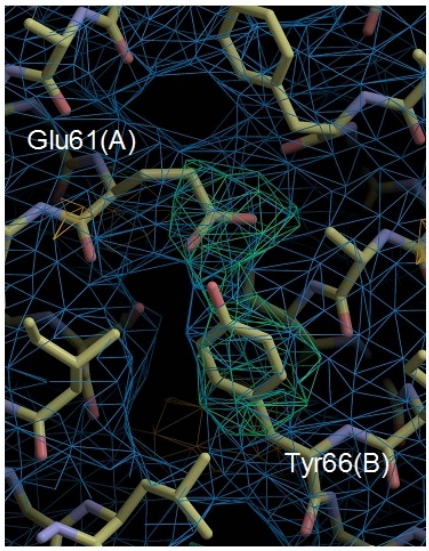

Figure 4.26: Proton binding site, represented by the side chains Glu61(A) of monomer A and Tyr66(B) of monomer B, of transmembrane ring of F_oF_1 ATP synthase from spinach chloroplasts. NCS averaged $2F_o$-F_c density (blue, contoured at 1.5 σ) and NCS averaged F_o-F_c omit density (green, contoured at 6 σ) (taken from Vollmar *et al.*, 2009)

This available native structure was used for molecular replacement for the data set 20090302_4192 (Table 4.5). The native structure as search model could be positioned very quickly although in large sections the electron density was not well defined. For the crystal grown in the presence of phloridzin an increase of the unit cell volume by 29% was found. It is not clear if this is extra volume can harbour some inhibitor molecules, which could not be resolved in a resolution of 4.25 Å, or if it is solvent.

5. Discussion

5.1. Purification

The crucial step in the purification procedure is the extraction of CF_oF_1 from the membranes in 1% (w/v) sodium cholate and 2% (w/v) DDM. This step is based on the method of Pick and Racker (137), but with different detergents. If the solubilisation of CF_oF_1 with ultrasound is not done carefully, the protein remains in the thylakoid membrane rather than moving into the detergent micelles. The protein is found in the pellet fraction after ultra centrifugation.

The anion exchange chromatography step reduces the amount of contaminations. CF_1 interacts with the functional groups of the column matrix and can be eluted by a linear sodium chloride gradient. The interaction between CF_1 and CF_o through the central and peripheral stalk, is strong enough, to hold both parts together. To avoid separation of both components it is essential to have 0.1% (w/v) dodecyl maltoside present in all buffers. The anion exchange chromatography also allows the exchange of the detergent. In the earlier steps, CF_oF_1 was kept soluble in dodecyl maltoside micelles. In the actual purification the buffer exchange after the concentration step is used to replace the detergent, i.e. for crystallisation trials of CF_oF_1 in washing buffer eight. The buffer volume used for the exchange is rather small. Consequently it may be possible that the detergent is not replaced completely and mixed micelles can form. An inhomogeneous detergent mixture may disturb the crystallisation process.

Mixed micelles would be one explanation for the results of the detergent assay for CF_oF_1 in washing buffer eight. The standard series analysed for this detergent shows a slight background colour which may originate from present glycerol in the buffer as suggested by Urbani and Warne (109). For the samples of CF_oF_1 in WB 8 (dilution 1:10) a clear orange colour can be seen. The assay is based on the reaction of sulphuric acid with anomer carbon atoms in sugar compounds of detergents such as dodecyl maltoside. C-HEGA-10 which is used in WB 8 does not have an anomer carbon atom as its sugar component, glucose, is not present in a circular form. The positive result in the samples of CF_oF_1 in WB 8 may be due to remaining dodecyl maltoside or glucose from purification. The former one may be present in mixed micelles and will have an effect on the crystallisation process. Glucose is also interesting, as for WB 11 analysed with this assay, a higher detergent concentration was estimated than expected. All buffers used contain 0.1% (w/v) DDM, which corresponds to a 10-fold critical micelle concentration (CMC). DDM forms detergent micelles with a molecular weight

of 70 kDa. Because of the exclusion size (100 kDa) of the membrane used in the concentration step, an "empty" micelle, without the CF_oF_1 complex (550 kDa), would pass the membrane pores and then be found in the supernatant. An essential prerequisite for micelle formation is an equilibrium with free detergent molecules, which was given at any time with the chosen detergent concentration. One would therefore expect that even as the protein becomes concentrated the concentration of the detergent stays constant (139). Contrary for CFoF1 in WB 11, containing dodecyl maltoside, a five fold higher detergent concentration was estimated. Taking the former argument into account this is very surprising. For WB 11 as for WB 8 it might be possible that there is still glucose present from the purification. Alternatively the chosen buffer components and the presence of CF_oF_1 changes the physical and chemical properties of DDM that it becomes concentrated as well. For clarification an alternative method such as dynamic light scattering should be used.

5.2. Crystallisation

After analysing all crystallisation results the established standard setup for further screening and co-crystallisation was set as follows:

method	hanging drop
reservoir volume	400 µl
drop volume	3 µl protein solution + 3 µl crystallisation buffer
temperature	15°C

These settings were combined with a number of different washing and crystallisation buffers. For the buffer solutions, the acid or base used for pH adjustment was essential. This is independent of buffer composition and buffer type, e.g. washing or crystallisation buffer. Using hydrochloric acid and sodium hydroxide improved the crystal quality significantly. Their use increased the reproducibility of the crystallisation process in general and assured the appearance of crystals of reasonable size (about 50 µm) after four days. It had no effect on the heterogeneity of crystal shape. The *c*-ring still crystallised in a mixture of compact three dimensional crystals and thin plates,which had a maximal thickness of 10 µm.

Decreasing the protein concentration reduced the formation of micro crystals. For washing buffer

eight 5 mg/ml and for washing buffer 11 6 mg/ml were found to be ideal. Smaller concentrations still allowed for crystal growth but over an extended period. This may be useful for a crystallisation series to test for the best harvesting point in correlation with the diffraction quality. It may also be possible that an extended incubation time helps to reduce the mosaicity. The unit cells have more time to arrange in a three dimensional lattice, which may favour a tighter packing. However extended incubation time has also the opposite effect of more probable denaturation of the protein molecules. Defect protein molecules integrated into a crystal lattice may increase the mosaicity.

ADP was added to stabilise the holo-enzyme, as it is necessary for the catalytic and regulatory binding sites in the F_1 part. It was found that the precipitate appearing after mixing protein solution and crystallisation buffer includes F_1 and peripheral stalk subunits. Elimination of the precipitate by centrifugation after the mixing of both solutions didn't result in crystal formation. The standard concentration of ADP for WB 8 was 3 mM and 4 mM for WB 11. A 200-fold lower concentration of 20 µM was also tested for washing buffer 11, but didn't result in crystal formation. Higher concentrations than 3 or 4 mM, produced large amounts of micro crystals. It is therefore suggested that, although not essential for the stability of the membrane integrated *c*-ring, ADP seems to have an effect on the crystallisation process and may help to form nuclei for crystal growth.

A list of crystallisation buffers tested, can be found in the Appendix 7.1. The protein was found to crystallise in several buffer components with different concentrations and at different pH values. Variation of the PEG 400 concentration had no effect on the crystallisation process. 30% (v/v) PEG 400 is widely used for crystallisation experiments and was kept as a constant parameter. The standard crystallisation buffers for WB 8 and 11 are given in the table below:

Washing buffer 8	Washing buffer 11
30% (v/v) PEG 400	30% (v/v) PEG 400
100 mM $CdCl_2$	100 mM $CdCl_2$
100 mM $LiCl_2$	-
100 mM sodium acetate (pH 4.6/HCl)	100 mM sodium acetate (pH 4.6/HCl)

A screening with various di- and tri-valent ions showed positive crystallisation results for several new substances. Some crystals, like those grown with copper sulphate instead of cadmium chloride, were analysed in diffraction experiments. They showed improved spot quality and a data set was collected. At the moment for most new components only the crystallisation result can be analysed. But the findings and results with copper sulphate are promising. It may be useful to combine the

substances found in the crystallisation assays with the standard buffer.

Screenings with additives and inhibitors were set up for washing buffers four, eight, and 11. DCCD, phloretin, and phloridzin were tested. They are all small hydrophobic compounds, which can diffuse freely through the membrane or for a purified membrane protein through the surrounding detergent micelle.

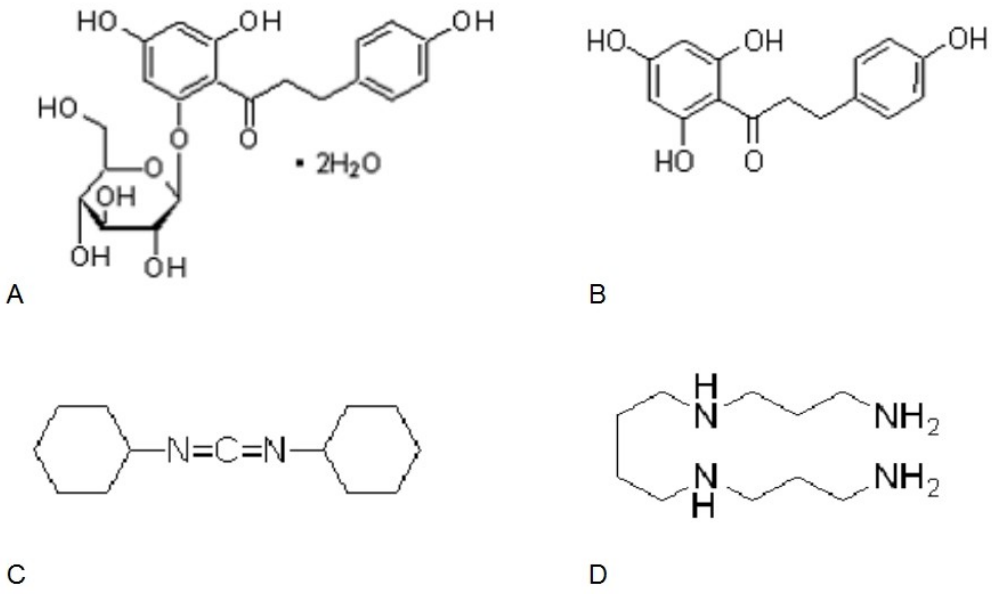

Figure 5.1: (A) Phloridzin; (B) Phloretin; (C) DCCD (N,N'-dicyclohexylcarbodiimide); (D) Spermine (all structures are taken from www.sigmaaldrich.com)

All three inhibitors as well as the additive spermine produced crystals within four days with each of the washing buffers tried and the corresponding standard crystallisation buffer. Spermine as additive supported a more regular crystal shape but did not improve the diffraction quality or resolution. It had also no effect if used in combination with any of the inhibitors.

In general the crystallisation process did not differ between native *c*-ring crystals and those grown in the presence of an inhibitor. Diffraction experiments done with crystals grown in the presence of an inhibitor showed a loss in resolution. This was accompanied by an increase in unit cell dimensions, especially along the a axis. The unit cell volume increased by about 29%, which gives either more space for additional solvent or for inhibitor molecules.

DCCD is known as an inhibitor and the binding site on F_o is known. For the inhibitory mechanism it

is known that DCCD accepts the proton, if present, from the *c*-ring binding site and binds afterwards covalently to the essential aspartate or glutamate. The crystallisation was done at pH 4.6. However almost no DCCD inhibition of the spinach ATP synthase can be detected at a pH < 5.0 (140). Why there is no inhibition at low pH is still under debate. It may simply be possible that, because of a proton excess at a low pH, the inhibitor becomes protonated and therefore inactive and does not bind at all. Free DCCD molecules effect the crystallisation process, which may result in *c*-ring crystals with a weak order and consequently in low resolution.

For inhibitors phloretin and phloridzin nothing is known about a binding site or a mechanism. Phloretin is not known to bind specifically to ATP synthase. Instead it is suggested to act as an uncoupler in mitochondrial oxidative phosphorylation (141). Cseh and Benz (142) studied the effect of phloretin on artificial lipid monolayers created from different lipids. They suggested that phloretin interacts with the membrane in three different ways. It can adsorb to the surface, integrate in between the phosphate heads of lipid molecules or insert deeply in between the alkyl side chains of the lipids. For a membrane protein soluble in detergent micelles it is also likely that phloretin integrates between the detergent molecules and may therefore be able to interact with the protein.

Phloridzin is suggested to bind to a distinct binding site in CF_1 (143) and inhibits hydrolysis of ATP. As a consequence, a proton gradient cannot be created. Compared to phloretin, phloridzin is linked to a glucose molecule. Zheng and Ramirez (144) compared the inhibitory effect of several polyphenolic phytochemicals, including phloretin and phloridzin, on ATP synthase from rat mitochondria. They suggest that the saturation of one OH-group in phloretin decreases the inhibitor efficiency. They do not specify in which position and do not take the glucose OH-groups into account. For phloretin for IC_{50} they determined 40% inhibition in the presence of 70 µM inhibitor. Less than 15% inhibition were found for phloridzin at the same concentration. Therefore it might be expected that phloridzin having one OH-group saturated with a glucose molecule is less efficient than phloretin. It was thought that according to these findings the necessary concentration for successful co-crystallisation may be higher for phloridzin than for phloretin. For crystallisation it is desired to have a homogeneous protein mixture including the inhibitor. Phloretin and phloridzin were tested in a concentration range including saturating concentrations. Interesting was the finding, contrary to the expected results, that a higher concentration for phloretin than for phloridzin was necessary for successful crystallisation.

Data sets were taken from *c*-ring crystals grown from CF_oF_1 in washing buffer 11 in the presence of either 70 µM phloridzin or 150 µM phloretin. Interesting are the results retrieved for cell

parameters, indexing, and processing. They are almost identical for both inhibitors. A reason might be a hydrolysing effect of the washing buffer and crystallisation buffer. A pH of 4.6 for both solutions allows for hydrolysis of phloridzin into glucose and phloretin.

A data set was collected for a crystal grown from CF_oF_1 in washing buffer eight with 25 µM phloridzin. 14fold NCS was used to improve the quality of the electron density map. However, at a resolution of 4.25 Å for the data set taken from a phloridzin-*c*-ring co-crystal, it is impossible to see such details like a bound inhibitor. The increased unit cell volume (see above) may rather originate from additional solvent than from bound inhibitor molecules. For future crystallisation experiments with an acidic crystallisation buffer it is recommended, to use only phloretin in co-crystallisation trials with the membrane integrated *c*-ring.

Hydrolysis, as for phloridzin into glucose and phloretin, may also be applicable for the detergent used in the experiments. Dodecyl maltoside contains maltose, which consists of two glucose molecules. An alternative detergent with the same length of alkyl chain and similar physical and chemical properties, like CMC and solubility, may be n-dodecyl 1-thio-β-maltoside. Replacing the oxygen of the anomere carbon atom in the glycosidic bond between maltose and the alkyl chain avoids hydrolysis. Furthermore, n-decyl 1-thio-β-D-glucopyranoside could be used. It consists of a shorter alkyl chain only one glucose molecule. n-dodecyl 1-thio-β-maltoside can still be hydrolysed and lose a glucose molecule of maltose.

Post-crystallisation treatment like dehydration was not successful for an isolated protein crystal but seems to be promising if the entire drop is used. The used setup and incubation times were chosen according to widely used procedures. The problem of precipitate present in the trial can be circumvented by transferring a crystal of interest into a drop, which has the same conditions under those the crystal was grown. This drop was setup at the same time as the crystallisation trial and therefore should be in the same equilibrium state. The drop containing the transferred crystal is moved between wells filled with increasing precipitant concentrations. As a result cracks should not occur and after the transfer there would only be little precipitate present. After reaching the desired state of drop shrinkage the crystal can be harvested with a nylon loop and analysed in diffraction experiments.

For the cryo buffers tested no significant improvement of the diffraction quality was observed for any crystal. Annealing of protein crystals was found to be more useful. The applied scheme included three 3 seconds thawing steps with 5 seconds freezing pause. After this procedure the spots in diffraction images were found to be better defined on the background and were less diffuse. This

procedure also helped to increase the resolution slightly. More interesting was the finding that a prefrozen crystal grown in the same plate and under the same conditions as those crystals used for the cryo buffer test showed higher resolution and much better diffraction. The most likely reason for this difference is the way of transport. The crystals for cryo buffer testing were transported in their crystallisation plates whereas the prefrozen ones were carried in a dry shipper with liquid nitrogen. The transport in the crystallisation plates may have caused severe damage in the crystal lattice because of movements, vibrations, and temperature differences. It is suggested that for future testing crystals are incubated in the buffer of interest and then flash frozen in a nylon loop for analysis at a synchrotron or on a home source.

5.3. Structure of the c_{14}-ring from Chloroplast ATP Synthase

5.3.1. Structural Comparison of Multimers

The overall shape of the membrane integrated rotor ring is a cylinder with a waist at the binding site, which is located in the C terminal helix. This seems to be a general scheme as it was also found for the structures of *Ilyobacter tartaricus* (82) and *Enterococcus hirae* (38). On the basis of NMR results a model has been created for the proton translocating enzyme of *Escherichia coli* (4). A low resolution structure of the mitochondrial ATP synthase from yeast also shows the same overall shape (3), but because of the limiting resolution only the protein backbone could be resolved. Figure 5.2 shows the structures solved for *Ilyobacter*, *Enterococcus*, and spinach as well as the theoretical model for *E. coli*. Every ring is presented according to its proposed orientation within the membrane and top view from the cytoplasm or stroma side respectively.

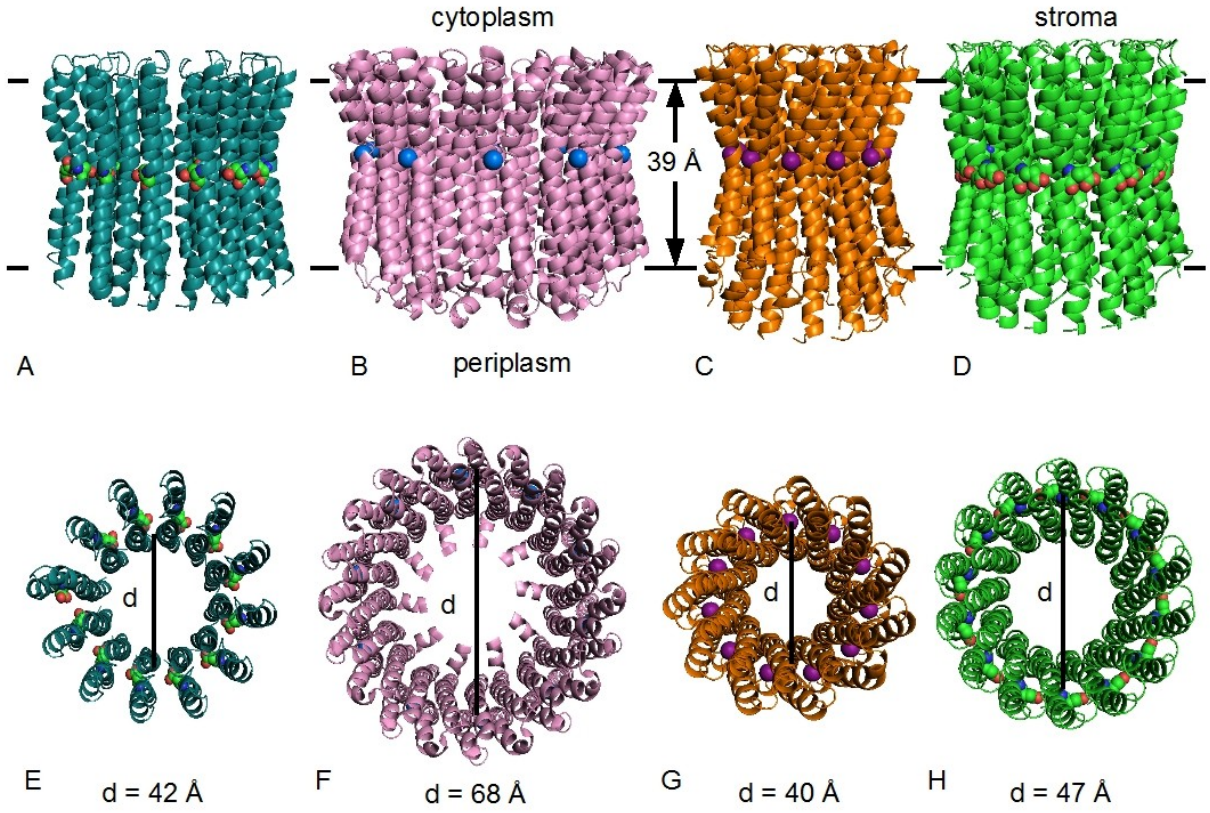

Figure 5.2: (A)-(D) Side view of membrane integrated rotor rings of F_oF_1 ATP synthases and V-ATPase; (E)-(H) Top view of the rotor rings; (A) and (E) Theoretical model of the membrane ring of the *Escherichia coli* enzyme based on PDB code 1C17 lacking a model for subunit *a*; (B) and (F) Structure for the V-ATPase *K*-ring from *Enterococcus hirae* (PDB code 2BL2); (C) and (G) Structure for the sodium translocating *c*-ring of F_oF_1 ATP synthase from *Ilyobacter tartaricus* (PDB code 1YCE); (D) and (H) Structure of the *c*-ring of the proton translocating F_oF_1 ATP synthase from spinach chloroplasts (PDB code 2W5J); d gives the diameter in Å of each ring, measured at the inner contact area between the parallel helices of opposite monomers and for *Enterococcus* two opposite binding sites were used; For the sodium ATPase from *Enterococcus* and *Ilyobacter* the binding site is indicated with a blue or magenta sphere for sodium. For the enzymes of *E. coli* and spinach the position of the binding site is indicated with the essential carboxylate shown as spheres.

The central pore in the rotor ring, as can be seen in the top view, is proposed to be sealed on the side of the termini of the *c*-subunits. This avoids uncontrolled ion traffic across the membrane if the central subunit *γ*, on top of the ring, is lost or stripped off. Thus, a break down of the membrane potential is prevented. In the structures of the membrane rings from *Ilyobacter* and *Enterococcus* with a resolution of 2.4 Å and 2.1 Å respectively, lipids could be identified in the central pore (38, 44, 145). The resolution for the spinach structure is too low to define clear electron density for disordered molecules like lipids, although non-assignable positive electron density is clearly present in the central cavity.

5.3.2. Binding site

The binding site is located on the periphery of the outer ring created by the C terminal helices of the *c*-subunits in the multimer. The C terminal helix of each monomer shows a kink at the binding site which creates a waist in the multimeric ring. The essential and highly conserved residue for any known F_oF_1 ATP synthase is a glutamate or aspartate. The distances between the adjacent binding sites are almost identical for the different species. On average it is 10.8 Å for spinach, for *Ilyobacter* 10.5 Å, and for E.coli 11.5 Å. In *Enterococcus hirae* the distance is twice as big, e.g. 20.3 Å. This is reasonable as it is suggested that the *K*-ring of the V-ATPase arose from gene duplication and followed by gene fusion of *c*-monomers from F-ATPases (36, 38). In every second potential binding site the essential carboxylate, glutamate 139, is replaced by a glycine. This is also supported with the finding that the four helices of one monomer can be divided into two pairs which are almost identical in sequence. The distances between the binding sites are kept almost identical in different species, but the number of monomers within the ring varies from 10 to 15. It seems that this gear distance is conserved for the enzyme in different species and therefore the diameter varies significantly to allow for flexibility in respect to the number of monomers. Alternatively, with a known diameter and a conserved distance between the binding sites, one can estimate the number of subunits from any ring with unknown stoichiometry (146).

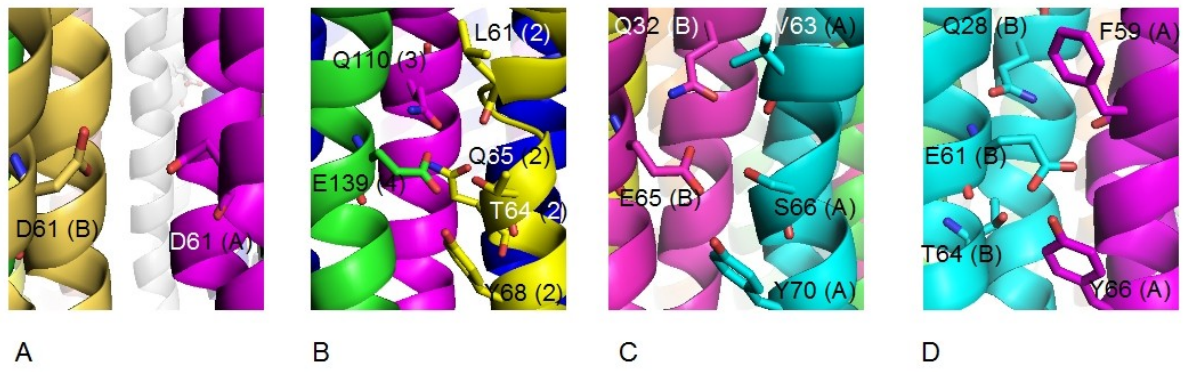

Figure 5.3: Proton/Ion binding sites of *c*-rings from different species. (A) Binding site of *Escherichia coli*; (B) Binding site of *Enterococcus hirae*; (C) Binding site of *Ilyobacter tartaricus*; (D) Binding site of spinach chloroplast; Given are the side chains necessary for sodium ion clustering or proton binding for the different species.

Figure 5.3 shows the binding sites of four different species. For *Escherichia coli* aspartate 61 is present as carboxylate to carry a proton. The two residues of adjacent monomers point towards each other, as Asp61 (B) shows the deprotonated state and Asp61 (A) the protonated state. They reach one of the two possible orientations by a rotation step at the interface of subunit *a* and *c* which is explained in Chapter 1.4.4.

In the examples (B) to (D), the translocated ion/proton is clustered with six residues in *Enterococcus*, five in *Ilyobacter*, and four side chains possibly involved have been found for spinach chloroplasts. All residues involved are directly in contact with the ion/proton and/or contribute to the hydrogen bonding network. In *Enterococcus* the sodium ion is coordinated by L61, T64, Q65, Y68 in chain two, Q110 in chain three, and E139 in chain four. Chain one is not part of the binding site but forms the back to the central pore. All chains belong to the same monomer.

In *Ilyobacter* two adjacent monomers create the binding site at their interface. The left chain viewed from the cytoplasm is named B and contributes residues with Q32 and E65 to the binding site. Chain A forms the opposite side with residues V63, S66, and Y70.

For spinach with a resolution of 3.8 Å it is not possible to assign electron density for water or protons. Alternatively to the protonation of the carboxylate Asp61 proposed for the *c*-ring of *Escherichia coli*, a proton may be bound to a water molecule and coordinated as hydronium ion in spinach. Side chains, contributing to the binding site, are offered by two adjacent monomers. The residues involved are Q28 and E61 in chain B as well as residues F59 and Y66 in chain A. T64 may have a supporting function in the hydrogen bonding network. In all three binding sites shown the

outward pointing tyrosine residue in position 66 (spinach), 68 (*Enterococcus*), and 70 (*Ilyobacter*) is not directly in contact with the ion but supports the coordinating hydrogen bonding network.

For spinach CF_oF_1, protonation and deprotonation of glutamate 61 is proposed. This is also suggested for the *E.coli* binding site as coordinating side chains are missing (4). Alternatively, a proton can be associated to a water molecule which then may be clustered in a similar way as a sodium ion. This second binding scheme was suggested by Boyer (85). von Ballmoos and Dimroth (86) analysed the covalent inhibition with DCCD over a pH range on the basis of binding site studies of Laubinger and Dimroth (148) and Kluge and Dimroth (88). DCCD showed a complete inhibition of the chloroplast enzyme only in the basic pH range 8-9 and almost no effect at a pH below 5.0 (140). This cannot be explained, if the proton translocating enzyme is expected to work with protonation/deprotonation in the DCCD interaction site. An alternative to the protonation/deprotonation of the carboxylate is the coordination as hydronium in a crown ether. In this form the coordination of a proton would correspond to the coordination found in sodium ATP synthases. It would also explain why the *Propionigenium modestum* enzyme, which preferentially binds sodium ions, and the proton translocating chloroplast ring show a similar pH dependent DCCD inhibition (86).

To allow for a controlled translocation of protons in chloroplast F_oF_1 ATP synthase, two different states of the binding site are proposed in this work. Each subunit has to alter between an open and a closed state to facilitate access to the hydrogen bonding network for protonation or deprotonation. This is thought to be implemented in a change of rotamers.

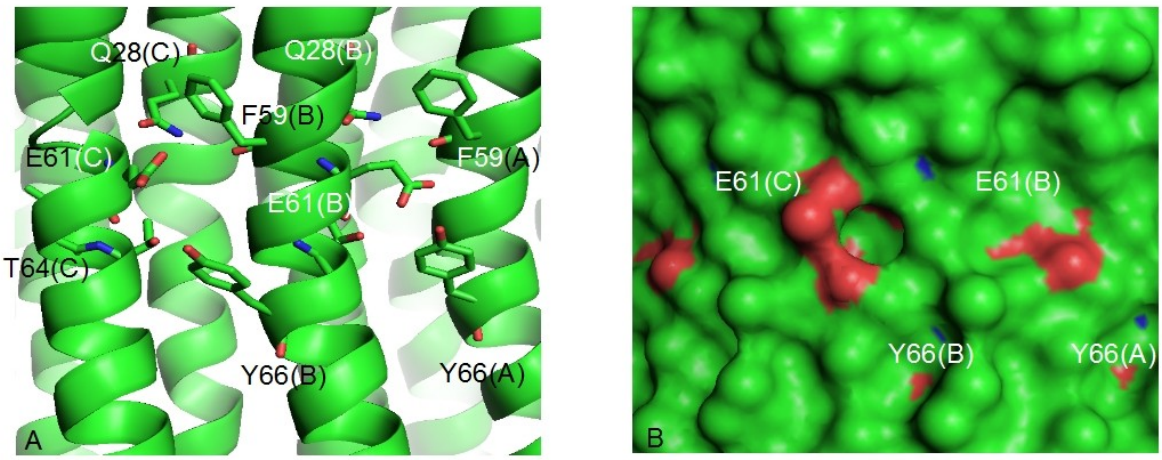

Figure 5.4: (A) Side chains creating the binding site; Between monomers (B) and (C) the binding site is in an open state; Between the monomers (A) and (B) the binding site is closed; (B) Surface calculated for image (A). One can clearly see the hole of the open binding site with negative charge in the back (red) for proton attraction.

Figure 5.4 shows the two different states in adjacent binding sites. Figure 5.4 (B) gives the surface of the same two binding sites as in 5.4 (A). The deprotonated/open site given as Glu61(C) in Figure 5.4 (A) allows for access to a cavity in the calculated surface as shown in Figure 5.4 (B). This cavity is formed by the residues proposed to participate in the hydrogen bonding network for proton binding.

5.3.3. Theoretical Model of Subunit *a*

Figure 5.5 represents a theoretical model of subunit *a* from spinach based on an *E. coli* model. The four helix bundle proposed for the *E.coli* subunit *a* was created through modelling and is part of the structure deposited with the PDB code 1C17. The cross-linking studies mentioned in 1.4.2 (47, 48, 49, 89, 50, 51, 52, 53, 90, 55, 54) and general known restraints in bond lengths and angles were used to create the model. CHAINSAW (127) was used to manipulate the *E. coli* model and create a "mixed" model as described in 3.4.4.1. All side chains were completed in COOT (126) according to the spinach sequence of subunit *a*. The resulting theoretical structure as shown below, is not determined by experimental data.

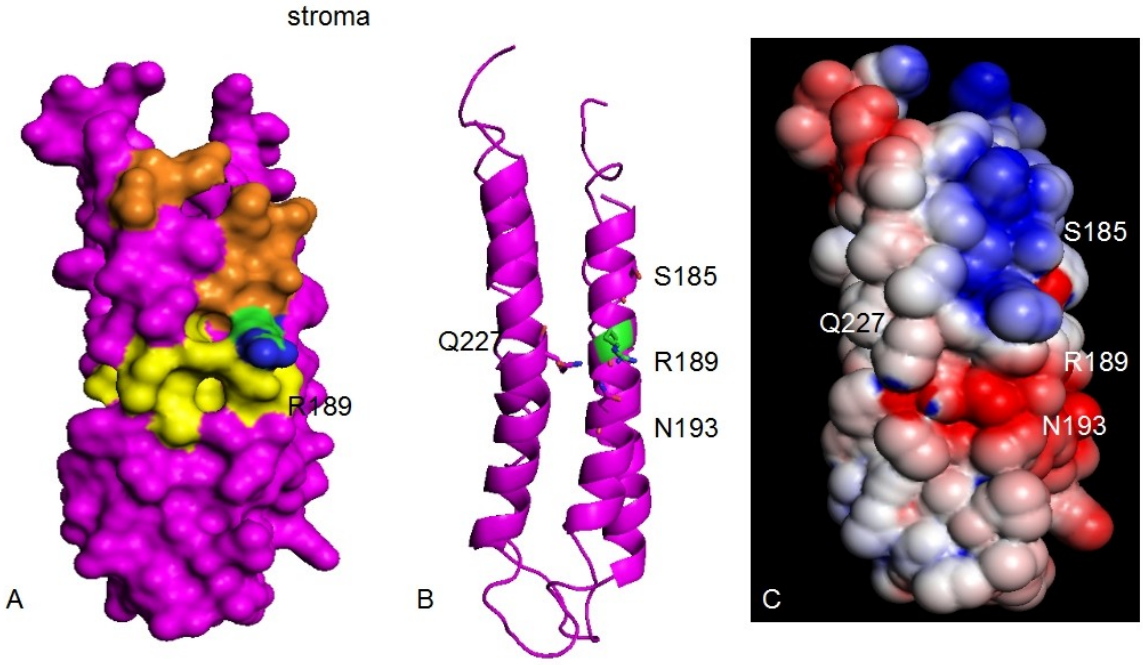

Figure 5.5: (A) View of the surface of subunit *a* showing the contact area with the membrane ring. Residues, which are proposed to form the cytoplasmic half channel are given in orange and those proposed to contribute to the periplasmic half channel are given in yellow. Essential Arg189 is given in green; (B) Underlying helix arrangement of (A). Residues proposed to be essential in protonation/deprotonation are shown as sticks; (C) Water accessible surface for the contact area to the *c*-ring coloured according to the electrostatic potential; blue positive and red negative

In figure 5.5 (A) the proposed aqueous half channel residues are indicated in a surface image. Yellow gives the periplasmic channel and orange the cytoplasmic channel. In green the highly conserved arginine 189 (for spinach) is shown. If the marked residues will be found to form the two half channels then Arg189 can indeed be seen as a barrier. The side chain of Arg189 protrudes far from the surface which makes interaction with subunit *c* in the membrane integrated rotor possible. Residues Ser185, Arg189, Asn193, and Gln227 for subunit *a* from spinach F_oF_1 ATP synthase (Figure 5.5 (B)) are thought to be essential for the mechanism in concert with the *c*-ring. The electrostatic surface calculated for subunit *a* (Figure 5.5 (C)) appears to correlate with the proposed half channels. The area extending from Arg189 towards the cytoplasm, including Ser 185, has a positive electrostatic potential (blue) and corresponds to the cytoplasmic half channel proposed for *E. coli* (52, 90). For the periplasmic half channel there is negative electrostatic potential (red).

5.3.4. Interaction between Subunit *a* and the *c*-Ring

Two main models for a mechanism and possible interaction between subunits *a* and *c* have been proposed. They are both described in detail in 1.4.4. Which model is most probable for the spinach *c*-ring is still speculative as a resolution of 3.8 Å does not reveal structural and mechanistic details. Concerning the the orientation of *c*Glu61 in the binding site (Figure 5.3 (D)), this suggests that a 140° rotation of the C terminal helix as proposed for *E. coli* (39) is not necessary.

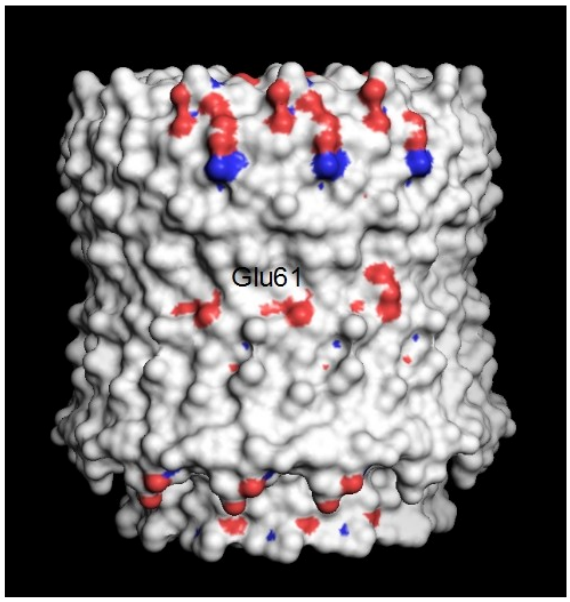

Figure 5.6: Surface view of the c-ring; for three adjacent subunits charged and polar side chains are indicated; red negative and blue positive

For the spinach binding site it seems to be sufficient to change the rotamer. This is also more efficient from a thermodynamic point of view. Less energy is necessary to switch between two rotamers while protonation and deprotonation occurs, than rotation of a complete helix as proposed for *E. coli* (39). A possible mechanism in spinach F_oF_1 ATP synthase could be as follows:
*c*Glu61 becomes deprotonated when entering the *a/c*-interface and getting into proximity of *a*Arg189 in subunit *a*. The arginine competes with the proton for the negative charge of *c*Glu61 and a stable salt bridge is favoured compared to a bound proton. This salt bridge formation is accompanied with a rotamer switch of glutamate 61 in subunit *c* to an exposed rotamer, which facilitates a stabilising ionic connection. Figure 5.4 (A) shows two adjacent binding sites with different rotamers. The water accessible area in subunit *a* (Figure 5.5 (C)) allows for the

establishment of a hydrogen bonding network. This network may be connected to the stroma via *a*Ser185, corresponding to the proposals for *E. coli* (52, 90). Residues *a*Asn193 and *a*Gln227 are correspond to *a*Asn214 and *a*Gln252 in *E. coli*. They are suggested to be part of the periplasmic half channel, which is in contact with a proton pool. Both residues may assist *a*Arg189 to load a proton on the free binding site, which actually is part in the stabilising salt bridge. However, a hydrogen bonding network for proton delivery in proximity to *a*Asn193 and *a*Gln227 with connection to the periplasm is not as obvious as for proton release in the area around *a*Ser185. An alternative periplasmic half channel as proposed to be intrinsic to the *c*-ring of the sodium translocating ATP synthase from *Ilyobacter* (33) is also not obvious from Figure 5.6 where charged residues are indicated. After having accepted a new proton, *c*Glu61 undergoes again a rotamer change so that the protonated residue is buried between the C terminal helices of adjacent *c* monomers. The buried rotamer produces less friction when moving within the membrane during rotation, than a deprotonated *c*Glu61 or an outward pointing side chain. The loaded binding site leaves the interface on one site simultaneously with a loaded one entering from the opposite side. The situation in the *a/c* interface as proposed for the ATP synthase from spinach chloroplasts can be seen in Figure 5.7.

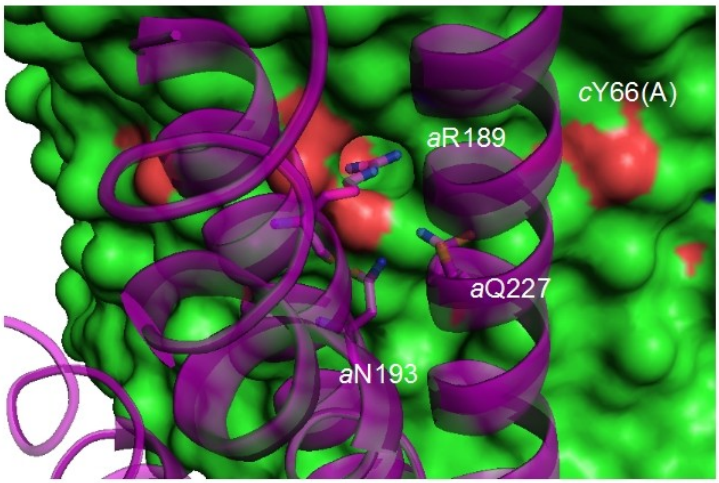

Figure 5.7: Proposed interaction between subunit a and c in the membrane of F_oF_1 ATP synthase from spinach chloroplasts. In the background the surface of the membrane ring is given with one open and adjacent closed binding sites. Subunit a is shown as transparent ribbons and sticks as it is only a theoretical model and not the result of a structure solution. The essential Arg189 has free access into the open binding site.

6. Literature

1. Brown, S.P., Miller, W.C., and Eason, J.E. (2005) Exercise Physiology: Basis of Human Movement in Health and Disease, Lipincott Williams & Wilkins

2. Pedersen, L.P. And Amzel, L.M. (1993) ATP Synthases Structure, Reaction Center, Mechanism, and Regulation of One of Nature's Most Unique Machines, *J. Biol. Chem.* **268**, 9937-9940

3. Stock, D., Leslie, A.G.W., and Walker, J.E. (1999) Molecular Architecture of the Molecular Motor in ATP Synthase, *Science* **286**, 1700-1705

4. Rastogi, V.K. and Girvin, M.E. (1999) Structural changes linked to proton translocation by subunit *c* of the ATP synthase, *Nature* **402**, 263-268

5. Seelert, H., Poetsch, A., Dencher, N.A., Engel, A., Stahlberg, H., and Müller, D.J. (2000) Proton-powered turbine of a plant motor, *Nature* **405**, 418-419

6. Jiang, W., Hermolin, J., and Fillingame, R.H. (2001) The preferred stoichiometry of *c* subunits in the rotary motor sector of *Escherichia coli* ATP synthase is 10, *Proc. Natl. Acad. Sci. U.S.A.* **98**, 4966-4971

7. Vonck, J. Krug von Nidda, T., Meier, T., Matthey, U., Mils, D.J., Kühlbrandt, W., and Dimroth, P. (2002) Molecular Architecture of the Undecameric Rotor of a Bacterial Na^+-ATP Synthase, *J. Mol. Biol.* **321**, 307-316

8. Pogoryelov, D., Yu, J., Meier, T., Vonck, J., Dimroth, P., and Müller, D.J. (2005) The c_{15} ring of the *Spirulina platensis* F-ATP synthase: F_1/F_o symmetry mismatch is not obligatory, *EMBO reports* **6**, 1040-1044

9. Dimroth, P., von Ballmoos, C., Meier, T., and Kaim, G. (2003) Electrical Power Fuels Rotary ATP Synthase, *Structure* **11**, 1469-1473

10. Nalin, C.M. and McCarty, R.E. (1984) Role of a Disulfide Bond in the γ Subunit in Activation of the ATPase of Chloroplast Coupling Factor 1, *J. Biol. Chem.* **259**, 7275-7280

11. Richter, M.L., Patrie, W.J., and McCarty, R.E: (1984) Preparation of the ε Subunit and the ε Subunit-deficient Chloroplast Coupling Factor 1 in Reconstitutively Active Form, *J. Biol. Chem.* **259**, 7371-7373

12. Digel, J.G., Moore, N.D., and McCarty, R.D. (1998) Influence of Divalent Cations on Nucleotide Exchange and ATPase Activity of Chloroplast Coupling Factor1, *Biochemistry* **37**, 17209-17215

13. Johnson, E.A., and McCarty, R.E. (2002) The carboxyl terminus of the epsilon subunit of the chloroplast ATP synthase is exposed during illumination, *Biochemistry* **41**, 2446-2451

14. Nowak, K.F. and McCarty, R.E. (2004) Regulatory Role of the C-Terminus of the ε Subunit from the Chloroplast ATP Synthase, *Biochemistry* **43**, 32739-3279

15. Boekema, E.J. and Böttcher, B. (1992) The structure of ATP synthase from chloroplasts: Conformational changes of CF_1 studied by electron microscopy, *Biochim. Biophys. Acta* **1098**, 131-143

16. Böttcher, B., Schwarz, L., and Gräber, P. (1998) Direct indication for existence of a double stalk in CF_oF_1, *J. Mol. Biol.* **281**, 757-762

17. Mellwig, C. and Böttcher, B. (2003) A unique resting position of the ATP-Synthase from Chloroplasts, *J. Biol. Chem.* **278**, 18544-18549

18. Groth, G. and Pohl, E. (2001) The structure of the Chloroplast F_1-ATPase at 3.2 Å resolution, *J. Mol. Biol.* **276**, 1345-1352

19. Cross, R.L. (1988) The number of functional catalytic sites on F_1-ATPases and the effect on quaternary structural asymmetry on their properties, *J. Bioenerg. Biomembr.* **20**, 395-405

20. Abrahams, J.P., Leslie, A.G.W., Lutter, R., and Walker, J.E. (1994) Structure at 2.8 Å resolution of F_1-ATPase from bovine heart mitochondria, *Nature* **370**, 621-628

21. Gibbons, C., Montgomery, M.G., Leslie, A.G.W., and Walker J.E. (2000) The structure of the central stalk in bovine F_1- ATPase at 2.4 Å resolution, *Nature Struct. Biol.* **7**, 1055-1061

22. Watts, S.D, Zhang, Y., Fillingame, R.H:, Capaldi, R.A. (1995) The *γ* subunit in the *Escherichia coli* ATP synthase complex (ECF_oF_1) extends through the stalk and contacts the *c* subunits to the F_o part, *FEBS Lett.* **368**, 235-238

23. Hermolin, J., Dmitriev, O.Y., Zhang, Y., and Fillingame, R.H: (1999) Defining the Domain of Binding of F_1 Subunit *ε* with the Polar Loop of F_o Subunit *c* in the *Escherichia coli* ATP Synthase, *J. Biol. Chem.* **274**, 17011-17016

24. Sabbert, D., Engelbrecht, S., and Junge, W. (1996) Intersubunit rotation in active F-ATPase, *Nature* **381**, 623-625

25. Junge, W., Lill, H., and Engelbrecht, S. (1997) ATP synthase: an electrochemical transducer with rotatory mechanics, *Trends. Biochem. Sci.* **22**, 420-423

26. Elston, T., Wang, H., and Oster, G. (1998) Energy transduction in ATP synthase, *Nature* **391**, 510-513

27. Samra, H.S., Gao, F., He, F., Hoang, E., Chen, Z., Gegenheimer, P.A., Berrie, C.L., and Richter, M.L. (2006) Structural Analysis of the Dithiol-containing Domain of the Chloroplast ATP Synthase *γ* Subunit, *J. Biol. Chem.* **281**, 31041-31049

28. Uhlin, U., Cox, G.B., and Guss, J.M. (1997) Crystal structure of the *ε* of the proton-translocating ATP synthase from *Escherichia coli*, *Structure* **5**, 1219-1230

29. Wilkens, S. and Capaldi, R.A. (1998) Solution Structure of the ε Subunit of the F_1-ATPase from *Escherichia coli* and Interactions of This Subunit with β Subunit in the Complex, *J. Biol. Chem.* **273**, 26645-26651

30. Rodgers, R.J.W. and Wilce, M.C.J. (2000) Structure of the γ-ε complex of ATP synthase, *Nature Struct. Biol.* **7**, 1051-1054

31. Lill, H., Hensel, F., Junge, W., and Engelbrecht, S. (1996) Cross-linking of Engineered of Subunit δ to $(\alpha\beta)_3$ in Chloroplast F-ATPase, *J. Biol. Chem.* **271**, 32737-32742

32. Engelbrecht, S., Giakas, E., Marx, O., and Lill, H. (1998) Fluorescence resonance energy transfer mapping of subunit δ in spinach chloroplast F_1 ATPase, *Eur. J. Biochem.* **252**, 277-283

33. von Ballmoos, C., Cook, G.M., and Dimroth, P. (2008) Unique Rotary ATP Synthase and Its Biological Diversity, *Annu. Rev. Biophys.* **37**, 43-64

34. Birkenhäger, R., Hoppert, M., Deckers-Hebestreit,G., Mayer, F., and Altendorf, K. (1995) The F_o complex of the *Escherichia coli* ATP synthase-Investigation by electron spectroscopic imaging and immunoelectron microscopy, *Eur. J. Biochem.* **230**, 58-67

35. Hatch, L.P., Cox, G.B., and Howitt, S.M. (1995) The Essential Arginine Residue at Position 210 in the *a* Subunit of the *Escherichia coli* ATP Synthase Can Be Transferred to Position 252 with Partial Retention of Activity, *J. Biol. Chem.* **270**, 29407-29412

36. Nelson, N (1992) Structural conservation and functional diversity of V-ATPases, *J. Bioenerg. Biomembr.* **24**, 407-414

37. Nishi, T. and Forgac, M. (2002) The vacuolar (H^+)-ATPases – nature's most versatile proton pumps, *Nat. Rev. Mol. Cell Biol.* **3**, 94-103

38. Murata, T., Yamato, I., Kakinum, Y., Leslie, A.G.W., and Walker, J.E. (2005) Structure of the Rotor of the V-Type Na^+-ATPase from *Enterococcus hirae*, *Science* **308**, 654-659

39. Girvin, M.E., Rastogi, V.K., Abildgaard, F., Markley, J.L., and Fillingame, R.H. (1998) Solution Structure of the Transmembrane H-Transporting Subunit *c* of the F_1F_o ATP Synthase, *Biochemistry* **37**, 8817-8824

40. Hoppe, J., Friedl, P., Schairer, H.U., Sebald, W., von Meyenburg, K., and Jørgensen, B.B. (1983) The topology of the proton translocating F_o component of the ATP synthase from *E.coli* K12: studies with proteases, *EMBO J.* **2**, 105-110

41. Groth, G. and Walker, J.E. (1997) Model of the *c*-subunit oligomer in the membrane domain of F-ATPases, *FEBS Lett.* **410**, 117-123

42. Khorana, H.G. (1953) The Chemistry of Carbodiimides, *Chem. Rev.* **53**, 145-166

43. Capaldi, R.A. and Aggeler, R. (2002) Mechanism of the F_1Fo-type ATP synthase, a biological rotary motor, *Trends Biol. Sci.* **27**, 154-160

44. Oberfeld, B., Brunner, J., and Dimroth, P. (2006) Phospholipids Occupy the Internal Lumen of the c Ring of the ATP Synthase of *Escherichia coli*, *Biochemistry* **45**, 1841-1851

45. Meier, T., Matthey, U., Henzen, F., Dimroth, P., and Müller, D.J. (2002) The central plug in the reconstituted undecameric *c* cylinder of a bacterial ATP synthase consists of lipids, *FEBS Lett.* **505**, 353-356

46. Wada, T., Long, J.C., Zhang, D., and Vik, S.B. (1999) A Novel Labelling Approach Supports the Five-transmembrane Model of Subunit *a* of the *Escherichia coli* ATP Synthase, *J. Biol. Chem.* **274**, 17353-17357

47. Valiyaveetil, F.I. and Fillingame, R.H. (1997) On the role of Arg-210 and Glu-219 of subunit a in proton translocation by the *Escherichia coli* F_oF_1-ATP synthase, *J. Biol. Chem.* **272**, 32635-32641

48. Valiyaveetil, F.I. and Fillingame, R.H. (1998) Transmembrane Topography of Subunit *a* in *Escherichia coli* F_1F_o ATP Synthase, *J. Biol. Chem.* **273**, 16241-16247

49. Jiang, W. And Fillingame, R.H. (1998) Interacting helical faces of subunits *a* and *c* in the F_1F_o ATP synthase of *Escherichia coli* defined by disulfide cross-linking, *Proc. Natl. Acad. Sci. U.S.A.* **95**, 6607-6612

50. Angevine, C.M. and Fillingame, R.H. (2003) Aqueous Access Channels in Subunit *a* of Rotary ATP Synthase, *J. Biol. Chem.* **278**, 6066-6074

51. Angevine, C.M., Herold, K.A.G., and Fillingame, R.H. (2003) Aqueous access pathways in subunit a of rotary ATP synthase extend to both sides of the membrane, *Proc. Natl. Acad. Sci. U.S.A.* **100**, 13179-13183

52. Schwem, B.E. and Fillingame, R.H. (2006) Cross-linking between Helices within Subunit *a* of *Escherichia coli* ATP Synthase Defines the Transmembrane Packing of a Four-helix Bundle, J. *Biol. Chem.* **281**, 37861-37867

53. Angevine, C.M., Herold, K.A.G., Owen, D.V., and Fillingame, R.H: (2007) Aqueous Access Pathways in ATP Synthase Subunit *a*, *J. Biol. Chem.* **282**, 9001-9007

54. Steed, P.R. and Fillingame, R.H. (2008) Subunit a Facilitates Aqueous Access to a Membrane-embedded Region of Subunit *c* in *Escherichia coli* F_1F_o ATP Synthase, *J. Biol. Chem.* **283**, 12365-12372

55. Moore, K.J. and Fillingame, R.H. (2008) Structural Interactions between Transmembrane Helices 4 and 5 of Subunit *a* and the Subunit *c* Ring of Escherichia coli ATP Synthase, *J. Biol. Chem.* **283**, 31726-31735

56. Jones, P.C., Hermolin, J., Jiang, W., and Fillingame. R.H. (2000) Insights into the Rotary Catalytic Mechanism of F_oF_1 ATP Synthase from the Cross-linking of Subunits *b* and *c* in the *Escherichia coli* Enzyme, *J. Biol. Chem.* **275**, 31340-31346

57. Schneider, E. and Altendorf, K. (1984) Subunit *b* of the membrane moiety (F_o) of ATP synthase (F_1F_o) from *Escherichia coli* is indispensable for H^+ translocation and binding of the water-soluble F_1 moiety, *Proc. Natl. Acad. Sci. U.S.A.* **81**, 7279-7283

58. Aris, J.P. and Simoni, R.D. (1983) Cross-linking and Labelling of the *Escherichia coli* F_1F_o-ATP Synthase Reveal a Compact Hydrophilic Portion of F_o Close to an F_1 Catalytic Subunit, *J. Biol. Chem.* **258**, 14599-14609

59. Kane Dickson, V., Silvester, J.A., Fearnley, I.M., Leslie, A.G.W., and Walker, J.E. (2006) On the structure of the stator of the mitochondrial ATP synthase, *EMBO J.* **25**, 2911-2918

60. Boyer, P.D. (1993) The binding change mechanism for ATP synthase – some probabilities and possibilities, *Biochim. Biophys. Acta* **1140**, 215-250

61. Boyer, P.D. (2000) Catalytic site forms and controls in ATP synthase catalysis, *Biochim. Biophys. Acta* **1458**, 252-262

62. Cross, R.L. (1981) The Mechanism and Regulation of ATP Synthesis by F_1-ATPases, *Annu. Rev. Biochem.* **50**, 681-714

63. Noji, H., Yasuda, R., Yoshida, M., and Kinosita Jr, K. (1997) Direct observation of the rotation of F_1-ATPase, *Nature* **386**, 299-302

64. Kato-Yamada, Y., Noji, H., Yasuda, R., Kinosita Jr, K., and Yoshida, M. (1998) Direct Observation of the Rotation of ε Subunit in F_1-ATPase, *J. Biol. Chem.* **273**, 19375-19377

65. Yasuda, R., Noji, H., Kinosita Jr, K., and Yoshida, M. (1998) F_1-ATPase Is a Highly Efficient Molecular Motor that Rotates with Discrete 120° Steps, *Cell* **93**, 1117-1124

66. Yasuda, R., Noji, H., Yoshida, M., Kinosita Jr, K., and Itoh, H. (2001) Resolution of distinct rotational substeps by submillisecond kinetic analysis of F_1-ATPase *Nature* **410**, 898-904

67. Jagendorf, A.T. And Uribe, E. (1966) ATP formation caused by acid-base transition of spinach chloroplasts, *Proc. Natl. Acad. Sci. U.S.A.* **55**, 170-177

68. Kaim, G. and Dimroth, P. (1999) ATP synthesis by F-type ATP synthase is obligatory dependent on the transmembrane voltage, *EMBO J.* **18**, 4118-4127

69. Mitchell, P. (1961) Coupling of phosphorylation to electron and hydrogen transfer by a chemi-osmotic type of mechanism, *Nature* **191**, 144-148

70. Kaim, G. and Dimroth, P. (1998) Voltage-generated torque drives the motor of the ATP synthase, *EMBO J.* **17**, 5887-5895

71. Steigmiller, S., Turina, P., and Gräber, P. (2008) The thermodynamic H^+/ATP ratios of the H^+-ATPsynthases from chloroplast and *Escherichia coli*, *Proc. Natl. Acad. Sci. U.S.A.* **105**, 3745-3750

72. Dimroth, P., von Ballmoos, C., and Meier, T. (2006) Catalytic and mechanical cycles in F-ATP synthases, *EMBO Rep.* **7**, 276-282

73. Junge, W., Pänke, O., Cherepanov, D.A., Gumbiowski, K., Müller, M., and Engelbrecht, S. (2001) Inter-subunit rotation and elastic power transmission in F_oF_1-ATPase, *FEBS Lett.* **504**, 152-160

74. Pänke, O., Cherepanov, D.A., Gumbiowski, K., Engelbrecht, S., and Junge, W. (2001) Viscoelastic dynamics of actin filaments coupled to rotary F-ATPases: Torque profile of the enzyme, *Biophys. J.* **81**, 1220-1233

75. Sielaff, H., Rennekamp, H., Wächter, A., Xie, H., Hilbers, F., Feldbauer, K., Dunn, S.D., Engelbrecht, S., and Junge, W. (2008) Domain compliance and elastic power transmission in rotary F_oF_1-ATPase, *Proc. Natl. Acad. Sci. U.S.A.* **105**, 17760-17765

76. Kaim, G. and Dimroth, P. (1995) Formation of a functionally active sodium-translocating hybrid F_1F_o ATPase in *Propionigenium modestum* by homologous recombination, *Eur. J. Biochem.* **218**, 937-944

77. Sorgen, P.L., Caviston, T.L., Perry, R.C., and Cain. B.D. (1998) Deletions in the second stalk of F_1F_o-ATP synthase in *Escherichia coli*, *J. Biol. Chem.* **273**, 27873-27878

78. Sorgen, P.L., Bubb, M.R., and Cain, B.D. (1999) Lengthening the Second Stalk of F_1F_o ATP Synthase in *Escherichia coli*, *J. Biol. Chem.* **274**, 36261-36266

79. Müller, M., Pänke, O., Junge, W., and Engelbrecht, S. (2002) F_1-ATPase: The terminal end of subunit *γ* is not required for ATP hydrolysis-driven rotation, *J. Biol. Chem.* **277**, 23308-23313

80. Matthey, U., Kaim, G., Braun, D., Wüthrich, K., and Dimroth, P. (1999) NMR studies of subunit *c* of the ATP synthase from *Propionigenium modestum* in dodecyl sulphate micelles, *Eur. J. Biochem.* **261**, 459-467

81. Assadi-Porter, F.M. and Fillingame, R.H. (1995) Proton-Translocating Carboxyl of Subunit *c* of F_1F_o H^+-ATP Synthase: The Unique Environment Suggested by the pKa Determined by ^1H NMR, *Biochemistry* **34**, 16186-16193

82. Meier, T., Polzer, P., Diederichs, K., Welte, W., and Dimroth, P. (2005) Structure of the Rotor Ring of F-Type Na^+-ATPase from *Ilyobacter tartaricus*, *Science* **308**, 659-662

83. Kaim, G., Gerike, U., and Dimroth, P. (1997) Molecular basis for coupling ion selectivity of F_1F_o ATP synthases: probing the liganding groups for Na^+ and Li^+ in the *c* subunit of the ATP synthase from *Propionigenium modestum*, *Biochemistry* **36**, 9185-9194

84. Murata, T., Yamato, I., Kakinuma, Y., Shirouzu, M., Walker, J.E., Yokoyama, S., and Iwata, S. (2008) Ion binding and selectivity of the rotor ring of the Na^+-transporting V-ATPase, *Proc. Natl. Acad. Sci. U.S.A.* **105**, 8607-8612

85. Boyer, P.D. (1988) Bioenergetic coupling to protonmotive force: should we be considering hydronium ion coordination and not group protonation?, *Trends. Biochem. Sci.* **13**, 5-7

86. von Ballmoos, C. and Dimroth, P. (2007) Two Distinct Proton Binding Sites in the ATP Synthase Family, *Biochemistry* **46**, 11800-11809

87. Graf, T. and Sebald, W. (1978) The dicyclohexylcarbodiimide-binding protein of mitochondrial ATPase complex from beef heart. Isolation and amino acid composition, *FEBS Lett.* **94**, 218-222

88. Kluge, C. and Dimroth, P. (1993) Kinetics of inactivation of the F_1F_o ATPase of *Propionigenium modestum* by dicyclohexylcarbodiimide in relationship to to H^+ and Na^+ concentration: probing the binding site for coupling ions, *Biochemistry* **32**, 10378-10386

89. Fillingame, R.H., Angevine, C.M, and Dmitriev, O.Y. (2002) Coupling proton movements to *c*-ring rotation in F_1F_o ATP synthase: aqueous access channels and helix rotations at the *a-c* interface, *Biochim. Biophys. Acta* **1555**, 29-36

90. Moore, K.J., Angevine, C.M., Owen, D.V., Schwem, B.E., and Fillingame, R.H. (2008) The Cytoplasmic Loops of Subunit *a* of *Escherichia coli* ATP Synthase May Participate in the Proton Translocating Mechanism, *J. Biol. Chem.* **283**, 13044-13052

91. Roberts, D.D., Lewis, S.D., Ballou, D.P., Olsen, S.T., and Shafer, J.A. (1986) Reactivity of small thiolate anions and cysteine-25 in papain toward methyl methanethiosulfonate, *Biochemistry* **25**, 5595-5601

92. Mordoch, S.S., Granot, D., Lebendiker, M., and Schuldiner, S. (1999)Scanning Cysteine Accessibility of EmrE, an H^+-coupled Multidrug Transporter from *Escherichia coli*, Reveals a Hydrophobic Pathway for Solutes, *J. Biol. Chem.* **274**, 19480-19486

93. Greie, J.C., Heitkamp, T., and Altendorf, K. (2004) The transmembrane domain of subunit *b* of the *Escherichia coli* F_1F_o ATP synthase is sufficient for H^+-translocating activity together with subunits a and c, *Eur. J. Biochem.* **271**, 3036-3042

94. von Ballmoos, C., Meier, T., and Dimroth, P. (2002) Membrane embedded location of Na^+ or H^+ binding sites on the rotor ring of F_1F_o ATP synthases, *Eur. J. Biochem*. **269**, 5581-5589

95. Meier, T., Matthey, U., von Ballmoos, C., Vonck, J., Krug von Nidda, T., Kühlbrandt, W., and Dimroth, P. (2003) Evidence for Structural Integrity in the Undecameric *c*-Rings Isolated from Sodium ATP Synthases, *J. Mol. Biol.* **325**, 389-397

96. Vik, S.B. and Antonio, B.J. (1994) An mechanism of proton translocation by F_1F_o ATP synthases suggested by double mutants of the a subunit, *J. Biol. Chem.* **269**, 30364-30369

97. Fillingame, R.H., Jiang, W., and Dmitriev, O.Y. (2000a) Coupling H^+ transport to rotary catalysis in F-type ATP synthases: structure and organisation of the transmembrane rotary motor, *J. Exp. Biol.* **203**, 9-17

98. Fillingame, R.H., Angevine, C.M., and Dmitriev, O.Y. (2003) Mechanics of coupling proton movements to *c*-ring rotation in ATP synthase, *FEBS Lett.* **555**, 29-34

99. Feniouk, B.A., Kozlova, M.A., Knorre, D.A., Cherepanov, D.A., Mulkidjanian, A.Y., and Junge, W. (2004) The proton-driven rotor of ATP synthase: ohmic conductance (10 fS), and absence of voltage gating, *Biophys. J.* **86**, 4094-4109

100. Dmitriev, O.Y., Jones, P.C., and Fillingame, R.H. (1999) Structure of the subunit *c* oligomer in the F_1F_o ATP synthase: Model derived from solution structure of the monomer and cross-linking in the native enzyme, *Proc. Natl. Acad. Sci. U.S.A.* **96**, 7785-7790

101. Fillingame, R.H., Jiang, W., and Dmitriev, O.Y. (2000b) The Oligomeric Subunit *c* Rotor in the F_o Sector of ATP Synthase: Unresolved Questions in Our Understanding of Function, *J. Bioener. Biomemb.* **32**, 433-439

102. Aksimentiev, A., Balabin, I.A., Fillingame, R.H., and Schulten, K. (2004) Insights into the Molecular Mechanism of Rotation in the F_o Sector of ATP Synthase, *Biophys. J.* **86**, 1332-1344

103. Strotmann, H., Hesse, H., and Edelmann, K. (1973) Quantitative determination of coupling factor CF_1 of chloroplasts, Biochim. Biophys. Acta **314**, 202-210

104. Groth, G. and Schirwitz, K. (1999) Rapid purification of membrane extrinsic F_1-domain of chloroplast ATP synthase in monodisperse form suitable for 3D-crystallisation, *Eur. J. Biochem.* **260**, 15-21

105. Bhairi, S. (2007) Detergents: A guide to properties and uses of detergents in biological systems, Calbiochem®

106. Laemmli, U.K. (1970) Cleavage of Structural Proteins of the Head of Bacteriophage T4, *Nature* **227**, 680-685

107. Heukeshoven, J. and Dernick, R. (1988) Improved silver staining procedure for fast staining in PhastSystem Development Unit I. Staining of sodium dodecyl sulfate gels, *Electrophoresis* **9**, 28-32

108. DuBois, M., Gilles, K.A., Hamilton, J.K., Rebers, P.A., and Smith, F. (1956) Colorimetric Method for Determination of Sugars and Related Substances, *Anal. Chem.* **28**, 350-356

109. Urbani, A. and Warne, T. (2005) A colorimetric determination for glycosidic and bile salt-based detergents: applications in membrane protein research, *Anal. Biochem.* **336**, 117-124

110. Chayen, N.E. (2005) Methods for separating nucleation and growth in protein crystallisation, *Prog. Biosphy. Mol. Biol.* **88**, 329-337

111. Chayen, N.E., Stewart, P.D.S., Maeder, D.L., and Blow, D.M. (1990) An Automated-System for Microbatch Protein Crystallisation and Screening, *J. Appl. Crystallogr.* **23**, 297-302

112. Chayen, N.E., Stewart, P.D.S., and Blow, D.M. (1992) Microbatch Crystallisation under Oil – a New Technique Allowing Many Small-Volume Crystallisation Trials, *J. Cryst. Growth* **122**, 176-180

113. D'Arcy, A., Elmore, C., Stihle, M., and Johnston, J.E. (1996) A novel approach to crystallise proteins under oil, *J. Cryst. Growth* **168**, 175-180

114. D'Arcy, A., MacSweeney, A., and Haber, A. (2004) Practical aspects of using the microbatch method in screening conditions for protein crystallization, *Methods* **34**, 323-328

115. Carter Jr, C.W. and Carter C.W. (1979) Protein Crystallisation Using Incomplete Factorial Experiments, *J. Biol. Chem.* **254**, 12219-12223

116. Jancarnik, J. and Kim, S.H: (1991) Sparse-Matrix Sampling – a Screening Method for Crystallization of Proteins, *J. Appl. Crystallogr.* **24**, 409-411

117. Landau, E.M. and Rosenbusch, J.P. (1996) Lipidic cubic phase: A novel concept for the crystallisation of membrane proteins, *Proc. Natl. Acad. Sci. U.S.A.* **93**, 14532-14535

118. Heras, B., Edeling, M.A., Byriel, K.A:, Jones, A., Raina, S., and Martin, J.L. (2003) Dehydration Converts DsbG Crystal Diffraction from Low to High Resolution, *Structure* **11**, 139-145

119. Heras, B. and Martin, J.L. (2005) Post-crystallization treatments for improving diffraction quality of protein crystals, *Acta Cryst.* **D 61**, 1173-1180

120. Garman, E.F. (2003) 'Cool' crystals: macromolecular cryocrystallography and radiation damage, *Curr. Opin. Struct. Biol.* **13**, 545-551

121. Garman, E.F. and Owen, R.L. (2006) Cryocooling and radiation damage in macromolecular crystallography, *Acta Cryst.* **D 62**, 32-47

122. Leslie, A.G.W. (1992) Joint CCP4 and ESF-EACMB Newsletter Protein Crystallography, p.26, Daresbury Laboratory, Warrington, UK

123. Evans, P.R. (2005) Scaling and assessment of data quality, *Acta Cryst.* **D 62**, 72-82

124. Collaborative Computational Project, Number 4 (1994) *Acta. Cryst.* **D 50**, 760-763

125. Vagin, A.A. and Teplyakov, A. (1997) MOLREP: an Automated program for Molecular Replacement, *J. Appl. Cryst.* **30**, 1022-1025

126. Emsley, P. and Cowtan, K.D. (2004) Coot: model-building for molecular graphics, *Acta Cryst.* **D 60**, 2126-2132

127. Stein, N. (2008) CHAINSAW: a program for mutating pdb files used as templates in molecular replacement, *J. Appl. Cryst.* **41**, 641-643

128. Murshudov, G.N., Vagin, A.A., and Dodson, E.J. (1997) Refinement of Macromolecular Structures by the Maximum-Likelihood Method, *Acta Cryst.* **D 53**, 240-255

129. McCoy, A.J., Grosse-Kunstleve, R.W., Adams, P.D., Winn, M.D., Storoni, L.C., and Read, R.J. (2007) Phaser crystallographic software, *J. Appl. Cryst.* **40**, 658-674

130. Cowtan, K.D. and Zhang, K.Y. (1999) Density modification for macromolecular phase improvement, *Prog. Biophys. Mol. Biol.* **72**, 245-270

131. Winn, M.D., Isupov, M., and Murshudov, G.N. (2001) Use of TLS parameters to model anisotropic displacement in macromolecular refinement, *Acta Cryst.* **D 57**, 122-133

132. Laskowski, R.A., MacArthur, M.W., Moss, D.S., and Thornton, J.M. (1993) PROCHECK: a program to check the stereochemical quality of protein structures, *J. Appl. Cryst.* **26**, 283-291

133. Hooft, R.W.W., Vriend, G., Sander, C., and Abola, E.E. (1996) Errors in protein structures, *Nature* **381**, 272-272

134. DeLano, W.L. (2002) The PyMOL Molecular Graphics System, DeLano Scientific, San Carlos, CA, U.S.A.

135. Baker, N.A., Sept, D., Joseph, S., Holst, M.J., and McCammon, J.A. (2001) Electrostatics of nanosystems: application to microtubulus and the ribosome, *Proc. Natl. Acad. Sci. U.S.A.* **98**, 10037-10041

136. Dolinsky, T.J., Czodowski, P., Li, H., Nielsen, J.E., Jensen, J.H., Klebe, G., and Baker, N.A. (2007) PDB2PQR: Expanding and upgrading automated preparation of biomolecular structures for molecular simulations, *Nucleic. Acids Res.* **35**, W522-525

137. Büchner, C. (2004) Kristallisation und Strukturanalyse der chloroplastidären F_oF_1-ATPase, Dissertation, Heinrich-Heine-Universität, Düsseldorf

138. Pick, U. and Racker, E. (1979) Purification and Reconstitution of the N,N'-Dicyclohexylcarbidiimide-sensitive ATPase Complex from Spinach Chloroplasts, *J. Biol. Chem.* **254**, 2793-2799

139. Warne, T., Chirnside, J., and Schertler, F.G. (2003) Expression and purification of truncated, non-glycosylated turkey beta-adrenergic receptors for crystallisation, *Biochim. Biophys. Acta* **1610**, 133-140

140. Mills, J.D. And Hind, G. (1979) Light-induced Mg^{2+} ATPase activity of coupling factor in intact chloroplasts, *Biochim. Biophys. Acta* **547**, 455-462

141. De Jonge, P.C., Wieringa, T., van Putten, J.P.M., Krans, H.M.J., and van Dam, K. (1983) An uncoupler and an inhibitor of mitochondrial oxidative phosphorylation, *Biochim. Biophys. Acta* **722**, 219-225

142. Cseh, R. and Benz, R. (1999) Interaction of Phloretin with Lipid Monolayers: Relationship between Structural Changes and Dipole Potential Change, *Biophys. J.* **77**, 1477-1488

143. Pick, U. and Finel, M. (1983) Detection of conformational changes in chloroplast coupling factor 1 by 8-anilino-1-naphthalene-sulphonate fluorescence changes, *Eur. J. Biochem.* **135**, 559-567

144. Zheng, J. and Ramirez, V.D. (2000) Inhibition of mitochondrial proton FoF1-ATPase/ATP synthase by polyphenolic phytochemicals, *Br. J. Pharmacol.* **130**, 1115-1123

145. Matthies, D., Preiß, L., Klyszejko, A.L., Muller, D.J., Cook, G.M., Vonck, J., and Meier, T. (2009) The c_{13} Ring from a Thermoalkalophilic ATP Synthase Reveals an Extended Diameter Due to a Special Structural Region, *J. Mol. Biol.*, in press

146. Vollmar, M., Schlieper, D., Winn, M., Büchner, C., and Groth, G. (2009) Structure of the c_{14}-Rotor ring of the proton translocating chloroplast ATP synthase, *J. Biol. Chem.*, in press

147. Laubinger, W. and Dimroth, P. (1989) The sodium ion translocating adenosintriphosphatase of *Propionigenium modestum* pumps protons at low sodium ion concentrations, *Biochemistry* **28**, 7194-7198

148. Winter, R. and Noll, F. (1998) Methoden der Biophysikalischen Chemie, Teubner, Stuttgart

149. Massa, W. (2005) Kristallstrukturbestimmung, Teubner, Wiesbaden

150. Lodish, H., Berk, A., Matsudaira, P., Kaiser, C.A., Krieger, M., Scott, M.P., Zipursky, S.L:, and Darnell, J. (2004) Molecular Cell Biology, 5th Edition, W.H. Freemann and Company, New York

151. Blow, D. (2006) Outline of Crystallography for Biologists, Oxford University Press, Oxford

152. Bergfors, T.M. Protein Crystallization – Techniques, Strategies, and Tips (International University Line, La Jolla, 1999)

7. Appendix

7.1. List of Washing Buffers

Washing Buffer 1			Washing Buffer 6	
100 mM	Natriumcitrate pH 5.5		100 mM	Na-Acetate, pH 4.6
10% (w/v)	Glycerol		10% (w/v)	Glycerol
4%(w/v)	Glycine		4% (w/v)	Glycine
2 mM	$MgCl_2$		2 mM	$MgCl_2$
0.02% (w/v)	NaN_3		0.002% (w/v)	PMSF
0.002% (w/v)	PMSF		0.02% (w/v)	NaN_3
0.1% (w/v)	Dodecylmaltoside		0.01% (w/v)	Dodecylmaltoside
Washing Buffer 2			Washing Buffer 7	
100 mM	Natriumcitrate pH 5.5		100 mM	Na-Acetate pH 4.6
10% (w/v)	Glycerol		10%(w/v)	Glycerol
4%(w/v)	Glycine		4%(w/v)	Glycine
2 mM	$MgCl_2$		2 mM	$MgCl_2$
0.02% (w/v)	NaN_3		1 mM	EDTA, pH 7.0
0.002% (w/v)	PMSF		0.02% (w/v)	NaN_3
0.01% (w/v)	Dodecylmaltoside		0.002% (w/v)	PMSF
			0.01% (w/v)	Dodecylmaltoside
Washing Buffer 3			Washing Buffer 8	
100 mM	Natriumcitrate pH 5.5		25 mM	Bis-Tris-Propane, pH 6.5
10% (w/v)	Glycerol		10% (w/v)	Glycerol
4% (w/v)	Glycine		4% (w/v)	Glycine
4 mM	$MgCl_2$		2 mM	$MgCl_2$
0.02%(w/v)	NaN_3		1 mM	EDTA, pH 7.0
0.002% (w/v)	PMSF		0.02% (w/v)	NaN_3
0.1% (w/v)	Dodecylmaltoside		0.002% (w/v)	PMSF
			35 mM	C-HEGA-10

Washing Buffer 4			Washing Buffer 11	
25 mM	Tricine, pH 8.0		25 mM	Na-Acetate, pH 4.6/HCl
10% (w/v)	Glycerol		10% (w/v)	Glycerol
4% (w/v)	Glycine		4% (w/v)	Glycine
2 mM	$MgCl_2$		2 mM	$MgCl_2$
1 mM	EDTA, pH 7.0		1 mM	EDTA, pH 7.0
0.02% (w/v)	NaN_3		0.02% (w/v)	NaN_3
0.002% (w/v)	PMSF		0.002% (w/v)	PMSF
0.1% (w/v)	Dodecylmaltoside		0.1% (w/v)	Dodecylmaltoside
Washing Buffer 5			Washing Buffer 12	
35 mM	Bis-Tris-Propane, pH 6.5		25 mM	Tricine, pH 8.0
10% (w/v)	Glycerol		4% (w/v)	Glycine
4% (w/v)	Glycine		10% (w/v)	Glycerol
2 mM	$MgCl_2$		2 mM	$MgCl_2$
1 mM	EDTA, pH 7.0		1 mM	EDTA, pH 7.0
0.02% (w/v)	NaN_3		0.02% (w/v)	NaN_3
0.002% (w/v)	PMSF		0.002% (w/v)	PMSF
0.1% (w/v)	Dodecylmaltoside		0.1% (w/v)	Phosphatidyl choline
			0.1% (w/v)	Dodecylmaltoside
Washing Buffer 14			Washing Buffer 16	
25 mM	Na-Acetate, pH 4.6/HCl		25 mM	Na-Acetate, pH 4.6/HCl
10% (w/v)	Sucrose		4% (w/v)	Glycine
4% (w/v)	Glycine		2 mM	$MgCl_2$
2 mM	$MgCl_2$		1 mM	EDTA, pH 7.0
1 mM	EDTA, pH 7.0		0.02% (w/v)	NaN_3
0.02% (w/v)	NaN_3		0.002% (w/v)	PMSF
0.002% (w/v)	PMSF		0.1% (w/v)	Dodecylmaltoside
0.1% (w/v)	Dodecylmaltoside			

Washing Buffer 15	
25 mM	Na-Acetate, pH 4.6/HCl
10% (w/v)	Glycerol
4% (w/v)	Glycine
2 mM	$MgCl_2$
1 mM	EDTA, pH 7.0
0.02% (w/v)	NaN_3
0.002% (w/v)	PMSF
35 mM	C-HEGA-10

7.2. List of Crystallisation Buffers

30%(v/v) PEG 400; 50/100/150/200 mM Cr-chloride, 0.1 M Na-acetate (pH 4.6/HCl)
30%(v/v) PEG 400; 50/100/150/200 mM Cu-sulphate, 0.1 M Na-acetate (pH 4.6/HCl)
30%(v/v) PEG 400; 50/100/150/200 mM Co-chloride, 0.1 M Na-acetate (pH 4.6/HCl)
30%(v/v) PEG 400; 50/100/150/200 mM Li-sulphate, 0.1 M Na-acetate (pH 4.6/HCl)
30%(v/v) PEG 400; 50/100/150/200 mM Zn-chloride, 0.1 M Na-acetate (pH 4.6/HCl)
30%(v/v) PEG 400; 50/100/150/200 mM Ce-chloride, 0.1 M Na-acetate (pH 4.6/HCl)
30%(v/v) PEG 400; 50/100/150/200 mM Fe-3^+-chloride, 0.1 M Na-acetate (pH 4.6/HCl)
30%(v/v) PEG 400; 50/100/150/200 mM Mn-chloride, 0.1 M Na-acetate (pH 4.6/HCl)
30%(v/v) PEG 400; 50/100/150/200 mM Li-acetate, 0.1 M Na-acetate (pH 4.6/HCl)
30%(v/v) PEG 400; 50/100/150/200 mM Ni-sulphate, 0.1 M Na-acetate (pH 4.6/HCl)
30%(v/v) PEG 400; 50/100/150/200 mM Cu-chloride, 0.1 M Na-acetate (pH 4.6/HCl)
30%(v/v) PEG 400; 50 mM Hg-chloride, 0.1 M Na-acetate (pH 4.6/HCl)
30%(v/v) PEG 400; 50/100/150/200 mM Mg-sulphate, 0.1 M Na-acetate (pH 4.6/HCl)
30%(v/v) PEG 400; 50/100/150/200 mM Mg-acetate, 0.1 M Na-acetate (pH 4.6/HCl)
30%(v/v) PEG 400; 50/100/150/200 mM Fe-2^+-sulphate, 0.1 M Na-acetate (pH 4.6/HCl)
30%(v/v) PEG 400; 50/100/150 mM Fe-2^+-chloride, 0.1 M Na-acetate (pH 4.6/HCl)
30%(v/v) PEG 1500; 0.1 M $CdCl_2$; 0.1 M Na-acetate (pH 4.6/HAc)
30%(v/v) PEG 2000 MME; 0.1 M $CdCl_2$; 0.1 M Na-acetate (pH 4.6/HAc)
30%(v/v) PEG 400; 0.1 M $CdCl_2$; 10/50/100/150/200 mM NaCl; 0.1 M Na-acetate (pH 4.6/HCl)
25-35% (v/v) PEG 400; 0.1 M MES (pH 6.5/HCl)
25-35% (v/v) PEG 400; 0.1 M Na-acetate (pH 4.6/HAc)
25-35% (v/v) PEG 400; 0.1 M HEPES (pH 7.5/HCl)
25-35% (v/v) PEG 400; 0.1 M Na-citrate (pH 5.5/HCl)
30%(v/v) PEG 400; 0.1 M MOPS (pH 6.5/6.75/7.00/7.29/HCl)
30%(v/v) PEG 400; 0.1 mM $CdCl_2$; 0.1 M MOPS (pH 7.00/7.29/HCl)
30%(v/v) PEG 400; 0.1 M MES (pH 6.0/6.5/6.75/7.00/HCl)
MBClass SuiteI (QUIAGEN)
MBClass SuiteII (QUIAGEN)
30%(v/v) PEG 400; 0.1 M $CdCl_2$; 0.1 M Na-acetate (pH 4.6/HCl)
30%(v/v) PEG 400; 0.1 M $CdCl_2$; 0.1 M $LiCl_2$; 0.1 M Na-acetate (pH 4.6/HCl)
28-32%(v/v) PEG 400; 90-110 mM $CdCl_2$; 90-110 mM Na-acetate (pH 4.6/HCl)

7.3. Sequence Alignment

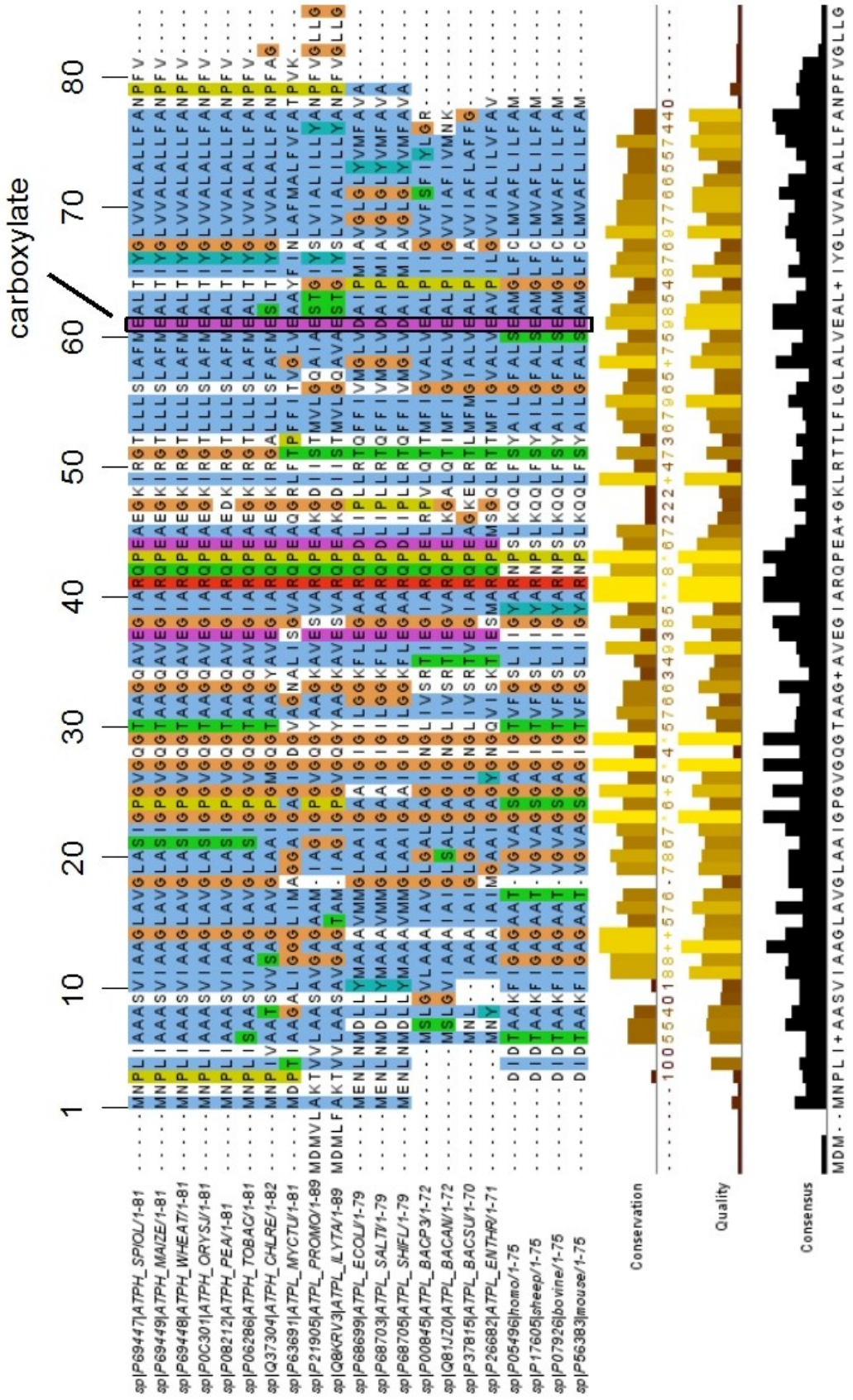

8. Acknowledgements

The last years have certainly been an interesting period. Lots of ups and downs, times of frustration close to desperation followed by feelings of elation. I would like to thank all people I met along this way in Düsseldorf as well as in the interesting places I had the chance to go to. My special thanks go to:

My supervisor Prof. Georg Groth for giving me the possibility to work on this highly interesting project, supporting my theories in experiments, and questioning my proposals, which made me think again and analysing problems from different points of view.

Prof. Lutz Schmitt for being my co-supervisor and having some spare time to read my thesis besides the overwhelming bureaucracy.

All present and former colleagues for coffee-breaks, a never ending flow of home made cakes (letting me survive some nights in the lab), and pizza orders and BBQ after a lab cleaning day. Anuschka, Benny, Daniel, Ellie, Erik, Jan, Judith, Kerstin, Mariana, Mel, Nicole, Silke, and Tom please keep on going and never give up. For every problem is a solution, one just have to find it.

Anuschka und Kerstin Ihr habt beide eben erst angefangen und ich hoffe auch nach einiger Zeit werdet Ihr immer noch Freude an der Wissenschaft haben. Es kann zwar frustrierend sein aber auch genauso begeisternd. Ich hoffe, Ihr entdeckt die positiven Aspekte und bleibt der Forschung erhalten.

Mariana, Du darfst jetzt meine Nachfolge auf dem Projekt antreten. Ich hoffe, dass Dir einiges an Frustration erspart bleibt und wünsche Dir, dass Du nicht den Spaß an der Arbeit verlierst.

Mel für die besten Schoko-Muffins der Welt

Benny, dass der Kleine Dich ab und an Mal lange schlafen lässt, um die nächtlichen Messzeiten am Fluorimeter auszugleichen. Aber Du weisst es gibt auch viel Schöneres als Labor, nämlich Windeln wechseln und Füttern.

Judith, falls das mit der Wissenschaft nicht so läuft wie Du willst kannst, Du ja eine Bäckerei auf machen. Mit Hefe kennst Du Dich ja jetzt bestens aus.

Jan und Nicole, bald wird es etwas turbulenter bei Euch. Ich hoffe, Ihr bekommt alles unter einen Hut und organisiert. Die Dreisamkeit hat auch etwas Schönes.

Ellie und Tom, Ihr seid beide einfach brilliant. Laßt Euch dabei aber nicht das Private zerstören. Lieber mal das Labor an der Uni bzw. in Jülich lassen. Macht weiter und mischt die Wissenschaft auf.

Daniel, Du bist erst vor einiger Zeit bei uns gelandet und hast mich somit nur auf dem Zieleinlauf begleiten können. Ich hoffe, dass in Düsseldorf alles für Dich nach Wunsch läuft und du die exzellente englische Küche nicht zu sehr vermisst. Beim nächsten Marmite-Brot denk' ich an Dich.

Lieber Sander, auch wenn Du nicht offiziell zu unserer Gruppe gehörst, hast Du Dir auf jeden Fall eine Kaffeetasse gesichert. Oops, ich muss meinen bei euch im Institut noch bezahlen. Danke für die vielen Tipps und Ratschläge sowie die durchwachten Nächte an der Beamline.

Liebe Christine, Du kannst das jetzt net lesen, da Du mich auf halber Strecke wegen dem wunderschönen Stockholm verlassen hast. Ich hoffe, wir sehen uns bald mal wieder zwischen Stockholm, Frankfurt und wo auch immer ich in England lande. Du hast immer einen Platz bei mir und natürlich eine Frau am Boden während Du in der Wand hängst.

Lieber Rolf, ich hoffe, dass ohne Wasserwerk die Kiste jetzt nahezu wartungsfrei läuft und Du Dich wieder auf das Überführen von Amminosäuren in die Gasphase konzentrieren kannst. Vielen Dank fürs Zuhören.

Lieber Arno, ich hoffe, Du hast genug Chlorophyll, um Deine Experimente zu machen und Deine Arbeit abzuschließen. Ich hab es leider nicht mehr zur Laser-Show geschafft.

Lieber Eckhard, auch wenn Du in Bochum sitzt vielen Dank für die Fahrten ans Synchroton. Mit Dir wird es beim Messen auf jeden Fall nicht langweilig und ich werd den Kaffee in Paris echt vermissen.

Lieber Guido, obwohl Du aus der anorganischen Chemie kommst und mit diesen kleinen Substanzen arbeitest danke Dir für die Einweisung in die Symmetrieoperationen innerhalb eines Moleküls.

Ein Danke an die Leute, die sonst nie erwähnt werden: Die Gärtner für den exzellenten Spinat. Iglo ist sicher neidisch. Den Jungs aus der Werkstatt für innovative Lösungen für Laborgeräte. Herrn Baum für die Wiederherstellung von elektronischem Equipment. Den Jungs im Chemikalienlager. Ihr seid die Flüssigstickstofflieferanten meines Vertrauens.

Herrn Lannert und Herrn Gutmann für einen wunderbaren Linux-Club und zahlreiche geeky sit-ins am Freitag Nachmittag. Ihr habt echt einen Linux-Liebhaber aus mir gemacht. Meine Shell spricht mit mir.

Martyn and Amy, for being patient. You had to wait so long but now it is done. I have finished. We can enjoy the summer now and play lots of wii. I will conquer your life now and you cannot get rid of me anymore.

Meiner Mutter und meinem Bruder für euren Rückhalt und euer unerschütterliches Vertrauen in mich. Liebe Mama, danke, danke, danke.

Erklärung

Die hier vorgelegte Dissertation habe ich eigenhändig und ohne unerlaubte Hilfe angefertigt.

Die Dissertation wurde in der vorgelegten oder in einer ähnlichen Form noch bei keiner anderen Institution eingereicht.

Düsseldorf, den 7.7.2009